

https://dspace.org/

Carbon nanotube production from greenhouse gases during syngas synthesis

Moothi, Kapil

2010-06-08T10:05:58Z
http://hdl.handle.net/10539/8170

Downloaded from a DSpace repository. https://dspace.org/

CARBON NANOTUBE PRODUCTION FROM GREENHOUSE GASES DURING SYNGAS SYNTHESIS

Kapil Moothi

A dissertation submitted to the Faculty of Engineering and the Built Environment, University of the Witwatersrand, in fulfillment of the requirement for the degree of Master of Science in Engineering.

Johannesburg, 2009

DECLARATION

I declare that this dissertation is my own, unaided work. It is being submitted for the Degree of Master of Science in the University of the Witwatersrand, Johannesburg. It has not been submitted before for any degree or examination in any other University.

_____

(Signature of candidate)

_____day of _____20_____

ABSTRACT

The impact of climate change around the world has led governments, institutions and industries to increase their efforts to combat it by seeking new and innovative technologies. Carbon dioxide (CO_2) is believed to be the primary reason for global warming. Therefore, the capture and transformation of some of the billions of tons of CO_2 produced annually by burning fossil fuels into useful products such as carbon nanotubes (CNTs) and carbon nanofibers (CNFs) is one of the methods being pursed in current research activities. The conversion of two major greenhouse gases, CO_2 and methane (CH_4), into CNTs and synthesis gas, which is a mixture of carbon monoxide (CO) and hydrogen (H_2) has been studied experimentally by passing a CO_2/CH_4 mixture through a vertically orientated Chemical Vapour Deposition (CVD) reactor at temperatures ranging from $650°C$ to $950°C$. Two different catalysts were used, a lanthanum nickel alloy ($LaNi_5$) and a mischmetal nickel alloy. Transmission electron microscopy (low and high magnification), Raman spectroscopy and gas chromatography were used to analyze the products from the experiment. The apparent activation energy for CH_4 and CO_2 consumption, and H_2 and CO production were estimated to be 41.7, 47.5, 54.5 and 47.5 kJ/ mol, respectively in the temperature range 1023 – 1123K. The CO_2 and CH_4 were decomposed, forming CNFs and CNTs as shown by the transmission electron microscope images. The findings showed that as the temperature increased the CNFs and CNTs became, less defined and fewer in number. The mischmetal nickel alloy had a smaller amount of amorphous carbon deposit compared to the lanthanum nickel alloy.

DEDICATION

I dedicate this body of work to my family, friends, teachers and professors, all of whom, no matter how big or small, had an effect on my life and my education. Thank you for your support and advice over the years.

"Experiments are the only means of knowledge at our disposal. The rest is poetry, imagination."

Max Planck

ACKNOWLEDGEMENTS

I would like to take this opportunity to express my token of appreciation to those who have helped me throughout this project. First, I would like to express my sincere thanks to Prof. Sunny E. Iyuke, my supervisor for his support, valuable experience and motivation during this study.

Thanks to Prof. Mike Witcomb from the WITS electron microscopy unit for assistance with the HMTEM work and Mr. Rudolph Erasmus from the School of Physics Department for help with the Raman Spectroscopy characterization of the samples.

I would also like to express my gratitude to the staff and students from the School of Chemical and Metallurgical Engineering for the creation of a friendly and stimulating working environment.

In addition, I recognize the financial support supplied from the University of the Witwatersrand, DST/NRF Centre of Excellence in Strong Materials and SANERI.

Last but foremost, I wish to extend a special thank you to my parents for the encouragement, guidance and understanding they provided throughout my undergraduate degree. I would not be who I am if it was not for you.

CONTENTS

DECLARATION i

ABSTRACT ii

DEDICATION iii

ACKNOWLEDGEMENTS iv

CONTENTS v

LIST OF FIGURES viii

LIST OF TABLES xiii

LIST OF SYMBOLS/ABBREVIATIONS xiv

CHAPTER ONE 1

1.0 Introduction 1

1.1 Background and Motivation 1

1.2 Aim and Objectives 2

1.3 Hypothesis 3

1.4 Dissertation Outline 3

CHAPTER TWO 4

2.0 Literature Review 4

2.1 Carbon 4

2.2 Carbon Nanotubes 5

2.3 Structure of Carbon Nanotubes 6

2.4 Growth Mechanism for Carbon Nanotubes 10

2.5 Synthesis Methods for Carbon Nanotubes 13

2.5.1 Arc Discharge 13

2.5.2 Laser Ablation 15

2.5.3 Chemical Vapour Deposition (CVD) 16

2.6 Properties and Applications of Carbon Nanotubes 19

2.6.1 Electronic 19

2.6.2 Thermal 20

2.6.3 Mechanical 21

2.6.4 Adsorption 21

2.6.5 Catalysis 22

2.7 Methane and Carbon Dioxide 22

2.8 Reforming 25

2.8.1 Network of Reactions 27

2.8.2 Kinetics 29

CHAPTER THREE 34

3.0 Experimental 34

3.1 Decomposition of Methane and Carbon Dioxide 34

3.2 Reforming of Methane with Carbon Dioxide 35

3.3 Equipment used for Analysis 37

3.3.1 Use of Transmission Electron Microscopy 37

3.3.2 Use of Raman Spectroscopy 37

3.3.3 Use of Gas Chromatography 40

CHAPTER FOUR 41

4.0 Results and Discussion 41

4.1 TEM images of CNFs produced using CH_4 41

4.1.1 Raman Spectroscopy Analysis (using CH_4 only) 48

4.2 TEM images of CNTs and CNFs produced using CO_2 50

4.2.1 Raman Spectroscopy Analysis (using CO_2 only) 59

4.3 TEM images obtained when dry reforming of CH_4 has taken place 66

4.3.1 Raman Spectroscopy Analysis (using CO_2/CH_4 reforming) 73

4.4 Kinetics 79

CHAPTER FIVE 87

5.0 Conclusion and Recommendations 87

5.1 Conclusion 87

5.2 Recommendations 88

REFERENCES 89

APPENDIX 1: POSTER, ORAL PRESENTATIONS AND PUBLICATIONS 113

LIST OF FIGURES

FIGURE PAGE

Figure 2.1: The structures of carbon (diamond, fullerene, graphite and CNT) 4

Figure 2.2: The basic atomic structures of CNTs (Dresselhaus *et al*., 2003) 6

Figure 2.3: Two dimensional hexagonal real lattice of graphene where the chiral vector $\overline{OA}$ or Ch is defined by unit vectors $a1$ and $a2$ (Dresselhaus *et al*., 2001) 7

Figure 2.4: Possible chiral vector specified by the pair of integers (n,m) for general nanotubes, including zigzag, armchair and chiral nanotubes. The encircled dots denote metallic nanotubes while the small dots are for semiconducting nanotubes 8

Figure 2.5: Three different types of SWCNTs a) armchair, b) zigzag and c) chiral (O'Connell, 2006) 10

Figure 2.6: Schematic of the two growth modes generally considered for CNTs, base growth and tip growth (Ando *et al*., 2004) 11

Figure 2.7: Schematic view of the mechanism for the formation of SWCNTs. a) adsorption and decomposition of the hydrocarbon, b) diffusion in the liquid surface layer of the particle, c) super-saturation of the surface and formation of the cap, d) growth of the SWCNT 12

Figure 2.8: Schematic representation of an arc discharge apparatus 14

Figure 2.9: Schematic representation of laser ablation apparatus (Kingston and Simard, 2003) 16

Figure 2.10: Schematic of catalytic CVD operated either as floating catalyst or as substrate catalyst (Iyuke and Mahalik, 2005) 18

Figure 2.11: a) standard FB-CVD reactor, b) FB-CVD reactor with gas pre-heating, and c) vibro-fluidized-bed reactor (Philippe *et al*., 2007) 18

Figure 2.12: Chemical Energy Transmission System (Richardson and Paripatyadar, 1990) 25

Figure 3.1: Diagrammatic representation (not to scale) of the CCVD used for production 35

Figure 3.2: Raman spectrum showing the most characteristic features of CNTs: radial breathing mode (RBM), the D band, G band and G' band (Belin and Epron, 2005) 39

Figure 4.1: CNT produced at $650°C$ using $LaNi_5$ 41

Figure 4.2: a) CNTs, b) a CNF and c) CNT produced at $650°C$ using $LaNi_5$ 42

Figure 4.3: HMTEM image of CNT produced at $650°C$ using $LaNi_5$ 43

Figure 4.4: CNTs produced at $750°C$ using $LaNi_5$ 44

Figure 4.5: HMTEM image of the CNTs produced at $750°C$ using $LaNi_5$ 45

Figure 4.6: CNTs produced at $750°C$ using $LaNi_5$ 45

Figure 4.7: HMTEM image of a CNT produced at $750°C$ using $LaNi_5$ 46

Figure 4.8: HMTEM image of a CNT produced at $850°C$ using $LaNi_5$ 47

Figure 4.9: Raman spectrum of carbon produced using CH_4 at $650°C$, with the D-band at 1360 cm^{-1} and G-band at 1600 cm^{-1} 48

Figure 4.10: Raman spectrum of carbon produced using CH_4 at $750°C$, with the D-band at 1352 cm^{-1}, G-band at 1585 cm^{-1} and G'-band at 2701 cm^{-1} 49

Figure 4.11: Raman spectrum of carbon produced using CH_4 at $850°C$, with the D-band at 1354 cm^{-1}, G-band at 1591 cm^{-1} and G'-band at 2714 cm^{-1} 50

Figure 4.12: CNFs and CNTs produced at $650°C$ using lanthanum nickel alloy 51

Figure 4.13: CNTs and CNFs produced at $700°C$ using lanthanum nickel alloy 51

Figure 4.14: a) CNFs and b) possible CNT produced at $700°C$ using lanthanum nickel catalyst 52

Figure 4.15: a) CNFs, b) CNFs (attached to catalyst particles) and c) a twisty CNF produced at $750°C$ using lanthanum nickel alloy 53

Figure 4.16: CNF produced at $850°C$ using lanthanum nickel alloy 54

Figure 4.17: a) CNF on the nickel catalyst, b) CNFs, c) CNF produced at $850°C$ using lanthanum nickel catalyst 55

Figure 4.18: a) CNFs and b) hollow CNF produced at $800°C$ using mischmetal nickel catalyst 56

Figure 4.19: a) CNF and b) CNFs and CNTs produced at $750°C$ using 1% Pt on alumina powder 57

Figure 4.20: Raman spectrum of carbon produced using CO_2 at $650°C$, with the D-band at 1352 cm^{-1}, G-band at 1593 cm^{-1} and G'-band at 2710 cm^{-1} 59

Figure 4.21: Raman spectrum of carbon produced using CO_2 at $700°C$, with the D-band at 1360 cm^{-1}, G-band at 1603 cm^{-1} and G'-band at 2698 cm^{-1} 60

Figure 4.22: Raman spectrum of carbon produced using CO_2 at $750°C$, with the D-band at 1356 cm^{-1}, G-band at 1591 cm^{-1} and G'-band at 2701 cm^{-1} 61

Figure 4.23: Raman spectrum of carbon produced using CO_2 at $850°C$, with the D-band at 1350 cm^{-1}, G-band at 1591 cm^{-1} and G'-band at 2685 cm^{-1} 62

Figure 4.24: Raman spectrum of carbon produced using CO_2 at $800°C$ 63

Figure 4.25: Raman spectrum of carbon produced using CO_2 at $750°C$ 64

Figure 4.26: Raman spectra of catalyst particles after the reaction using CO_2 a) $LaNi_5$ at $650°C$, b) $LaNi_5$ at $700°C$ and c) mischmetal nickel alloy at $800°C$ 65

Figure 4.27: a) CNTs and b) disordered CNTs produced at $750°C$ during dry reforming using $LaNi_5$ 66

Figure 4.28: a) Network of CNTs, b) CNTs and c) CNT produced at $750°C$ during dry reforming using mischmetal nickel alloy 67

Figure 4.29: a) CNT produced at $850°C$ during dry reforming using mischmetal nickel alloy and b) CNT not fully formed 68

Figure 4.30: HMTEM image of the catalyst particle (dark spot) and the carbon nanostructures (grey) 69

Figure 4.31: HMTEM image showing few CNTs are produced at $950°C$ 70

Figure 4.32: Composition of catalyst particle after dry reforming of CH_4 72

Figure 4.33: Raman spectrum of CNTs produced at $750°C$ during CO_2 reforming of CH_4, with the D-band at 1358 cm^{-1}, G-band at 1593 cm^{-1} and G'-band at 2710 cm^{-1} 73

Figure 4.34: Raman spectrum of CNTs produced at $850°C$ during CO_2 reforming of CH_4, with the D-band at 1360 cm^{-1} and G-band at 1601 cm^{-1} 74

Figure 4.35: Raman spectrum of CNTs produced at $750°C$ during CO_2 reforming of CH_4, with the D-band at 1358 cm^{-1}, G-band at 1599 cm^{-1} and G'-band at 2710 cm^{-1} 75

Figure 4.36: Raman spectrum of CNTs produced at $850°C$ during CO_2 reforming of CH_4, with the D-band at 1352 cm^{-1}, G-band at 1589 cm^{-1} and G'-band at 2705 cm^{-1} 76

Figure 4.37: Raman spectrum of sample when CNTs were not formed during dry reforming 77

Figure 4.38: Effect of different CO_2:CH_4 ratios on formation rate of CO over the nickel alloy catalyst at $750°C$, $800°C$ and $850°C$ (CO_2 changing, CH_4 constant) 81

Figure 4.39: Effect of different CO_2:CH_4 ratios on formation rate of CO over the nickel alloy catalyst at $750°C$, $800°C$ and $850°C$ (CH_4 changing, CO_2 constant) 82

Figure 4.40: Effect of different CO_2:CH_4 ratios on formation rate of H_2 over the nickel alloy catalyst at $750°C$, $800°C$ and $850°C$ (CO_2 changing, CH_4 constant) 83

Figure 4.41: Effect of different CO_2:CH_4 ratios on formation rate of H_2 over the nickel alloy catalyst at $750°C$, $800°C$ and $850°C$ (CH_4 changing, CO_2 constant) 84

Figure 4.42: Natural logarithm of reaction rate versus 1/T (K), where CO_2:CH_4:1 85

LIST OF TABLES

TABLE PAGE

Table 3.1: The conditions at which experiments are performed for the CCVD method 36

Table 4.1: Summary of carbon produced using CH_4 only, CO_2 only and CH_4/CO_2 reforming at different temperatures 78

LIST OF SYMBOLS/ABBREVIATIONS

CO_2	Carbon dioxide
CO	Carbon monoxide
CNT/CNTs	Carbon nanotube/ carbon nanotubes
CNF	Carbon nanofiber
CCVD	Catalytic chemical vapour deposition
CVD	Chemical vapour deposition
θ	Chiral angle
Ch	Chiral vector
DWCNT	Double-walled carbon nanotube
EDS	Energy Dispersive X-Ray Spectroscopy
GC	Gas chromatography
H_2	Hydrogen
HMTEM	High Magnification Transmission Electron Microscopy
La	Lanthanum
CETS	Chemical Energy Transmission System
CH_4	Methane
μm	Micron
MWCNT	Multi-walled carbon nanotube
nm	Nanometre
Ni	Nickel
RBM	Radial Breathing Mode
RWGS	Reverse Water-Gas Shift Reaction

STM	Scanning Tunneling Microscopy
SWCNT	Single-walled carbon nanotube
TGA	Thermogravimetic analysis
TEM	Transmission Electron Microscopy
r	Reaction rate (mol/g-s)
R	Ideal gas constant
P	Pressure (atm)
Ea	Apparent activation energy (kJ/mol)
K	Chemical equilibrium constant
T	Temperature (K)

CHAPTER ONE

1.0 Introduction

1.1 Background and Motivation

The world continues to become increasingly industrialized due to globalization, leading to humankind consuming fossil-fuel based resources at an ever-growing rate. This resulting in the emission of greenhouse gases (in particular carbon dioxide and methane), playing an increasing role in global warming. These emissions have to be mitigated in order for the effects of global warming to be diminished and controlled. CO_2 has an atmospheric lifetime that could effectively be tens of thousands of years whilst CH_4 has an atmospheric lifetime ranging from nine to 15 years. As discussed by Zwaan and Gerlagh (2006) the issue of climate uncertainty is one that calls for society to change its energy supply from one that is fossil fuel based to one that is free of carbon emissions.

In order to avert this concern, new and viable alternatives to current methods of CO_2 capture, use and sequestration need investigation. A promising field is converting it (and CH_4) to something else such as carbon nanotubes (CNTs) which are less harmful to the environment and even economically viable (Xu and Huang, 2007; Chai *et al.*, 2007). CNTs have arisen as a dynamic field of research due to their properties. A high thermal conductivity (6000 W/mK) in comparison to copper (401 W/mK), an electrical conductivity six times higher than copper (Bethune *et al.*, 1993), as well as extraordinary

mechanical properties i.e. a Young's modulus over 1 Tpa and an estimated tensile strength of 150 GPa (Serp *et al*., 2003; Treacy *et al*., 1996).

As a result of these unique and useful properties, CNTs have found potential application in the fields of hydrogen storage, field emitters, fuel cells (Lozovik *et al*., 2003; Conteau *et al*., 2003; Philip *et al*., 2003), polymer composites (Shofner *et al*., 2003), catalyst support (Bezemer *et al*., 2006) and water purification (Park *et al*., 2000). In order to realize large-scale CNT applications they are to be grown in large quantities. The Chemical Vapour Deposition (CVD) method has emerged as the best hope for cost-effective mass production of CNTs. The reforming of CH_4 with CO_2 process produces CNTs and valuable synthesis gas (a mixture of H_2 and CO). This method of production may well prove to be economically viable as the synthesis gas produced is with a low H_2/CO ratio, and sold to energy companies for Fischer-Tropsch synthesis to liquid hydrocarbons and oxygenated derivatives.

1.2 Aim and Objectives

The main aim of the study is to selectively produce CNTs from greenhouse gases in the reforming of CO_2/CH_4 with synthesis gas as a by product. Thus, the following objectives will be undertaken:

- Production of CNTs from CO_2 only, CH_4 only and reforming of CO_2/CH_4 by catalytic chemical vapour deposition method (CCVD).

- Characterize the as-synthesised CNTs using Raman spectroscopy and Transmission Electron Microscopy.
- Determine the best catalyst for carbon nanotube synthesis.

1.3 Hypothesis

Carbon nanotubes simultaneously produced from greenhouse gases during reforming of CO_2/CH_4 to synthesis gases.

1.4 Dissertation Outline

Chapter 1 looks at the background and motivation, aim and objectives and the hypothesis of this study. Chapter 2 is a literature review regarding CNTs, their types, structure, and growth mechanism, methods of production, properties and applications. Also discussed is CH_4 and CO_2 decomposition as well as dry reforming of CH_4.

Chapter 3 is the experimental section, consisting of CNT growth by Catalytic Chemical Vapor Deposition (CCVD) method and the characterization techniques used for the analysis of the as-grown CNTs and synthesis gas.

Chapter 4 presents the results and discussion. Finally, the conclusion and recommendations of this research are in Chapter 5.

CHAPTER TWO

2.0 Literature Review

2.1 Carbon

The most abundant element in the world is carbon and is the sixth element of the Periodic Table of Elements with a valency of four. The unique structure of carbon and its high valency allow it to exist in many alternative forms, referred to as allotropes. Carbon in its solid ground state, for example diamond, exhibits sp3 covalent bonding with carbon atoms bonded to four other carbon atoms in a tetrahedral 3-D lattice. Figure 2.1 shows the schematics of different carbon materials (Iyuke and Mahalik, 2005).

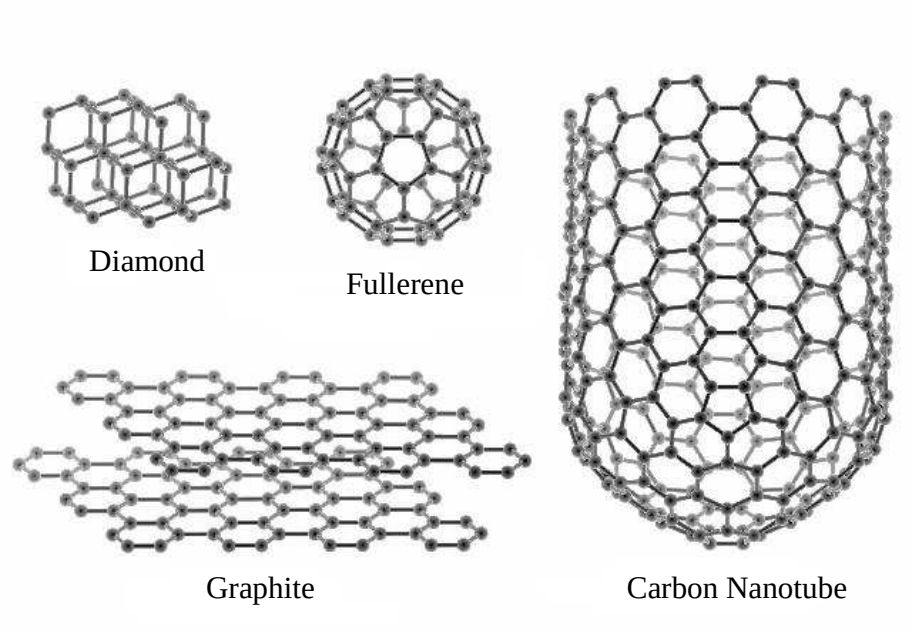


Figure 2.1: The structures of carbon (diamond, fullerene, graphite and CNT)

In the condensed phase, carbon has a hexagonal ground state of graphite with sp^2 hybridization. Another pure crystal form of carbon is fullerenes, with the spherical C_{60} molecule, commonly known as bucky balls observed by Smalley and his co-workers in 1985 (Kroto *et al*., 1985).

2.2 Carbon Nanotubes

Carbon nanotubes (CNTs), another form of allotropes of carbon were characterized in the early 1990's (Iijima, 1991; Iijima and Ichihashi, 1993; Thess *et al*., 1996) whereby two classes of CNTs were observed. A single-wall carbon nanotube (SWCNT) is a crystalline one-atom thick sheet of graphite rolled up into a hollow graphite cylinder with a diameter varying from $0.4nm$ to $2nm$ and a length in the order of microns (Szleifer and Yerushalmi-Rozen, 2005). CNTs consisting of a number of concentric graphitic layers with diameters varying from $10nm$ to $100nm$, and a length greater than $10\mu m$ are termed multi-walled carbon nanotubes (MWCNTs) (Kaneto *et al*., 1999). Figure 2.2 illustrates the different types of CNT structures i.e. SWCNTs, double-wall CNTs (DWCNTs), MWCNTs and 'peapods'. 'Peapods' are CNTs that are packed with fullerenes (Smith et al., 1998).

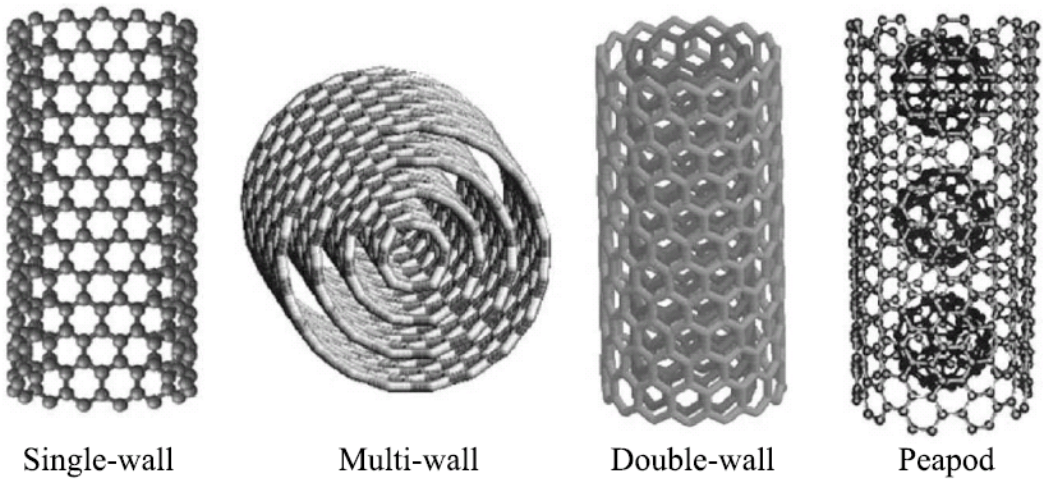


Figure 2.2: The basic atomic structures of CNTs (Dresselhaus *et al*., 2003)

2.3 Structure of Carbon Nanotubes

The CNT structure has been characterized using transmission electron microscopy (TEM) and scanning tunneling microscopy (STM), confirming that nanotubes are seamless cylinders derived from the honeycomb lattice of the graphene layers of single atomic crystalline graphite, shown in Figure 2.3.

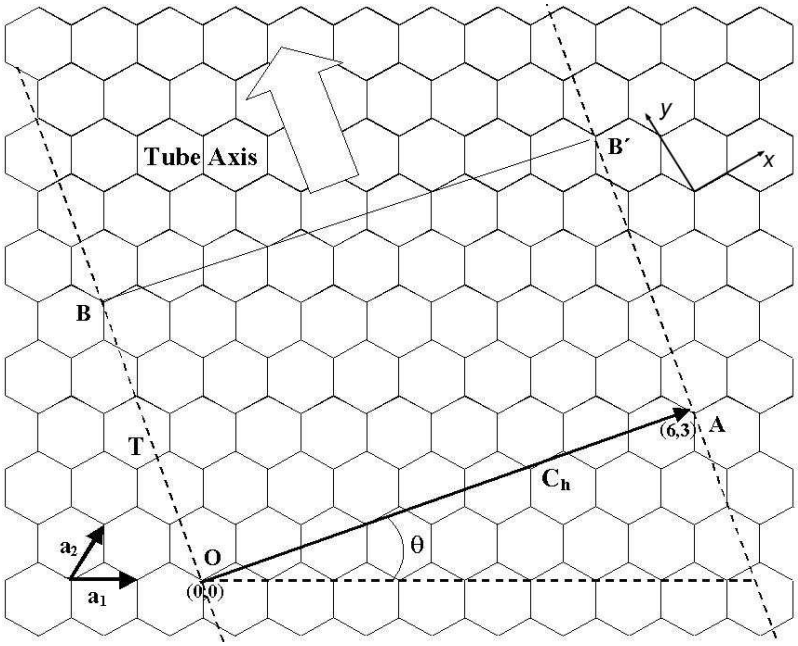


Figure 2.3: Two dimensional hexagonal real lattice of graphene where the chiral vector $\overline{OA}$ or Ch is defined by unit vectors $a1$ and $a2$ (Dresselhaus *et al*., 2001)

Specification of the structure of an individual tube is in terms of the vector Ch, which is joining two equivalent points on the original graphene lattice as depicted in Figure 2.3. The cylinder is produced by rolling up the sheet such that the two ends of the vector are superimposed.

Using the notation detailed by Dresselhaus *et al*. (2001), each pair of integers (n,m) represents a possible tube structure as illustrated in Figure 2.4.

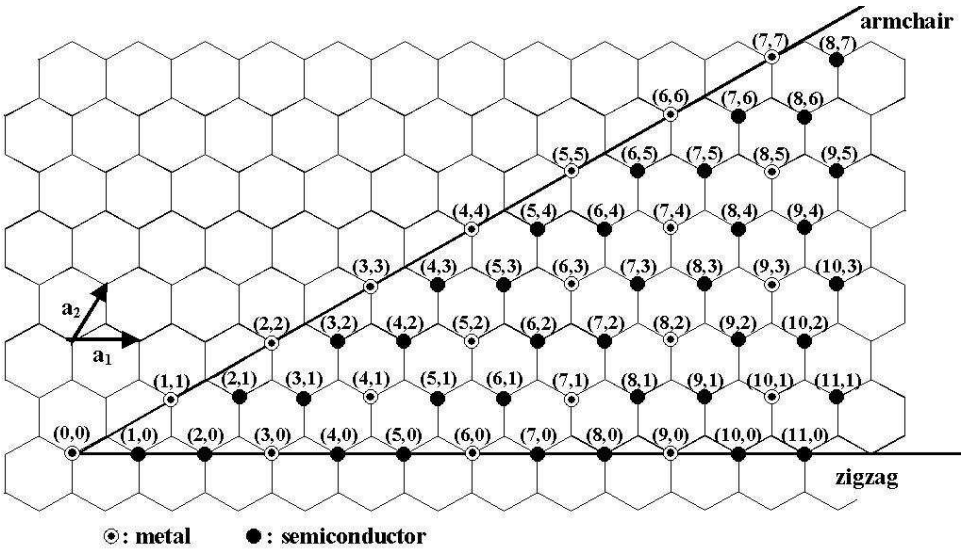


Figure 2.4: Possible chiral vector specified by the pair of integers (n,m) for general nanotubes, including zigzag, armchair and chiral nanotubes. The encircled dots denote metallic nanotubes while the small dots are for semiconducting nanotubes.

The vector Ch is expressed as shown in equation 2.1.

$$Ch = n(a1) + m(a2) \tag{2.1}$$

Where:

$a1$ and $a2$, are the unit cell base vectors of the graphene sheet

$0 \le m \le n$

There are three main groups of nanotubes, which depend on the indices (n,m). Armchair nanotubes formed when $n = m$ thus, the angle between the chiral vectors is $30°$. These nanotubes display metallic characteristics. Zigzag nanotubes as discussed by O'Connell

(2006) are classified as such when $m = 0$ and $n > 0$; whereas chiral nanotubes are created when 0 < |m| < n. Equation 2.2 gives the nanotube diameter.

$$d_t = \sqrt{3} a_{c-c} \left(n^2 + nm + m^2 \right)^{1/2} / \pi = Ch / \pi \quad (2.2)$$

Where:

Ch, is the length of the chiral vector

a_{c-c}, is the carbon atom bond length ($0.142nm$).

The angle between the zigzag axis and chiral vector is the chiral angle, θ given by equation 2.3.

$$\theta = \tan^{-1} \left(\frac{\sqrt{3} m}{2n + m} \right) \quad (2.3)$$

Classification of the different CNT structures together with a schematic model of the capping of the tubes is, depicted in Figure 2.5.

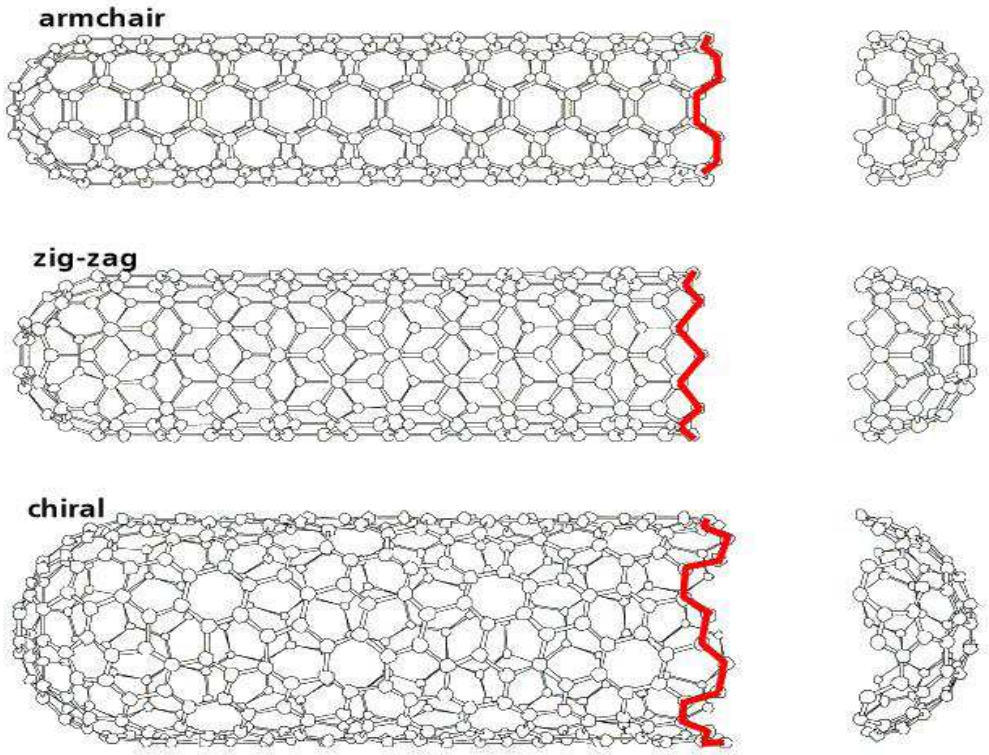


Figure 2.5: Three different types of SWCNTs a) armchair, b) zigzag and c) chiral (O'Connell, 2006)

2.4 Growth Mechanism for Carbon Nanotubes

The growth mechanism for formation of CNTs is unclear, as the growth dynamics of CNTs are not yet completely understood (Ando *et al*., 2004; Lee *et al*., 2001). This section provides an overview of research conducted in this aspect. As discussed by Vinciguerra *et al*. (2003), the growth of CNTs happens very rapidly since almost all of the growth transpires within the first 60 seconds. Studies conducted by Kim *et al*. (2002), have shown that growth rates as high as $60\ \mu m/\min$ are possible. The diameter of the CNTs that are grown is temperature dependent (Ducati *et al*., 2002).

CNTs grow from catalyst particles, as shown on the schematics in Figure 2.6. The strength of the interaction between the catalyst particle and the substrate determines the type of growth. Where the catalyst maintains its contact to the substrate it is base-growth, or it loses contact (tip-growth) (Dresselhaus *et al*., 2001). The growing CNT can have a catalyst particle on one or on both sides. CNTs do not grow on every accessible catalyst particle surface. It is not well understood as to which qualities the catalyst surface must provide to allow the nucleation necessary for the growth of a CNT (Rotkin and Subramoney, 2005; Ebbesen, 1997).

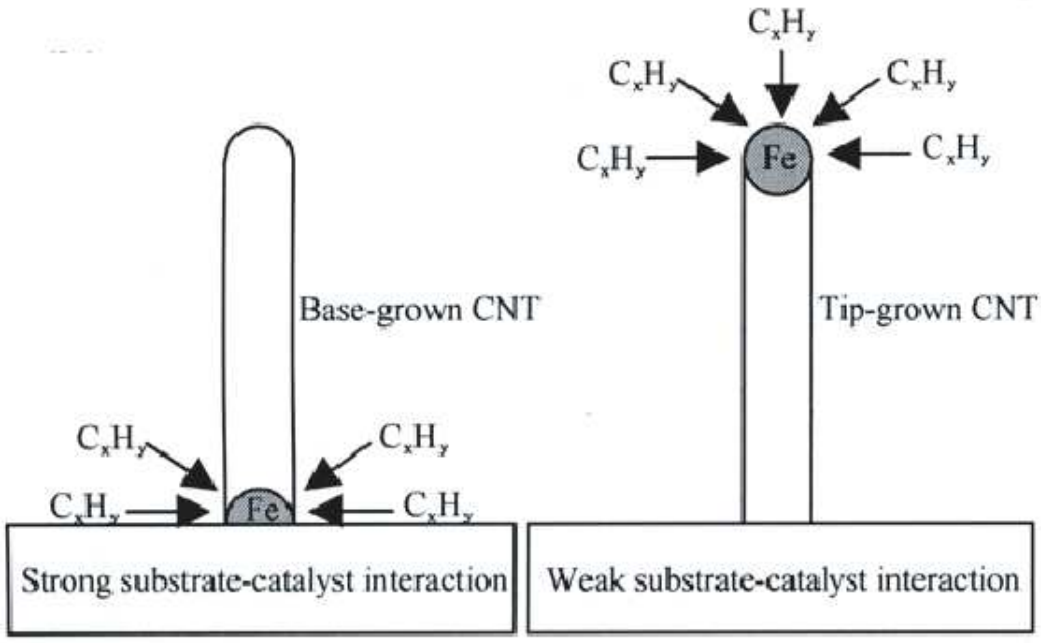


Figure 2.6: Schematic of the two growth modes generally considered for CNTs, base growth and tip growth (Ando *et al*., 2004)

The size of the catalyst particle also governs whether formation of SWCNTs or MWCNTs occurs. A catalyst particle size of a few nanometers would form SWCNTs,

whereas particles having a size of a few tens of nanometers would favour MWCNT formation (Lee *et al*., 2001; Kukovitsky *et al*., 2002). A possible mechanism for the growth of CNTs using a hydrocarbon discussed by Nagy *et al*. (2007) is shown in Figure 2.7.

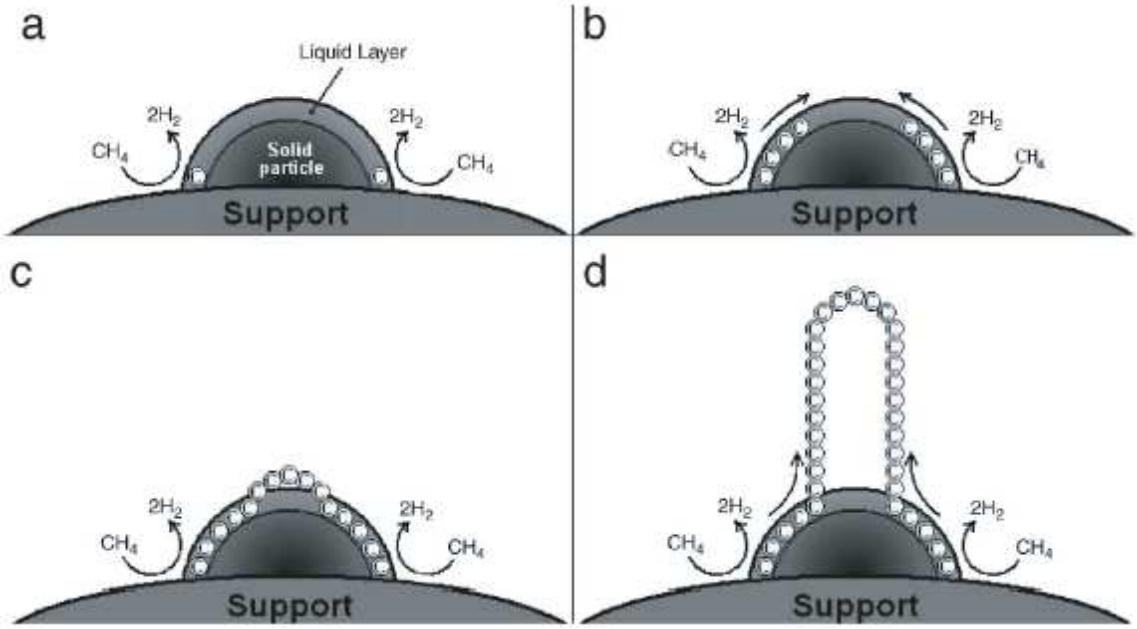


Figure 2.7: Schematic view of the mechanism for the formation of SWCNTs. a) adsorption and decomposition of the hydrocarbon, b) diffusion in the liquid surface layer of the particle, c) super-saturation of the surface and formation of the cap, d) growth of the SWCNT

Heating the methane feedstock causes its molecules to break up at the surface of the catalyst. The carbon atoms diffuse away (formation of radicals in gas phase) and form the SWCNT at another location. A possible explanation of this diffusion is due to the dissociation of methane into carbon and hydrogen being a highly exothermic reaction

resulting in local heating of the catalyst particle (Furer, 2006). The hydrogen reduces the catalyst locally and slows down a too fast radical formation. Consequently, this reduces the development of amorphous carbon on the surface. The carbon diffuses to a colder spot (Klinke *et al*., 2005) resulting in a carbon and a temperature gradient within the catalyst particle (Ducati *et al*., 2004).

2.5 Synthesis Methods for Carbon Nanotubes

Three methods currently used for the synthesis of CNTs are arc discharge, laser ablation and catalytic decomposition of hydrocarbons (generally referred to as the chemical vapour deposition (CVD) method). The carbon products obtained by these three methods differ from each other since each has its own growth dynamics and each method has its own advantages and disadvantages.

2.5.1 Arc Discharge

This method according to Keidar (2007) is the most practical method for synthesizing SWCNTs and has become a commonly used technique for carbon nanotube production. It produces SWCNTs with fewer defects than a method that operates at low temperature such as CVD. However, the tubes tend to be short with random sizes and directions and often require a lot of purification. It also has a drawback, as it is a non-continuous synthesis process. It needs periodic shutdowns to allow for replacement of the graphite electrode and product collection (Zeng *et al*., 2006).

The arc discharge technique involves the use of two high-purity graphite rods as the cathode (diameter of $8-12nm$) and anode (diameter of $6-8nm$). A DC electric discharge is established between the pair under an inert gas atmosphere (helium or argon) at a low pressure. A bias of 10-35V is applied to the electrodes (which are separated by $1mm$) to establish the discharge, producing currents of 60-100A and current densities of 150 A/cm^2. The resulting carbon vapour allows for assembly of CNTs, found in the cathode deposits. The main factor in establishing an optimum environment for carbon nanotube production is the stability of the discharge plasma (Kingston and Simard, 2003). SWCNT synthesis requires doping of the anode with a small amount of metallic catalyst particles such as Ni, Co, Mo and Fe (Zeng *et al*., 2006). Figure 2.8 shows a simplified schematic drawing of arc discharge apparatus (Kingston and Simard, 2003).

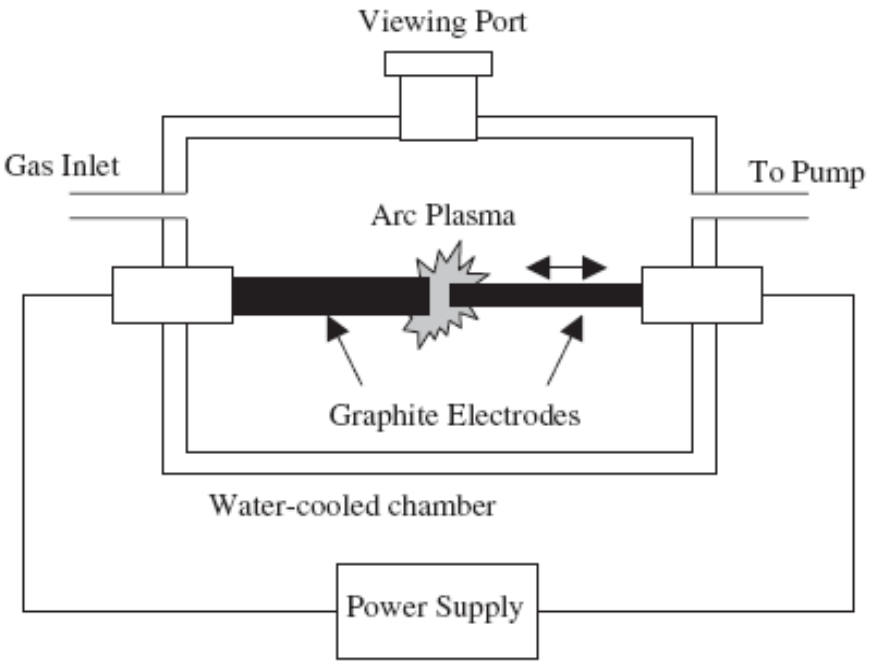


Figure 2.8: Schematic representation of an arc discharge apparatus

The synthesis of MWCNTs were the graphite anode is dipped into an open container of liquid nitrogen containing a short non-consumable copper or graphite cathode may prove economically viable as expensive inert gasses are not required (Zeng *et al*., 2006).

2.5.2 Laser Ablation

In this technique, laser pulses heat a carbon target, commonly graphite. The subsequent use of the resulting gas is the formation of SWCNTs (Munoz *et al*., 2000). This method has not achieved wide scale use, as it requires expensive equipment such as the laser to set-up, operate and maintain. As described by Maser *et al*. (2002), in order to achieve economically viable production of CNTs the following aspects are desired: continuous production; cheaper feedstock materials; and a more efficient process for the preparation of the target materials.

This process has a horizontal setup, consisting of a solid graphite target that is mounted in a quartz tube placed in a temperature-controlled oven. After sealing and evacuating the tube, a buffer gas (argon or helium) flows through it. The vapourisation of the target rod is performed by a pulsed Nd:YAG laser, producing a carbon based soot that is swept out of the furnace zone by the carrier gas. This soot, containing well graphitized MWCNTs and fullerenes is deposited on the water-cooled collector (Maser *et al*., 2002). Figure 2.9 depicts the apparatus used for laser ablation.

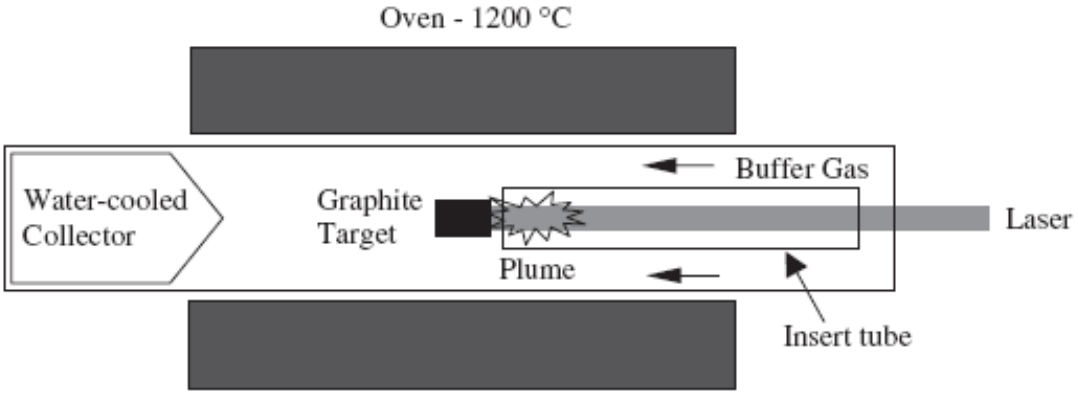


Figure 2.9: Schematic representation of laser ablation apparatus (Kingston and Simard, 2003)

Production of SWCNTs can transpire if the graphite rod is doped with transition metal catalysts such as Co, Ni and Fe. The most efficient way for SWCNT production is the use of equal parts of 0.5-1.0% each of Co and Ni powders in the graphite target. As a result, laser vapourisation has come be used almost exclusively for the fabrication of SWCNTs (Kingston and Simard, 2003). Munoz *et al*. (2000) observed that the type of ambient gas (argon, nitrogen or helium) and its pressure that is used influences the formation of the SWCNTs.

2.5.3 Chemical Vapour Deposition (CVD)

This process as described by McBride (2001) is one that allows the manufacturer to avoid the practice of separating nanotubes from the carbonaceous particulate that often accompanies the other two methods of synthesis. The basic principle of this method involves the cracking of gas-phase carbon-rich molecules (methane, acetylene or carbon

monoxide) in the presence of a catalyst at elevated temperatures. These reactive radical carbon molecules then diffuse and bond on the catalyst leading to the formation of CNTs.

CVD synthesis consists of two key categories, namely supported catalyst or floating catalyst growth. The catalysts used are typically Ni, Fe or Co. The choice of catalyst plays a central role in determining the formation of SWCNTs. The chemical and textual properties of the catalyst used affect the yield and quality of SWCNTs that are produced. The choice of carbon source is also a key element to the growth of SWCNTs containing no defects and amorphous carbon over-coating.

In supported growth process, prepared catalyst deposited on a support medium is placed in a tube at atmospheric pressure. The tube is inside a temperature-controlled furnace so that the carbon-rich gases can flow through the tube at temperatures ranging from $500-1100°C$ for the requisite time. For floating catalyst growth, the basic difference lies in that the catalyst and gas are injected into the system concurrently, in the gas phase (Kingston and Simard, 2003). CVD apparatus are designed to be either horizontal or vertical. A typical catalytic chemical vapour deposition system equipped with a horizontal tubular furnace as the reactor is shown in Figure 2.10.

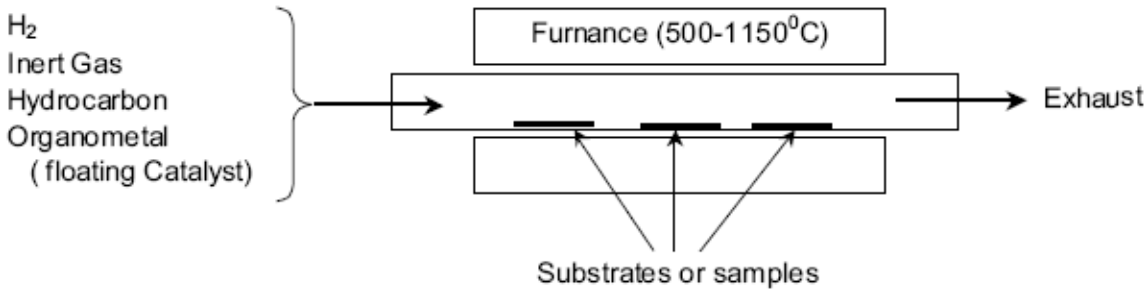


Figure 2.10: Schematic of catalytic CVD furnace operated either as floating catalyst or as substrate catalyst (Iyuke and Mahalik, 2005)

Vertically orientated CVD reactors are shown in Figure 2.11, configured to produce CNFs and MWCNTs under fluidized bed conditions (FB-CVD).

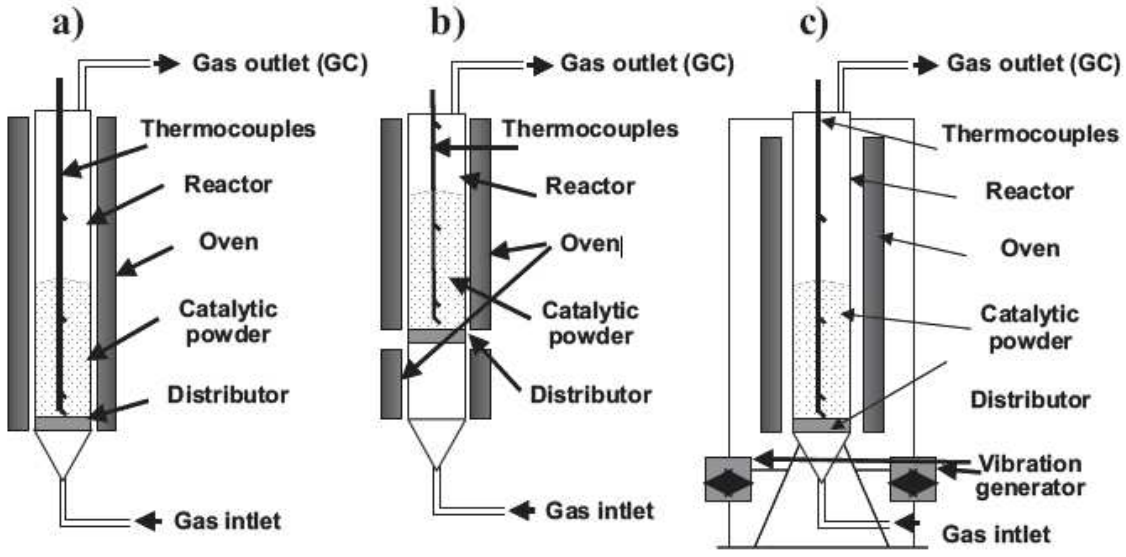


Figure 2.11: a) standard FB-CVD reactor, b) FB-CVD reactor with gas pre-heating, and c) vibro-fluidized-bed reactor (Philippe *et al*., 2007)

As discussed by Kong *et al*. (1998) it is critical to gain an understanding of the chemistry involved in the role of the catalyst and the CNT growth process. This will allow for the successful industrial application by CVD in the production of CNTs. The CVD process presents the best hope for large-scale production of CNTs owing to its relatively low cost and potentially high yield (Su *et al*., 2001; Xiang *et al*., 2007). Success of CNT utilization in various sectors is strongly dependent on the development of simple, efficient and inexpensive technologies for mass production.

2.6 Properties and Applications of Carbon Nanotubes

Many unique and fundamental properties (electronic, thermal, mechanical and adsorption) that CNTs possess make them potentially viable in a broad range of applications.

2.6.1 Electronic

The key factors in determining whether a SWCNT would exhibit behaviour of a conductor or a semi-conductor are the diameter and chirality of the carbon nanotube (Szleifer and Yerushalmi-Rozen, 2005; Katok *et al*., 2006; Kaneto *et al*., 1999; Odom *et al*., 1998). As the electrical properties of SWCNTs are dependant on the geometrical parameters of helicity (armchair, zigzag or chiral) and diameter, it has become important to be able to manipulate these parameters for feasible applications in the electronic

industry i.e. superconductors, single molecular transistors or magnetic recording devices (Lou *et al*., 2003).

SWCNTs with armchair structure are metallic whilst those with the zigzag arrangement demonstrate semi-conductor behaviour (Serp *et al*., 2003; Bethune *et al*., 1993). Hamada *et al*. (1992), describes that the variation of the band structure, which accounts for the differing conducting behaviour is due to the 2-D band structure of graphite. The unique properties of CNTs as described by Teo *et al*. (2003), where CNTs act as electrical conductors with a complete covalent bond allow them to avoid problems of atomic diffusion or electronic migration.

2.6.2 Thermal

A key feature of CNTs described by Thostenson *et al*. (2001), is the thermal stability it exhibits under reaction conditions of $2800°C$ (in a vacuum) whilst also displaying a thermal conductivity approximately twice as high as that of diamond. Thermogravimetic analysis (TGA) provides an easy method to learn about the resistance of CNTs towards temperature. It has been shown that activated carbon is less stable to oxidation than CNTs, with the CNTs being more reactive than graphite (Serp *et al*., 2003). Additionally, determination of thermal conductivity of CNTs is by phonons at all temperatures (Hone, 2004). CNTs present itself as an excellent material for field effect transistors (FETs) (Baughman *et al*., 2002) or as an alternative to the conventional silicon-based-microelectronics for circuits (Hoenlein *et al*., 2004).

2.6.3 Mechanical

CNTs being solely composed of strong covalently bonded carbon atoms, allow them to be one of the hardest wearing and durable substances discovered in modern times. This is revealed by the exceptionally high Young modulus, found to be in the terapascal (Tpa) range along with a traction resistance of 250 Gpa. This resistance to traction is one hundred times higher than displayed by steel, with the CNTs being six times lighter (Serp *et al*., 2003; Treacy *et al*., 1996). Krishnan *et al*. (1998) observed that values for the Young's modulus of CNTs are regularly higher in comparison with bulk graphite.

CNTs are highly flexible and are able to withstand twisting at right angles a number of times without any structural changes occurring. The millimeters-thick large area, self-standing blocks of CNTs as grown by Musso *et al*. (2007), have properties such as elasticity, resistance under compression and being highly hydrophobic. Due to CNTs being inherently stiff, they can be used as probe tips for atomic force microscopy (Hafner *et al*., 2001) and scanning tunneling microscopy (Biro *et al*., 1997; Hafner *et al*., 1999).

2.6.4 Adsorption

Studies undertaken by Yang *et al*. (2001) and Inoue *et al*. (1998) have shown that due to the porous nature of MWCNTs, they could prove to be useful for efficient gas storage. The adsorption of nitrogen on acid treated SWCNTS as observed by Eswaramoorthy *et al*. (1999), has shown that the micro pores of the CNTs can also accommodate molecules such as benzene. There are two different adsorption sites for gas in a SWCNT bundle i.e.

the inside of the SWCNTs and the interstitial channels of the bundle. Fujiwara *et al*. (2001) found that the inside of CNTs is more stable for nitrogen and oxygen gas adsorption than the interstitial channels of the bundles.

2.6.5 Catalysis

Carbon materials are recognized as a viable catalyst support in heterogeneous catalysis as the properties that they possess, such as being stable at high temperatures, showing resistance to both basic and acidic media and chemical inertness are highly wanted properties of catalyst supports (Rodriguez-Reinoso, 1998). The work undertaken by Serp *et al*. (2003) describes that carbon nanotube supports have some advantages in comparison to activated carbon, namely, minimization of self-poisoning due to the high purity of the material; their porous nature could be valuable for liquid-phase reactions; the specific metal-support interactions that exist are able to have a direct effect on catalytic activity and selectivity. As these properties expressed by CNTs exceed those of activated carbon they could prove to be an effective support for the Fischer-Tropsch reaction (Van Steen and Prinsloo, 2002; Bahome, 2007).

2.7 Methane and Carbon Dioxide

Studies have shown that CH_4 cracking produces CNTs, CNFs and hydrogen utilizing CVD apparatus (He *et al*., 2006; Gao *et al*., 2008). It was found that using CH_4 as a carbon feedstock, reaction temperatures ranging from $850-1000°C$, suitable catalysts

and flow rates, the growth of high quality SWCNTs is possible (Tibbetts, 1985; Kong *et al*., 1998; Cassell *et al*., 1999). Catalysts for the decomposition of CH_4 are Ni/Al, $Ni/Cu/Al_2O_3$ and MgO impregnated with one of the group 8 to 10 metals of the periodic table (He *et al*., 2006; Weizhong *et al*., 2004; Ichi-oka *et al*., 2007).

Investigations on the decomposition of CH_4 allow advancement in achieving a sustainable production of hydrogen (Dufour *et al*., 2009). This may lead to hydrogen emerging as an economically viable source of energy in fuel cells and other applications. It would be ideal as a synthetic fuel because it is lightweight, highly abundant and its oxidative product (water) is environmentally benign, although storage remains a problem (Schlapbach and Zuttel, 2001). CNTs, as single-walled or multi-walled systems would provide an effective storage means for hydrogen in vehicles (Winter and Nitsch, 1998).

Many investigations have been conducted to seek reduction of carbon dioxide using various methods although the CO_2 molecule is chemically quite stable (Tsuji *et al*., 1996; Ohme and Suzuki, 1996; Solymosi and Kiss, 1985). The ways of handling planet-warming CO_2 emissions: capture and storage of CO_2 from the flue gas of natural gas/coal fired power plants (Alie *et al*., 2005) which may require expensive technologies. Thermal decomposition utilizing high temperatures of approximately $2500°C$ for substantial conversion of CO_2 to CO (Khedr *et al*., 2006) or as a raw material in heterogeneous or homogeneous catalytic and non-catalytic processes (Xu *et al*., 2005). Nevertheless, studies have shown the decomposition of CO_2 at practical temperatures using appropriate catalysts. Lou *et al*. (2003) reported that large amounts of CNTs were synthesized by

reduction of CO_2 with metallic lithium at $550°C$ and 700atm using an autoclave. An inventive solution as discussed by Xu and Huang (2007) has been the use of CO_2, a non-toxic gas as a carbon source in the synthesis of MWCNTs at $790°C$ and $810°C$ by a horizontal CVD method over Fe/CaO catalyst. The reaction mechanism followed is that CO_2 reacts to CO and O, followed by CO disproportionation where two CO molecules react with each other to form carbon and CO_2. Motiei *et al*. (2001) report another method of CO_2 utilization for graphite production was CO_2 in a supercritical state used at conditions of $1000°C$ and 10 kbar according to the following chemical reactions:

$$Mg\ (g) + CO_2\ (g) \rightarrow MgO\ (g) + CO\ (gas)$$

$$Mg\ (l) + CO\ (g) \rightarrow MgO\ (g) + C\ (graphite)$$

Global Reaction: $Mg\ (g) + Mg\ (l) + CO_2\ (g) \rightarrow 2\ MgO\ (g) + C\ (graphite)$

The dissociation of CO_2 was also found to be possible on rare earth metals in a temperature range of 603 – 823K at atmospheric pressure (Arakawa *et al*., 1988). The increasing resistivity of the various metals is used as a measure of the CO_2 dissociation. Zhang *et al*. (1999) showed that Wustite ($Fe_{0.98}O$) can be used to reduce CO_2 at reaction conditions of 573K and atmospheric pressure to carbon. A proposed mechanism for the reduction is the conversion of CO_2 to CO and from CO to C. The CO is considered an intermediate as the CO conversion is faster than the conversion of CO_2.

2.8 Reforming

Carbon dioxide reforming (commonly known as dry reforming) of methane to produce synthesis gas (a mixture of CO and H_2) is a process that has been researched for many years. These greenhouse gases (CO_2 and CH_4) are the cheapest carbon-containing materials. Converting them into a valuable feedstock not only reduces their emissions into the atmosphere but can also prove to be economically beneficial. In comparison to steam reforming of methane (CH_4/H_2O) to synthesis gas, dry reforming has the following advantages. Production of synthesis gas with a lower H_2: CO ratio, which is suitable for use in the Fischer-Tropsch process to produce higher hydrocarbons; utilization of CO_2, rather then sequestration and storage; better use in chemical energy transmission systems (CETS) i.e. solar, nuclear or renewable energies (Zhang *et al*., 1996).

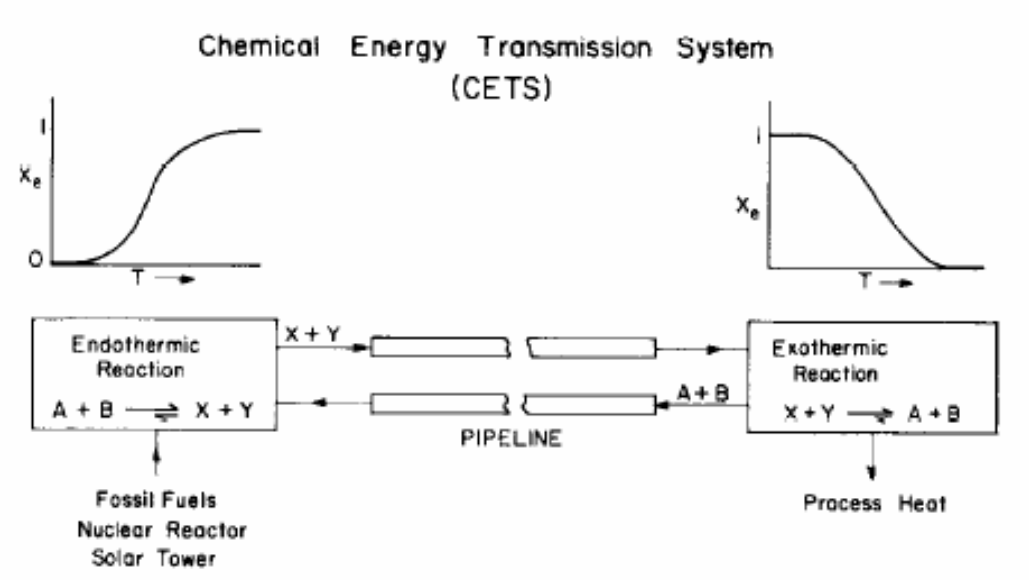


Figure 2.12: Chemical Energy Transmission System (Richardson and Paripatyadar, 1990)

According to the CETS design (Figure 2.12), abundant thermal energy from solar, nuclear, or fossil fuel sources is used to drive a reversible endothermic reforming reaction to equilibrium. The gaseous products can then be stored or transported to other process sites. When energy is needed, the reverse exothermic reaction can be driven to equilibrium, generating process heat. Products of the exothermic reaction can then be recycled back to the original reactor for reforming once again through the aid of the abundant thermal energy source (Richardson and Paripatyadar, 1990). Dry reforming has a further advantage to steam reforming in terms of a CETS because all species are in gas phase at atmospheric conditions, making transport and recycling of the species easier.

Edwards and Maitra (1995) discuss that suitably supported Group VIII elements in their reduced forms, especially Ni, Ru, Rh, Pd, Ir and Pt are effective catalysts for the dry reforming of methane. Some of the catalysts used in this reaction are NiO/Al_2O_3 (Chen *et al*., 2005), supported Ni-Ce and Ni-Co (Yang *et al*., 2002), Ni-MgO (Shamsi, 2004), Ni-SiO_2 (Effendi *et al*., 2003) and supported CoOx with MgO, ZrO_2 or CeO_2 (Mondal *et al*., 2007).

A long-standing problem with this process is that carbon deposits deactivate the catalysts (particularly the nickel-based catalysts) during the reaction (Chen *et al*., 2001). Research has been conducted to reduce the coke formation on the catalyst by making it more carbon resistant (Hou *et al*., 2005, Takanabe *et al*., 2005). The conversion of CO_2 to carbon has been found to be efficient, even more so than converting it to synthesis gas

(Ross, 2005). Carbon nanofibres (CNFs), including CNTs, were discovered on the catalysts used for dry reforming by Gallego and his co-workers (Gallego *et al*., 2008).

2.8.1 Network of Reactions

In addition to the main reaction (equation 2.4), there are possible side reactions that are thermodynamically favourable at $750°C$ (Bradford and Vannice, 1999). These are Reverse Water-Gas Shift Reaction (RWGS), steam reforming of CH_4, CH_4 decomposition, carbon removal reactions and reactant cross products (Song *et al*., 2008; Zang, 2008). The reactions are listed as:

$$CH_4 + CO_2 \Leftrightarrow 2CO + 2H_2 \quad (2.4)$$

$$H_2 + CO_2 \Leftrightarrow CO + H_2O \quad (2.5)$$

$$CH_4 + H_2O \Leftrightarrow CO + 3H_2 \quad (2.6)$$

$$CH_4 \Leftrightarrow C + 2H_2 \quad (2.7)$$

$$C + CO_2 \Leftrightarrow 2CO \quad (2.8)$$

$$C + H_2O \Leftrightarrow CO + H_2 \quad (2.9)$$

$$CH_4 + 2CO_2 \Leftrightarrow 3CO + H_2O + H_2 \quad (2.10)$$

$$CH_4 + 3CO_2 \Leftrightarrow 4CO + 2H_2O \quad (2.11)$$

It is possible to determine the number of independent reactions that are required to describe the system. Achievement of this is by obtaining the rank of the stoichiometric coefficient matrix (Fogler, 1986). The stoichiometric coefficient matrix expressed by

equation 2.12 where the coefficients of reactants are taken with a negative sign and those of products are taken with a positive sign (equations 2.4 – 2.11).

$$\begin{array}{cccccc} CH_4 & CO_2 & CO & H_2 & H_2O & C \end{array}$$

$$\begin{pmatrix} -1 & -1 & 2 & 2 & 0 & 0 \\ 0 & -1 & 1 & -1 & 1 & 0 \\ -1 & 0 & 1 & 3 & -1 & 0 \\ -1 & 0 & 0 & 2 & 0 & 1 \\ 0 & -1 & 2 & 0 & 0 & -1 \\ 0 & 0 & 1 & 1 & -1 & -1 \\ -1 & -2 & 3 & 1 & 1 & 0 \\ -1 & -3 & 4 & 0 & 2 & 0 \end{pmatrix} \quad (2.12)$$

Reducing the matrix, equation 2.13 can be derived from equation 2.12. The rank of the matrix shown by equation 2.13 is three, and correspondingly any three independent equations can be selected to describe the reaction system sufficiently. Hence, equations 2.4, 2.5, and 2.7 as 1 set of independent reactions could be chosen.

$$\begin{array}{cccccc} CH_4 & CO_2 & CO & H_2 & H_2O & C \end{array}$$

$$\begin{pmatrix} -1 & -1 & 2 & 2 & 0 & 0 \\ 0 & -1 & 1 & -1 & 1 & 0 \\ 0 & 0 & 0 & 0 & 0 & 0 \\ -1 & 0 & 0 & 2 & 0 & 1 \\ 0 & 0 & 0 & 0 & 0 & 0 \\ 0 & 0 & 0 & 0 & 0 & 0 \\ 0 & 0 & 0 & 0 & 0 & 0 \\ 0 & 0 & 0 & 0 & 0 & 0 \end{pmatrix} \quad (2.13)$$

2.8.2 Kinetics

Generally, catalysts are used to speed up chemical reactions. Therefore, an effective catalyst should be able to adsorb the reactants, and at the same time, facilitate the formation of the products. The entire reaction process should have a zero net-effect on the catalyst, leaving it unaltered and available for further reaction. The chemical equilibrium of a chosen reaction, if it can be reached, is determined entirely by the thermodynamics of that reaction. Consequently, an unfavoured reaction, from the thermodynamic perspective, will remain unfavoured – irrespective of whether a catalyst is present or not. The introduction of a catalytic substance only affects the kinetics of the system (Abild-Pedersen, 2005). The concepts discussed in the following concern interacting reactants on heterogeneous catalysts, such as metal surfaces, where the catalyst and the reactants are in different phases.

The study of the kinetics of dry reforming began with work conducted by Bodrov *et al.*, in 1967 over a variety of Ni-based catalysts. It was found that the kinetics for CO_2 reforming of CH_4 over a Ni film in a temperature range of $800-900°C$, matched the kinetic model they had constructed from a similar study of steam (H_20) reforming of CH_4 (Bodrov and Apelbaum, 1967). The model proposed by Bodrov to describe the dry reforming reaction is shown below, whereby * denotes an active site on the catalyst surface, $\rightarrow$ depicts a slow irreversible reaction, and $\leftarrow\rightarrow$ represents a quasi-equilibrated reaction:

$$CH_4 + * \rightarrow CH_2* + H_2 \qquad (2.14)$$

$CO_2 + * \leftarrow \rightarrow CO + O*$ (2.15)

$O* + H_2 \leftarrow \rightarrow H_2O + *$ (2.16)

$CH_2* + H_2O \leftarrow \rightarrow CO* + 2H_2$ (2.17)

$CO* + \leftarrow \rightarrow CO + *$ (2.18)

This model uses the assumption that CH_4 does not react with CO_2 but rather with the H_20. After the CH_4 has dissociated to CH_2 and H_2 (equation 2.14), and after the Reverse Water-Gas Shift Reaction has produced H_2O (equations 2.15 and 2.16), the remaining methane-derived CH_2 species is reformed with H_2O to produce a net result of 2CO and $2H_2$ (equations 2.17 and 2.18). Since the Reverse Water-Gas Shift Reaction is assumed to be fast relative to the first step of methane activation and decomposition, it is expected that the kinetics be nearly the same for CO_2 reforming as for H_2O reforming of methane (Witmore, 2007). Current research on the initial proposal of the reaction mechanism by Brodov has yielded interesting results with proposals of both modified and alternative reaction mechanisms, which are dependent on catalyst type, carrier or temperature. An understanding of the elementary steps which may or may not be involved in the mechanism is necessary in order for the kinetics of the overall catalytic dry reforming reaction to be understood fully.

Studies by Rostrup-Nielsen (1972) on the equilibria of CH_4 and CO decomposition on different Ni catalysts (temperature range $450-750°C$) showed that equilibrium constants of CO dispropotionation and CH_4 decomposition were influenced by Ni catalysts. This resulted in higher equilibrium concentrations of CO and CH_4, respectively

than those predicted using graphite equilibria. This deviation from the thermodynamic graphite calculation was accounted for by the presence of a more disordered structure of the carbon i.e. whiskers (or CNFs). Subsequent research in this area by Rostrup-Nielsen (1994) details insights into the carbon deposition reactions over Ni catalysts.

In steam methane reforming, were the primary carbon deposition route is methane decomposition; Rostrup-Nielsen (1994) describes carbon formation to be related to one of two conditions. One limit, which results in carbon formation, is a kinetic allowance in spite of overall thermodynamics. The conditions allow methane to decompose into carbon instead of reacting with steam even though thermodynamics predict no carbon formation after equilibrium of the reforming and shift reactions. The other limit in which carbon may form is dictated by thermodynamics; carbon will be formed if the equilibrated gas shows affinity for carbon.

Rostrup-Nielsen and Hansen (1993) conducted research of CH_4 decomposition, CO disproportionation, and dry reforming using Ni and noble metals as catalysts. Equilibrium constants for methane decomposition were discovered to be smaller for noble metals than Ni, deviating more from the graphite equilibrium. At $500°C$, the highest rate of carbon formation through methane decomposition followed the order Ni >> Rh> Ir,Ru > Pt, Pd, whilst at $650°C$, the order was Ni > Pd, Rh > Ir > Pt > Ru. In the dry reforming studies that was conducted in the temperature range of $550-600°C$, the activity followed the order Ru, Rh > Ir > Ni, Pt, Pd.

Wang and Au (1996) showed that the isotopic effects of CH_4/CD_4 in CO_2 reforming of CH_4 over Ni/SiO_2 catalyst indicated that dissociation of CH_4 is the rate-determining step. However, Slagtern *et al*. (1997) reported that the surface reaction between C species from CH_4 cracking and oxygen-adsorbed species derived from CO_2 dissociation is the rate-determining step. Hu and Ruckenstein (1997) also concluded the surface reaction between C and O species to be the rate-determining step over Ni catalysts through transient response analysis. Bradfrod and Vannice (1996) investigated and developed a kinetic model based on CH_4 dissociative adsorption to form CH_x species and CH_xO decomposition as rate-determining steps. In addition, Tsipouriari and Verykios (2001) reported another kinetic model by using the assumption that CH_4 cracking and surface reaction between C and oxycarbonate species are rate-determining steps over Ni/La_2O_3 catalyst. The proposed mechanistic steps, which lead to the production of CO and H_2:

$CH_4 + S \leftrightarrow S\text{-}CH_4$ equilibrium

$C\text{-}CH_4 \rightarrow S\text{-}C + 2H_2$

$CO2 + La_2O_3 \leftrightarrow La_2O_2CO_3$ equilibrium

$La_2O_2CO_3 + C\text{-}S \rightarrow La_2O_3 + 2CO + S$

$H_2 + 2S \leftrightarrow 2S\text{-}H$ equilibrium

$La_2O_2CO_3 + H\text{-}S \leftrightarrow La_2O_3 + CO + S\text{-}OH^-$

$S\text{-}OH^- + C\text{-}S \leftrightarrow S\text{-}CO + S\text{-}H$ (s)

$S\text{-}OH + S\text{-}H \leftrightarrow H_20 + 2S$

$S\text{-}CO \leftarrow > CO + S$

$CO_2 + S \leftrightarrow S\text{-}CO_2$

S-CO +H-S ←→ S-CO + OH-S slow

S-OH + H-S ←→ H_2O + 2S

Erdohelyi *et al*. (1993) studied CH_4 dissociation, CO_2 dissociation and the dry reforming reaction using Rh catalysts on various supports. The dissociation of CH_4 on Rh, at 423K, produced H_2 and small amounts of C_2H_6; the intermediate species CH_3, rapidly decomposes further to surface carbon and hydrogen atoms, as no CH_3 or CH_x species were identified. It was shown that the dissociation of CO_2 was aided by the addition of CH_4; the hydrogen formed in the CH_4 decomposition promotes the dissociation of CO_2. In the dry reforming studies, no deactivation of the Rh catalysts occurred; signifying that the surface carbon formed reacted away efficiently before stable amorphous or graphitic carbon is formed.

CHAPTER THREE

3.0 Experimental

The production of the CNTs and CNFs in this research is by Catalytic Chemical Vapour Deposition (CCVD). Ultra High Purity (UHP) i.e. 99.0% purity grade gases as supplied by AFROX (African Oxygen) Ltd were used.

3.1 Decomposition of Methane and Carbon Dioxide

Catalysts used as supplied by Sigma Aldrich without any further pre-treatment before the experimental runs. Approximately 10g of catalyst (unless otherwise stated) is placed on quartz wool which is located 28cm (from the bottom) within a vertically orientated tube of Figure 3.1 An electric furnace heats the mullite tube (inner diameter of 50mm; length of 1050mm). Before the commencement of an experimental run the reactor (Figure 3.1) was purged with argon so as to free the line from oxygen, detect leaks and to prevent the formation of nitrites (Kuwana *et al.*, 2005). Experiments conducted at temperatures ranging from $650-1000°C$ for CO_2 and $650-850°C$ for CH_4. The CO_2 decomposition temperatures were selected as suggested in section 2.7. The feed flowrate used was 487 ml/min. Effluent gas sampled using a sample collection cylinder for gas chromatography (GC) analysis. The detailed CCVD apparatus is shown in Figure 3.1, utilized for growth of the CNTs and CNFs.

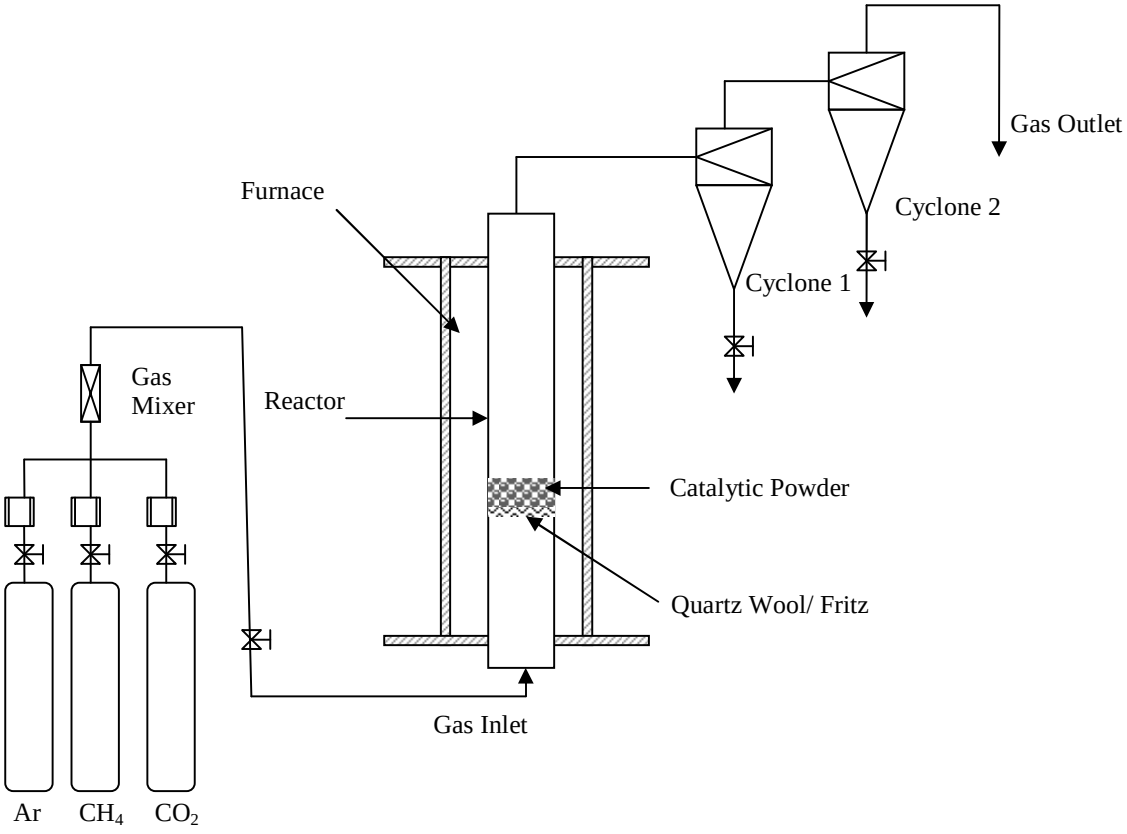


Figure 3.1: Diagrammatic representation (not to scale) of the CCVD used for production

3.2 Reforming of Methane with Carbon Dioxide

For the dry reforming of CH_4, the catalyst was loaded onto a quartz fritt (porosity of 40-90 micron) positioned in the centre of a quartz tube (inner diameter of 50mm and length of 1000mm). The feed gases of CO_2 and CH_4 were supplied at an equal flowrate (unless otherwise stated). Experiments were conducted at temperatures ranging from $650-950°C$, this is based on the acceptable temperature range used for CO_2 reforming of CH_4 (discussed in section 2.8). For the kinetic experiments at $750°C$, the CH_4 flowrate was kept constant at 308 ml/min and the CO_2 flowrate was varied from 154 to

927 ml /min. Then experiments are conducted were the CO_2 flowrate was kept constant at 308 ml/min and the CH_4 flowrate changed from 154 to 927 ml/min. Similar experiments were done at $800°C$ and $850°C$. The duration of each experimental run is 60 minutes. The growth conditions used for the experimental runs are presented in Table 3.1.

Table 3.1: The conditions at which experiments are performed for the CCVD method

Temperature (^oC)	**Catalyst**	**CO_2 (ml/min)**	**CH_4 (ml/min)**
650	$LaNi_5$ alloy		487
750	$LaNi_5$ alloy		487
850	$LaNi_5$ alloy		487
650	$LaNi_5$ alloy	487	
700	$LaNi_5$ alloy	487	
750	$LaNi_5$ alloy	487	
850	$LaNi_5$ alloy	487	
800	Mischmetal Nickel alloy	487	
750	1% Pt. on Alumina (2.5g)	487	
750	Ni (2.5g) & LaO_5 (2.5g)	487	
750	$LaNi_5$ alloy	154, 308, 616, 927	308
		308	154, 308, 616, 927
800	$LaNi_5$ alloy	154, 308, 616, 927	308
		308	154, 308, 616, 927
850	$LaNi_5$ alloy	154, 308, 616, 927	308
		308	154, 308, 616, 927
950	$LaNi_5$ alloy	487	487
750	Mischmetal Nickel alloy	487	487
850	Mischmetal Nickel alloy	487	487
950	Mischmetal Nickel alloy	487	487

3.3 Equipment used for Analysis

Characterization of the carbon products is by using Transmission Electron Microscopy (TEM) and Raman Spectroscopy (J-Y T64000) techniques due to the nanometer scale dimensions involved. TEM (Joel JEM 100S) and high magnification TEM (Philips CM200) was utilized. Gas chromatography (Agilent Technology 6820) was used for analysis of the exit gas samples.

3.3.1 Use of Transmission Electron Microscopy

In order to observe the products, 5ml of methanol was added to the samples and placed in a sonic bath for 10 minutes. A few drops of the resulting suspension were deposited onto a lacey carbon film on a copper grid. The methanol was evaporated (air-dried) before the copper grid was loaded into the sample chamber of the TEM for observation.

3.3.2 Use of Raman Spectroscopy

Raman spectroscopy is of crucial importance for better understanding of the structure and the type of CNTs as well as providing crucial information about the quality of CNTs, whether as-grown CNTs have defects or are well graphitized. This tool also gives information about the type of CNTs whether they have armchair, zigzag, or chiral structures. It is a quick and non-destructive tool for CNT characterization since SWCNTs and MWCNTs give characteristic peaks. The Raman spectra of CNTs are unique and distinct due to their one dimensional (1D) nature (Shiri, 2007). It is used in the study of

vibration, rotational and other low-frequency modes in a system. Incoming photons from a laser scatter in-elastically with phonons or other excitations in the system. The energy of the scattered photons can be shifted up or down. This shift in energy gives information about the phonon modes in the system. This in-elastic scattering of the light is termed Raman scattering (Rao *et al*., 1997; Dresselhaus *et al*., 2005).

The characteristic features of CNTs in the Raman shift (Figure 3.2) are: (a) a low frequency peak < 200cm^{-1}, whose frequency depends on the diameter of the tube (RBM: radial breathing mode); (b) a large structure (1340 cm^{-1}) assigned to residual ill-organized graphite, namely the 'D-Band' (D meaning disorder) (Maultzsch *et al*., 2002) whereas in perfectly ordered graphite there is no 'D band'; (c) a high-frequency bunch, the 'G-Band' between 1500 and 1600 cm^{-1} (G meaning graphite); (d) a second order observed mode between 2450 and 2650 cm^{-1} assigned to the first overtone of the D mode and often called G' mode; (e) a combination mode of the D and G modes between 2775 and 2950 cm^{-1} (Belin and Epron, 2005).

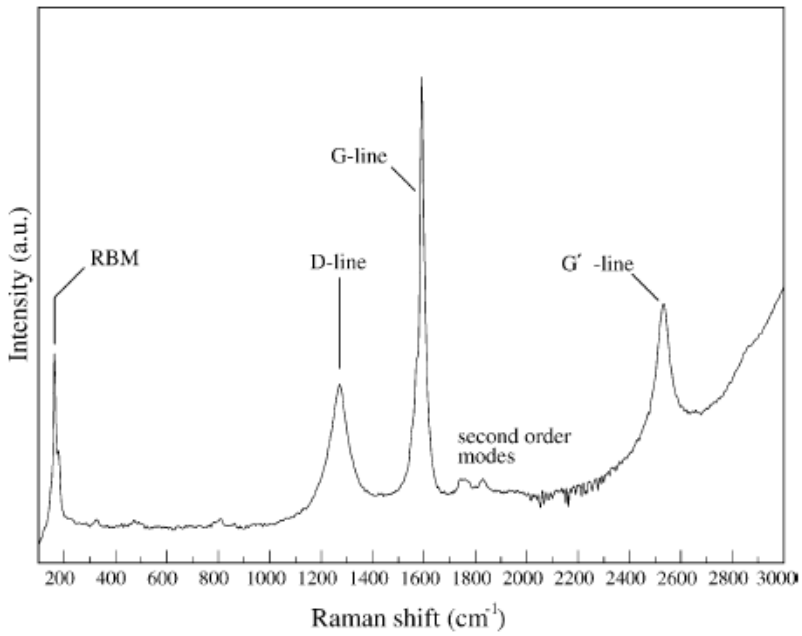


Figure 3.2: Raman spectrum showing the most characteristic features of CNTs: radial breathing mode (RBM), the D band, G band and G' band (Belin and Epron, 2005)

The distinction between SWCNTs and MWCNTs is possible due to the ratio of the integrated D- and G-band being inversely proportional to the crystallite size of graphite. The ratio of the D- and G- band is also used as an indicator of the amount of disorder within CNTs. An I_D/I_G ratio in the range 0.1 – 0.2 indicates the defect level in the atomic carbon structure is low, signifying reasonable crystalline quality (Eklund *et al*., 1995; Dresselhaus *et al*., 2002).

The samples did not need any pre-treatment to be inspected using Raman Spectroscopy. The carbon products were analyzed at nominally room temperature and the power at the sample was kept low (~1.2 MW) to minimize local heating. The argon laser line was at an excitation wavelength of 514.5 nm.

3.3.3 Use of Gas Chromatography

A gas chromatograph is a chemical analysis instrument that separates gas mixtures into individual components. It usually consists of a double column system with two detectors, namely the thermal conductivity detector (TCD) and flame ionization detector (FID) which is used for detecting inorganic and organic compounds, respectively. A carrier gas transports the gas mixture of unknown components and composition through a tube, called a column. This column restricts different components at different temperatures and allows certain components to continue to the detector, depending on the temperature of the column. The components are identified electronically by the detector at different times (retention time), by generating a chromatogram.

Samples of the exit gas collected during experimental runs are injected into the gas chromatograph to determine if the input gases did break down. If decomposition of the input gasses did occur the gas chromatograph provides information about the extent of the decomposition. The TCD, equipped with carboxen-1000 (2.0 m x 1/8 inch, stainless steel) packaging was used to analyze the gasses. Since the detector works on the gas stream's Thermal Conductivity Differences, argon was used as the carrier gas. Argon has a low thermal conductivity and is inert in nature, which eliminates contamination of the sample. The flow of argon is kept constant at 10 Psi. The preloaded 'method' used is an initial temperature hold at $35°C$ for 5 minutes. This is followed by a ramp up to the maximum temperature of $150°C$ at a rate of $20°C$ per minute. The oven is kept at this temperature for three additional minutes with the complete cycle duration lasting 13.75 minutes.

CHAPTER FOUR

4.0 Results and Discussion

4.1 TEM images of CNFs produced using CH_4

TEM experiments conducted to confirm the growth of CNTs or CNFs. The TEM images provided information on the structural (diameter and length) and morphological characteristics of the carbon products. Figure 4.1 shows a characteristic TEM image of a straight CNT produced at $650°C$ using lanthanum nickel alloy ($LaNi_5$) as catalyst. Figure 4.2 shows TEM micrographs of CNTs and CNFs produced at $650°C$ with $LaNi_5$ catalyst.

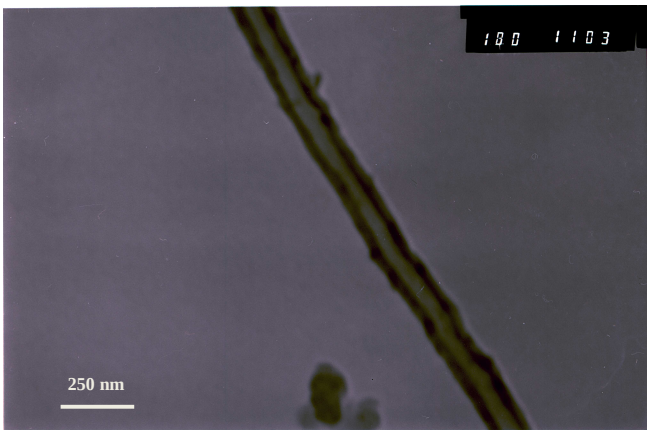
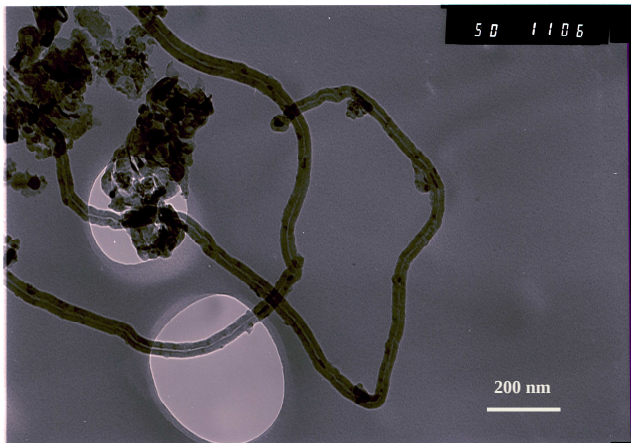
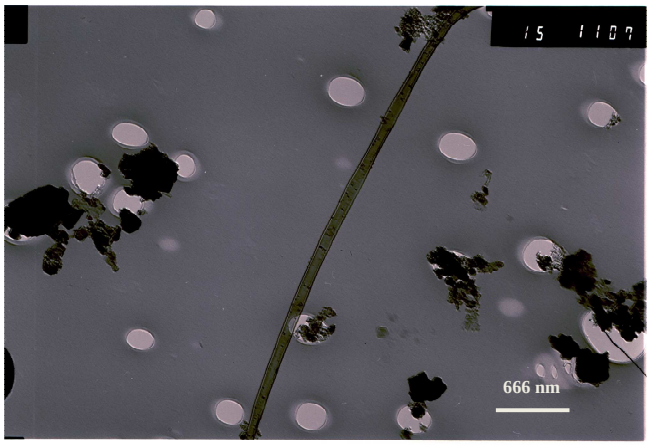


Figure 4.1: CNT produced at $650°C$ using $LaNi_5$

a)



b)



c)

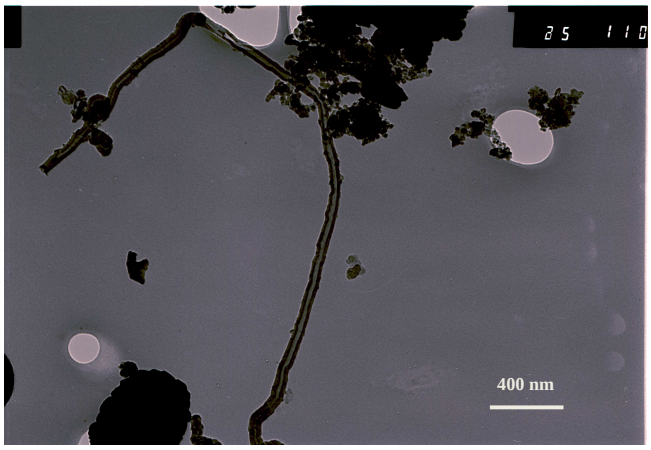


Figure 4.2: a) CNTs, b) a CNF and c) CNT produced at $650°C$ using $LaNi_5$

Figure 4.3 is a HMTEM image of a CNT produced at $650°C$ using $LaNi_5$. The outer diameter of this CNT is $60\ nm$. Figure 4.4 clearly shows the hollow core of a nanotube produced at $750°C$ using $LaNi_5$. This CNT is $\sim 3.5\ \mu m$ in length and most of it is uncontaminated by the catalyst.



Figure 4.3: HMTEM image of CNT produced at $650°C$ using $LaNi_5$

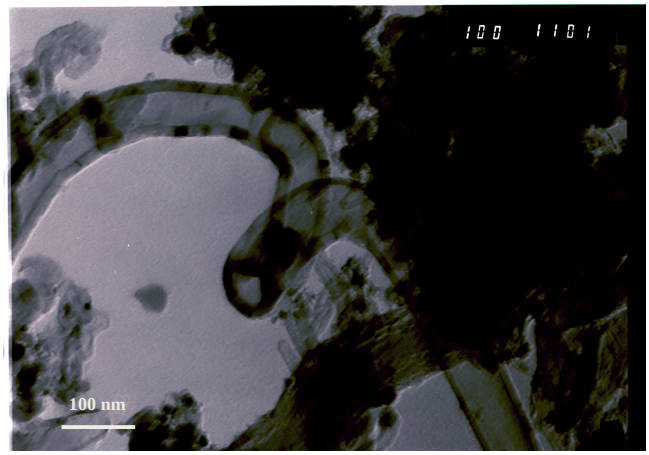


Figure 4.4: CNTs produced at $750°C$ using $LaNi_5$

The two CNTs depicted in Figure 4.5 show multiple wall structure of the nanotubes, with (a) having an inner diameter of $6.6\,nm$ and an outer diameter of $16.6\,nm$; (b) $10\,nm$ inner diameter and outer diameter of $23.2\,nm$. The concentric arrangement of the graphene sheets parallel to the tube axis, which is typical for a multi-walled tube structure, is confirmed in Figure 4.5. The CNTs shown in Figures 4.5 – 4.7 were produced at $750°C$ using $LaNi_5$.

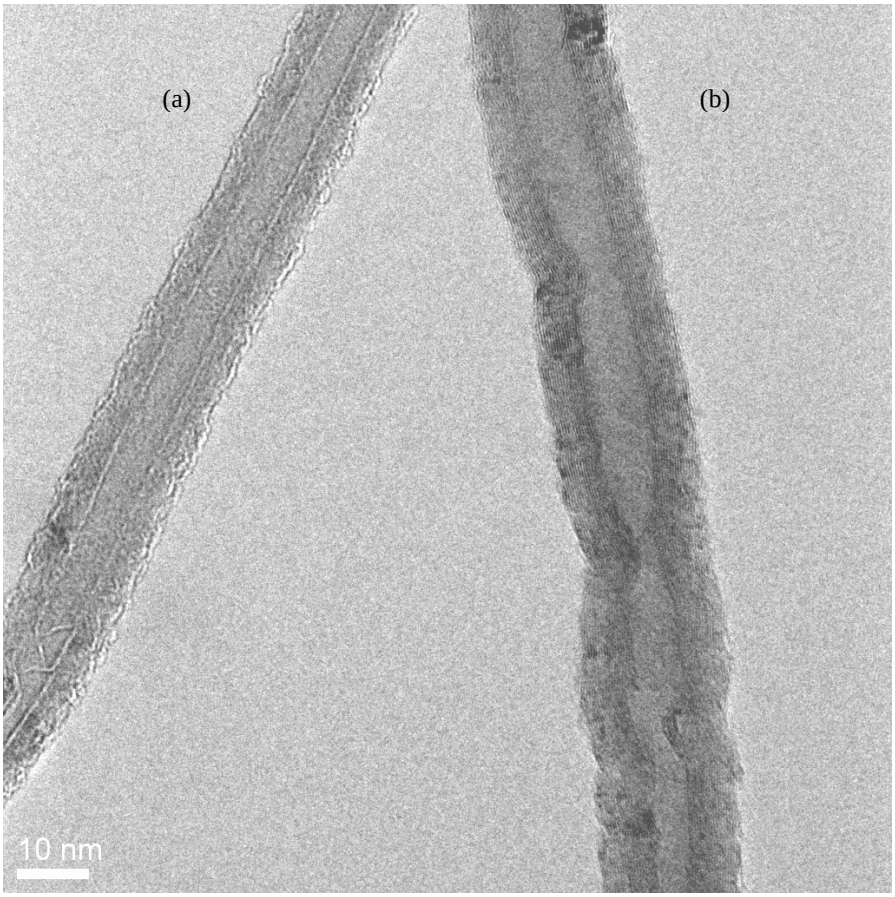


Figure 4.5: HMTEM image of the CNTs produced at $750°C$ using $LaNi_5$

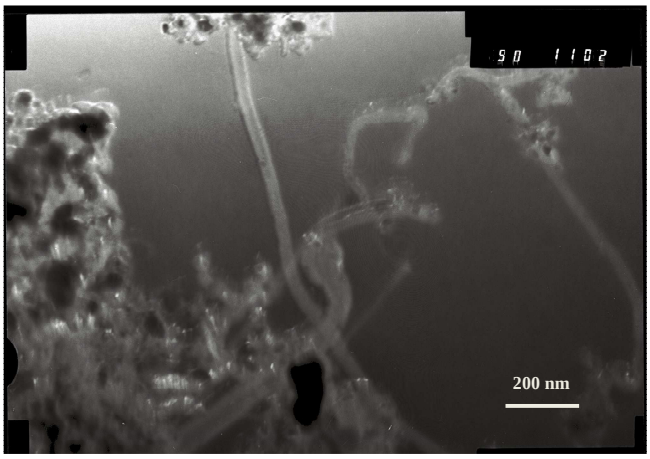


Figure 4.6: CNTs produced at $750°C$ using $LaNi_5$

HMTEM of the carbon nanostructures as shown in Figures 4.7 and 4.8 which indicate that multi-wall carbon nanotubes are produced at temperatures of $750°C$ and $850°C$, respectively. The CNT shown in Figure 4.7 has an outer diameter of $26.3\,nm$ and the CNT in Figure 4.8 has an outer diameter of $75.2\,nm$.

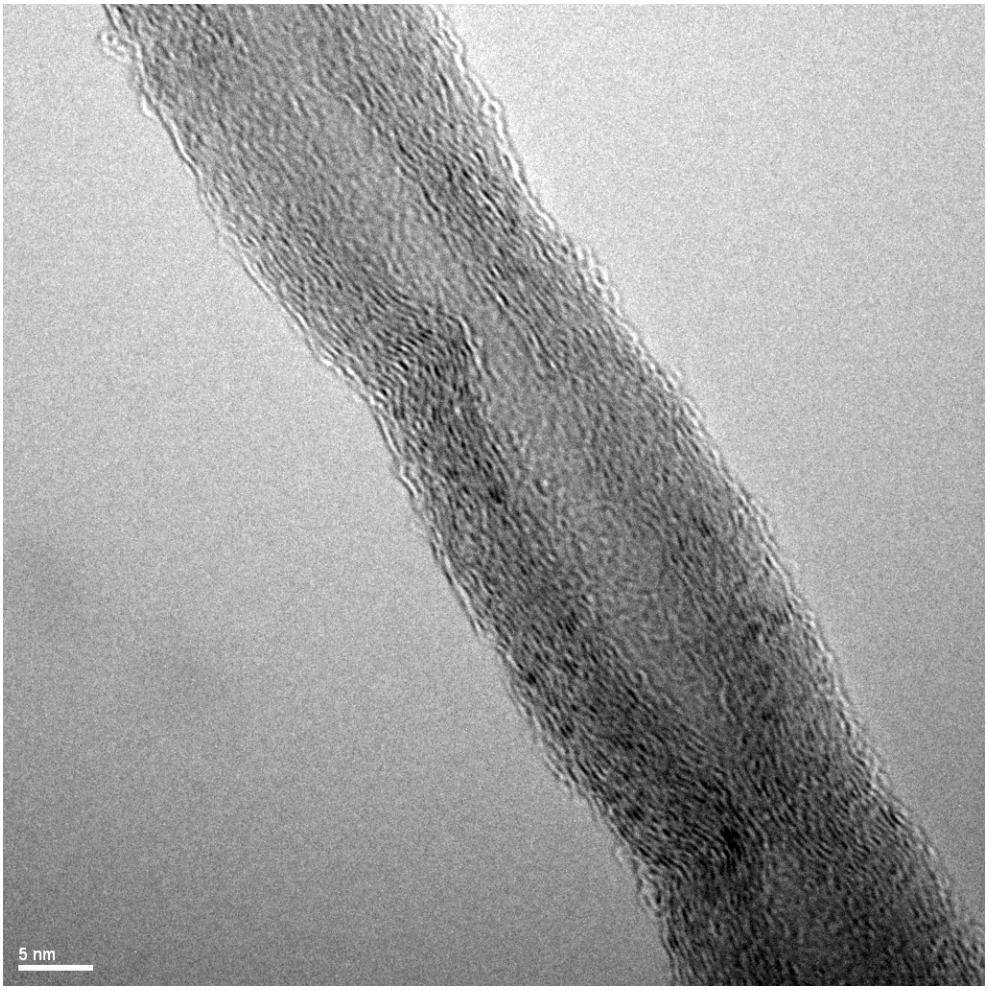


Figure 4.7: HMTEM image of a CNT produced at $750°C$ using $LaNi_5$

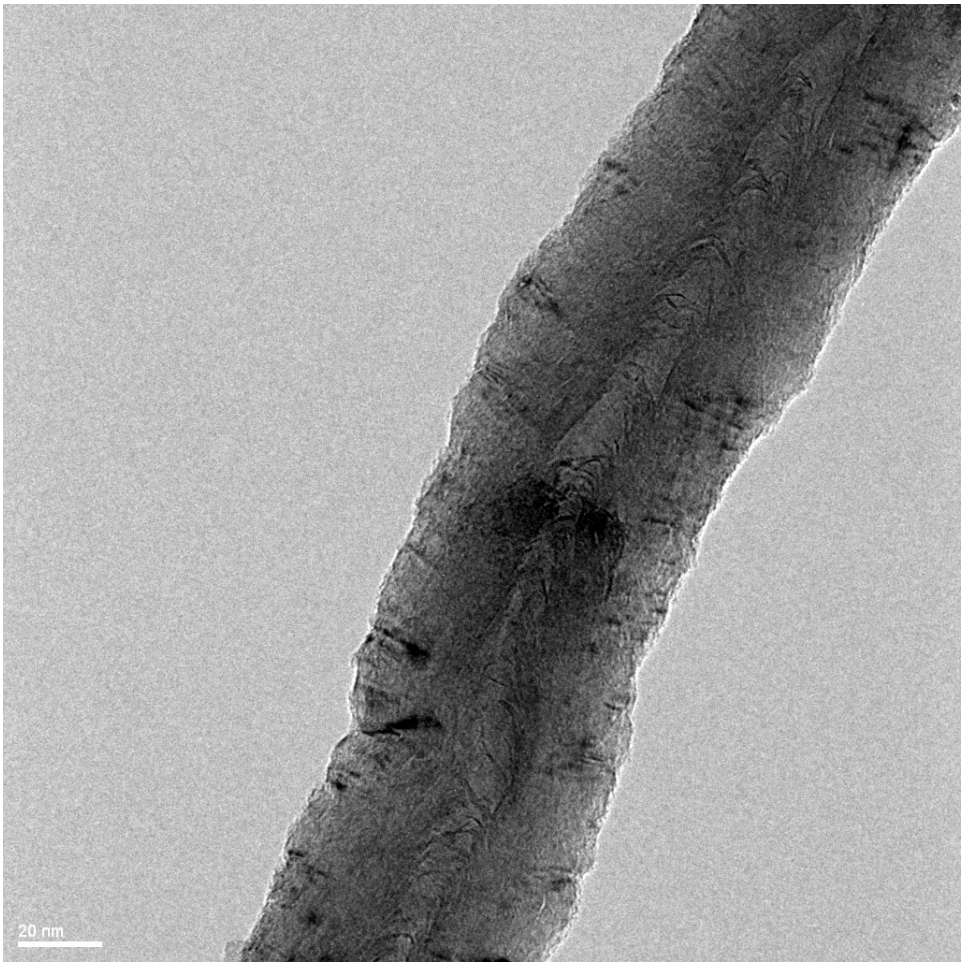


Figure 4.8: HMTEM image of a CNT produced at $850°C$ using $LaNi_5$

The synthesized CNTs ranged in length from several hundreds of nanometres to several microns across all the samples. Methane produces well-defined CNTs with a low content of amorphous carbon adhering to the external walls at all temperatures, which is in agreement with the documented literature (He *et al*., 2006; Gao *et al*., 2008; Chai *et al*., 2007). The most effective catalysts in the decomposition of methane to CNTs are Fe and Ni based (He *et al*., 2006; Zhao *et al*., 2007; Li *et al*., 2008). Due to this reason methane is easily decomposed by the nickel alloy ($LaNi_5$) catalyst at temperatures ranging from $650°C$ to $850°C$ (Inoue *et al*., 2008). Analysis by gas chromatography showed that there

is decomposition of CH_4 at $750°C$ to 13.65% H_2 and 28.02% other hydrocarbons that were not calibrated for (remainder 58.33% CH_4).

4.1.1 Raman Spectroscopy Analysis (using CH_4 only)

Raman spectra for the samples produced using methane and $LaNi_5$ are displayed in Figures 4.9 – 4.11. From Figures 4.9 – 4.11 it can be seen that the peaks correspond to those that signify the presence of CNTs. The first peak is between 1300 and 1400 cm^{-1} (D-band), the second is just before 1600 cm^{-1} (G-band) and the last around 2700 cm^{-1} (G'-band), which indicates the presence of CNTs.

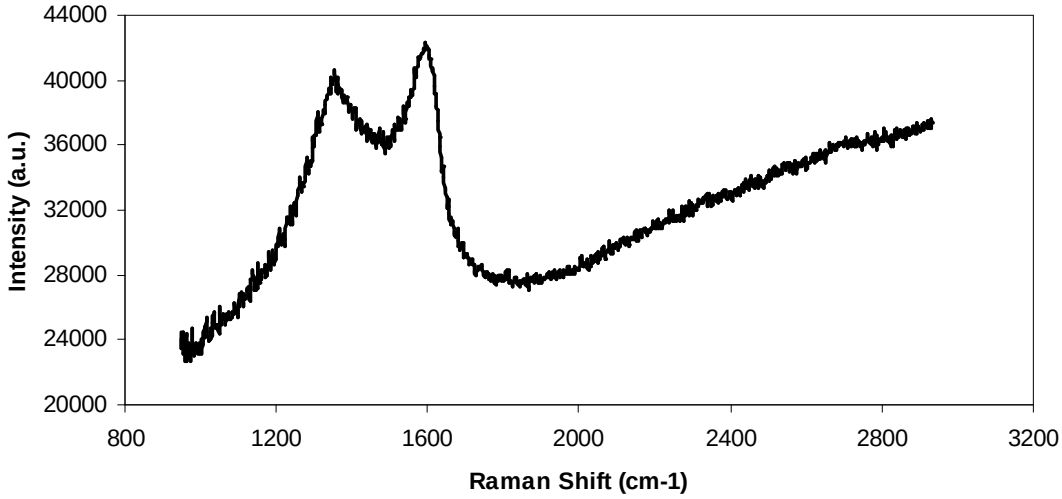


Figure 4.9: Raman spectrum of carbon produced using CH_4 at $650°C$, with the D-band at 1360 cm^{-1} and G-band at 1600 cm^{-1}

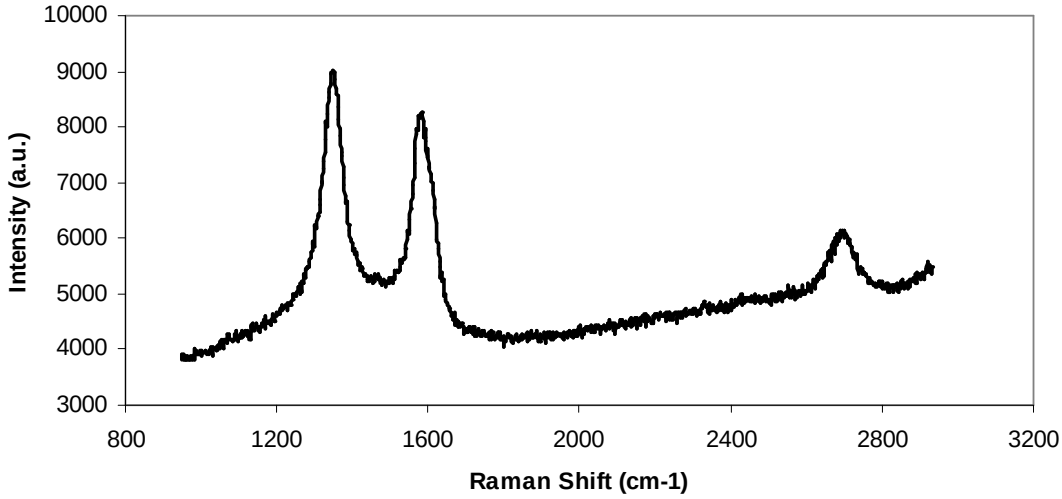


Figure 4.10: Raman spectrum of carbon produced using CH_4 at $750°C$, with the D-band at 1352 cm^{-1}, G-band at 1585 cm^{-1} and G'-band at 2701 cm^{-1}

The Raman spectra show that CNTs with essentially similar properties are produced at the temperatures of $650°C$, $750°C$ and $850°C$ using methane. This confirms the TEM images shown in Section 4.1. Most of the CNTs produced using $LaNi_5$ catalyst are not agglomerated and entangled with each other. Such CNTs are ideal for integration into devices i.e. CNT – based field effect transistors (FET) etc.

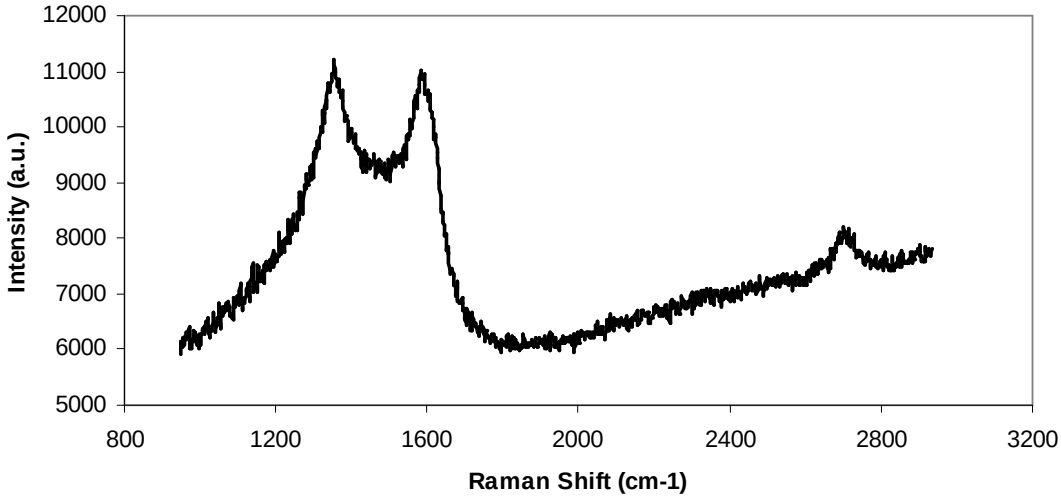


Figure 4.11: Raman spectrum of carbon produced using CH_4 at $850°C$, with the D-band at 1354 cm^{-1}, G-band at 1591 cm^{-1} and G'-band at 2714 cm^{-1}

Durrer *et al*. (2008) showed that SWCNTs might be grown for use in devices such as CNT sensors. The CNTs grown using CH_4 may have potential applications in electronics, thus ways to improve their crystalline quality and control their chirality need investigation.

4.2 TEM images of CNTs and CNFs produced using CO_2

Figure 4.12 shows that CNTs, helical and straight fibers with various diameters were synthesized at $650°C$ using $LaNi_5$ as a catalyst. Some of the CNTs and CNFs grow from the large catalyst particle also shown in the TEM image.

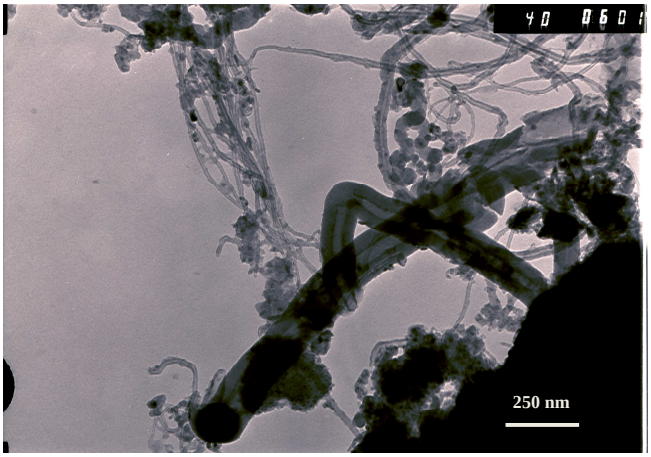


Figure 4.12: CNFs and CNTs produced at $650°C$ using lanthanum nickel alloy

CNFs and CNTs in Figure 4.13 are produced at $700°C$ using $LaNi_5$ and appear to overlap each other. The longest of the fibres in the TEM image is $\sim 2.3\,\mu m$. Metal catalyst particles are visible in the image including carbon structures such as amorphous carbon and graphitic particles.

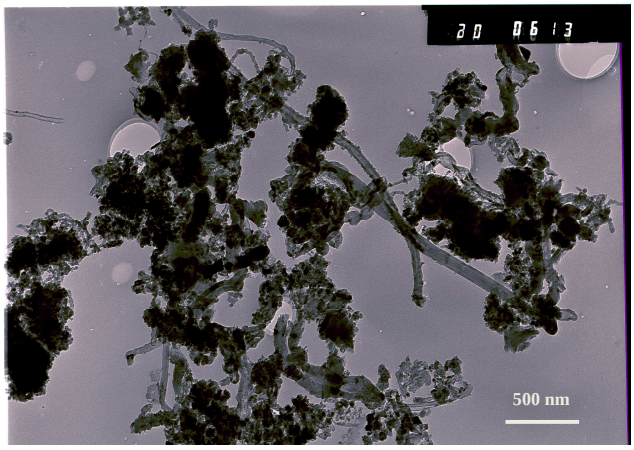
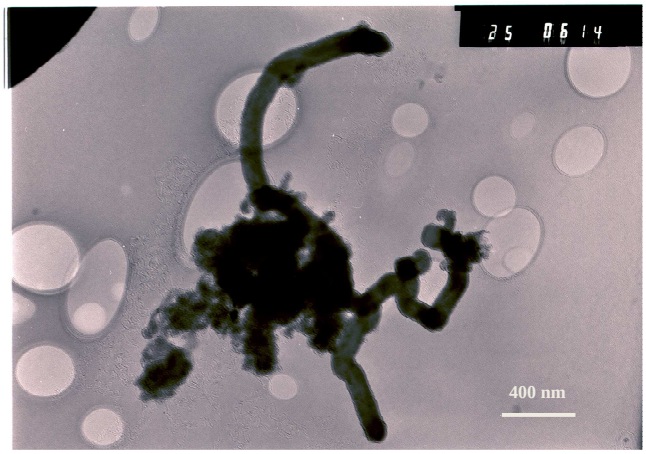


Figure 4.13: CNTs and CNFs produced at $700°C$ using lanthanum nickel alloy

a)



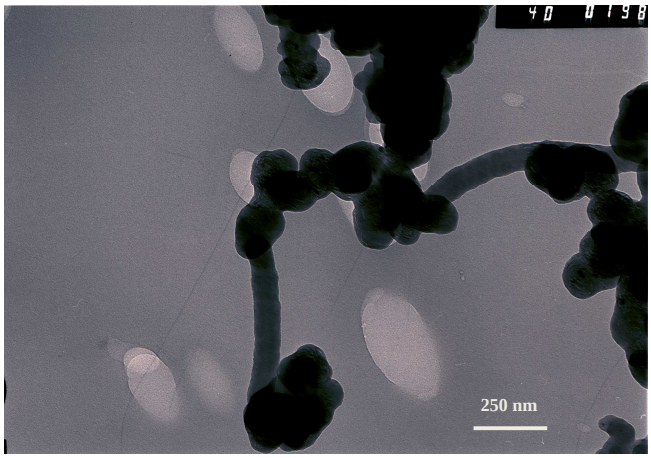
b)



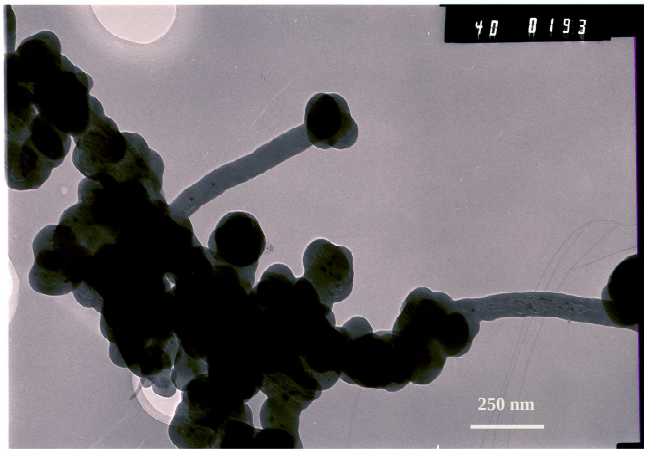
Figure 4.14: a) CNFs and b) possible CNT produced at $700°C$ using lanthanum nickel catalyst

At $750°C$ CNFs are produced using the $LaNi_5$ catalyst, as shown in Figures 4.15. Figure 4.15 (a) and (b) shows the catalyst particles that catalyses nanofiber growth are attached on the ends of the nanofibers. The diameter of the vertical nanofiber in Figure 4.15 (a) is $\sim 72.5\, nm$.

a)



b)



c)

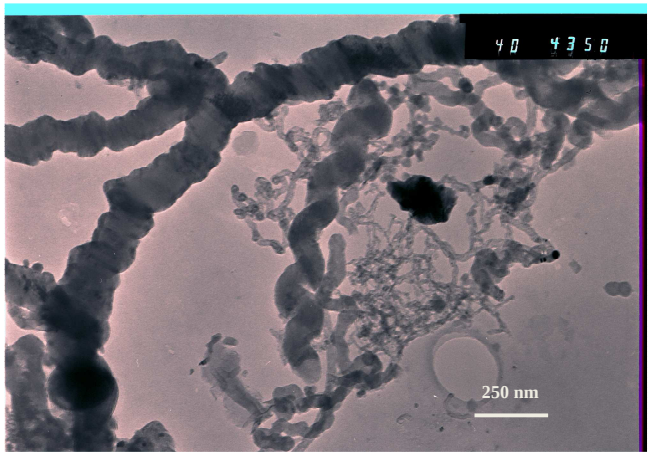


Figure 4.15: a) CNFs, b) CNFs (attached to catalyst particles) and c) a twisty CNF produced at $750°C$ using lanthanum nickel alloy

In Figure 4.16 the CNF has a diameter of $\sim 217.5\,nm$ and does not appear to have any catalyst particles embedded inside its structure.

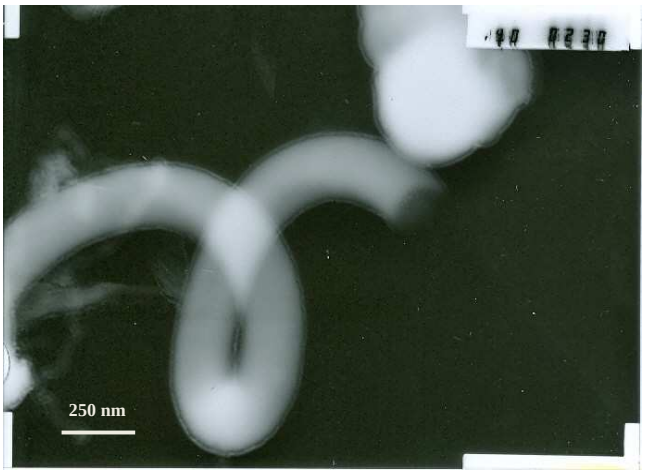
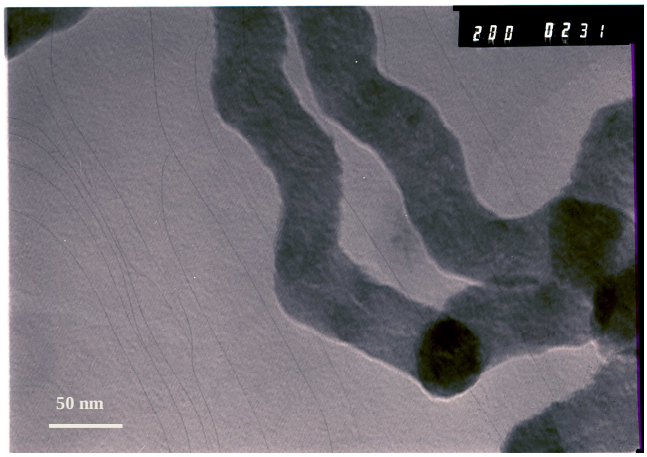


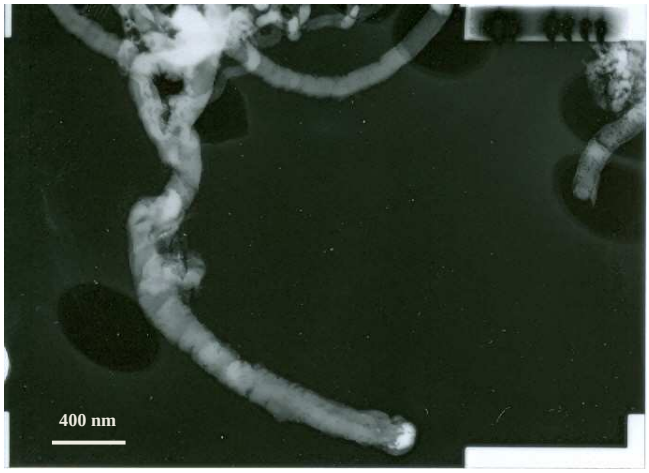
Figure 4.16: CNF produced at $850°C$ using lanthanum nickel alloy

The CNFs in Figure 4.17 are produced at $850°C$ using $LaNi_5$. It is widely believed that there is a correlation between catalyst particle size and CNF diameter (Cheung *et al.*, 2002). Figure 4.17 (a) displays the catalyst particle at the tip of the nanofiber indicating that the as-grown CNF has the same diameter as the catalyst particle.

a)



b)



c)

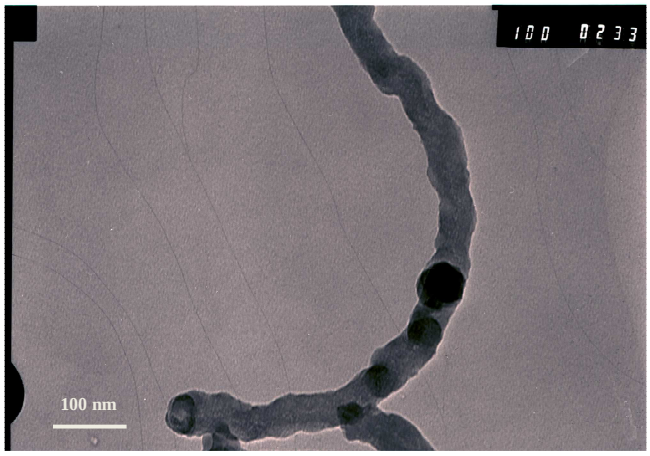
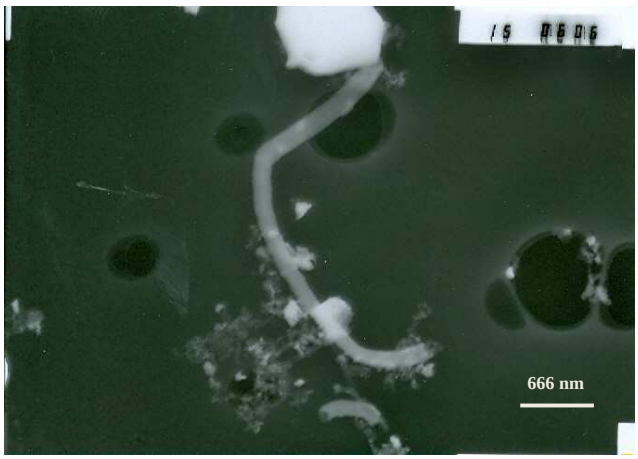


Figure 4.17: a) CNF on the nickel catalyst, b) CNFs, c) CNF produced at 850°*C* using lanthanum nickel catalyst

Figure 4.18 displays CNFs produced at $800°C$ using a mischmetal nickel alloy as the catalyst. In Figure 4.18 (a) the nanofibers are relatively free of any catalyst particles in their structure, with the longest nanofiber $\sim 3.6\ \mu m$ long.

a) 

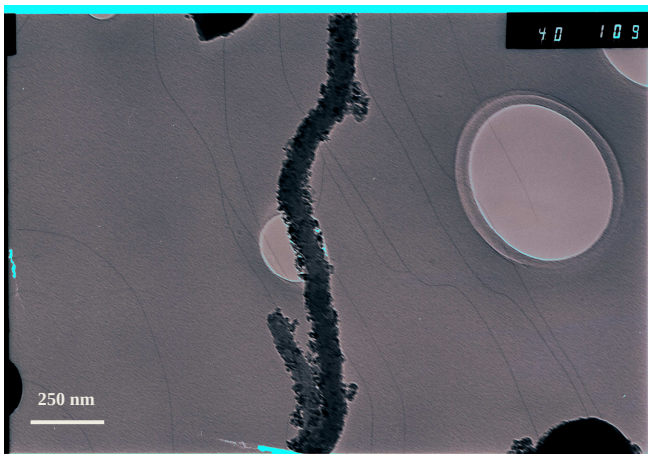
b) 

Figure 4.18: a) CNFs and b) hollow CNF produced at $800°C$ using mischmetal nickel catalyst

CNFs produced at $750°C$ using platinum and alumina powder catalyst is shown in Figure 4.19. Figure 4.19 (a) shows a CNF $\sim 1.44\ \mu m$ in length that does not have any

catalyst particles inside it or at its ends. Figure 19 (b) shows that CNTs may also be formed at these conditions.

a)



b)

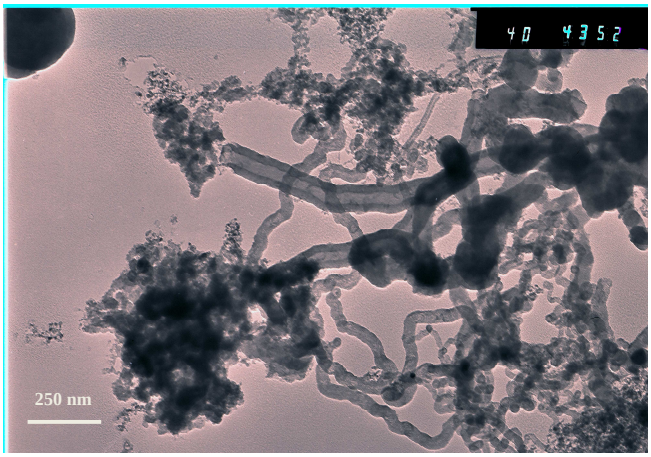


Figure 4.19: a) CNF and b) CNFs and CNTs produced at $750°C$ using 1% Pt on alumina powder

From Figure 4.12 to Figure 4.19 it is easily seen that CNFs are produced using CO_2 at temperatures ranging from $650°C$ to $850°C$. At $650°C$ and $700°C$ there are CNTs being produced (Figures 4.12 – 4.14). This means that at relatively low temperatures it is possible to produce CNTs using only CO_2. The CNFs become more distinct and longer as

the temperature increases (greater degree of graphitisation) as can be seen at $800°C$ and $850°C$ (Figures 4.16 – 4.18). The TEM micrographs indicate that the CNFs produced by CO_2 have an array of varying lengths and diameters. In some of the TEM images, the catalyst particles on which the CNTs and CNFs were grown were observed; showing the catalytic nature of this process. The reaction temperature played a crucial role in the synthesis process of CNTs and CNFs, which is in agreement with literature (Xu and Huang, 2007).

The breakdown of CO_2 may be attributed to the type of catalysts used. The $LaNi_5$ catalyst contains lanthanum, a rare earth metal with the property of being able to decompose CO_2 into CO, C and O_2. Gas Chromatography analysis showed that CO_2 is decomposed during the experiment at $650°C$ using $LaNi_5$ to the extent of 5.33% O_2 and 2.02 % CO (remainder 92.65% CO_2). Mischmetal, an inter-metallic alloy composed of rare earth metals which is produced by fused chloride electrolysis of the light lanthanide elements i.e. from lanthanum to lutetium together with scandium and yttrium (Lannou *et al*., 2003) allows it to also decompose CO_2. CO_2 is more chemically stable than gaseous hydrocarbons at high temperature, so it is difficult to be activated or decomposed to CNTs and CNFs (Lou *et al*., 2003). The $LaNi_5$ and mischmetal nickel catalyst have shown that although decomposition of CO_2 is difficult it is still possible at the relatively low temperatures of $650°C$, $750°C$ and $850°C$.

4.2.1 Raman Spectroscopy Analysis (using CO_2 only)

The Raman spectra for the samples are displayed in Figures 4.20 – 4.26. Figures 4.20 and 4.21 are of samples produced using $LaNi_5$ at $650°C$ and $700°C$, respectively.

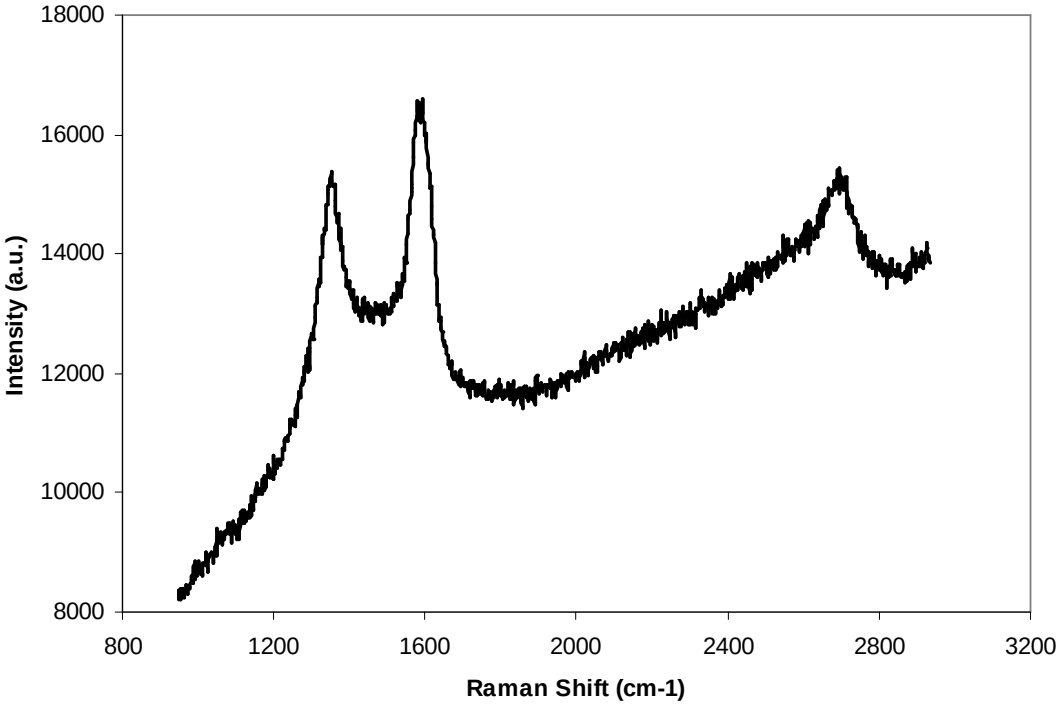


Figure 4.20: Raman spectrum of carbon produced using CO_2 at $650°C$, with the D-band at 1352 cm^{-1}, G-band at 1593 cm^{-1} and G'-band at 2710 cm^{-1}

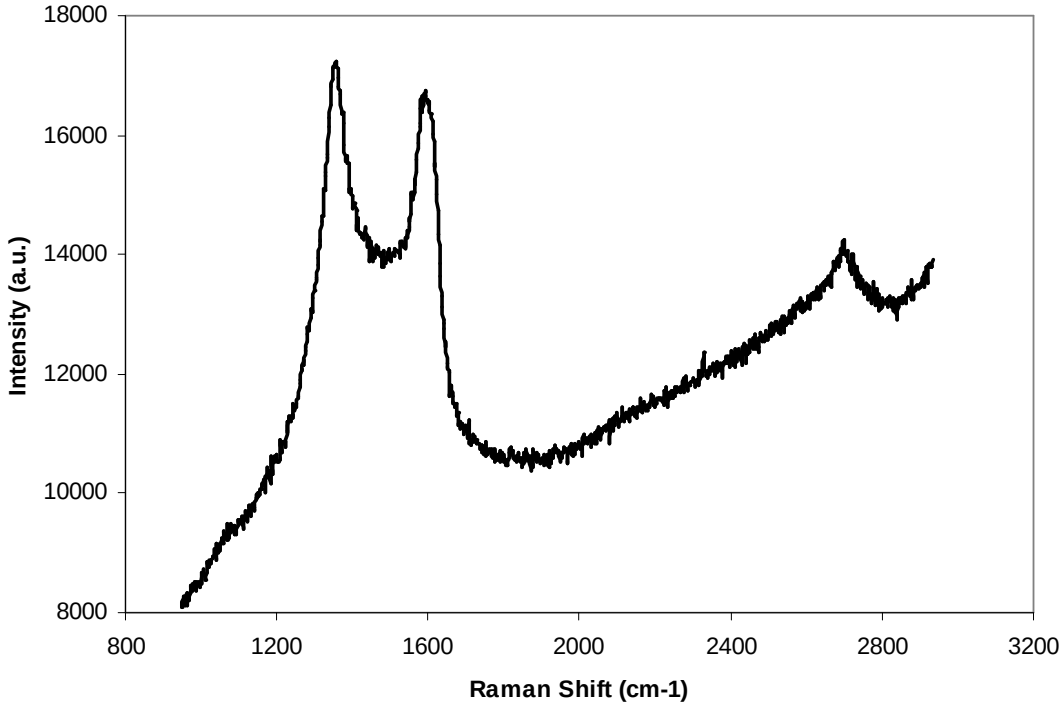


Figure 4.21: Raman spectrum of carbon produced using CO_2 at $700°C$, with the D-band at 1360 cm^{-1}, G-band at 1603 cm^{-1} and G'-band at 2698 cm^{-1}

Studies have shown CNTs produced using lanthanum nickel alloy as catalyst are good hydrogen storage materials (Yi *et al*., 2006; Zhang *et al*., 2004). The CNTs shown in Section 4.2 produced using CO_2 and $LaNi_5$ may also have such properties, and accordingly exploration into this aspect may yield similar results.

Figures 4.22 and 4.23 shows samples produced using $LaNi_5$ at 750°*C* and 850°*C*, respectively.

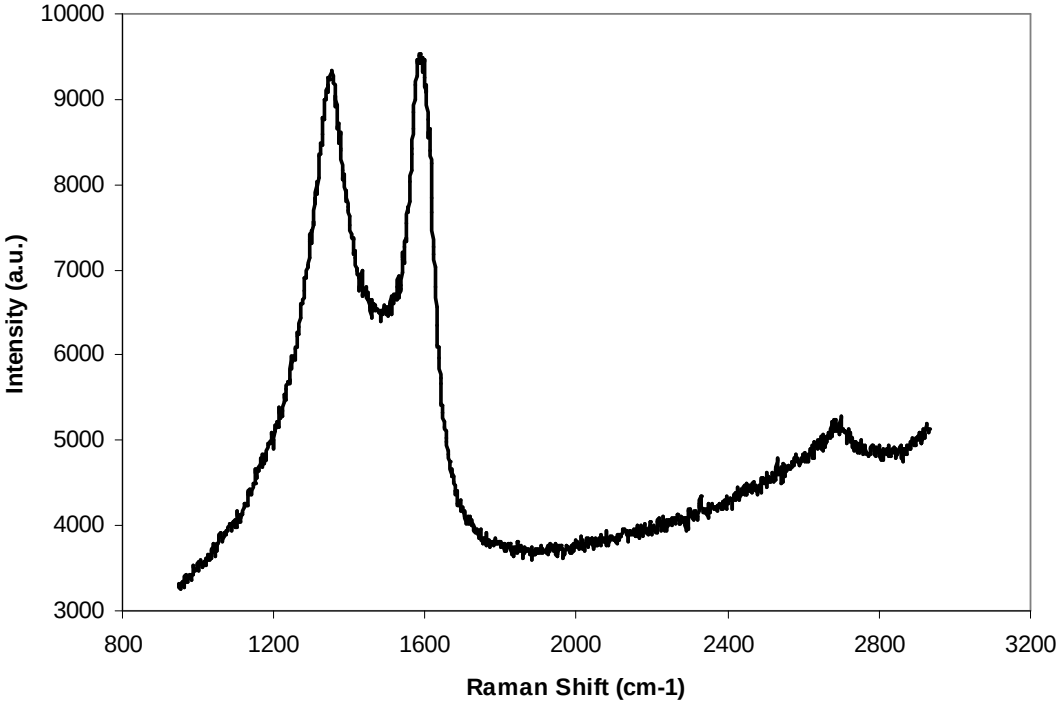


Figure 4.22: Raman spectrum of carbon produced using CO_2 at 750°*C*, with the D-band at 1356 cm^{-1}, G-band at 1591 cm^{-1} and G'-band at 2701 cm^{-1}

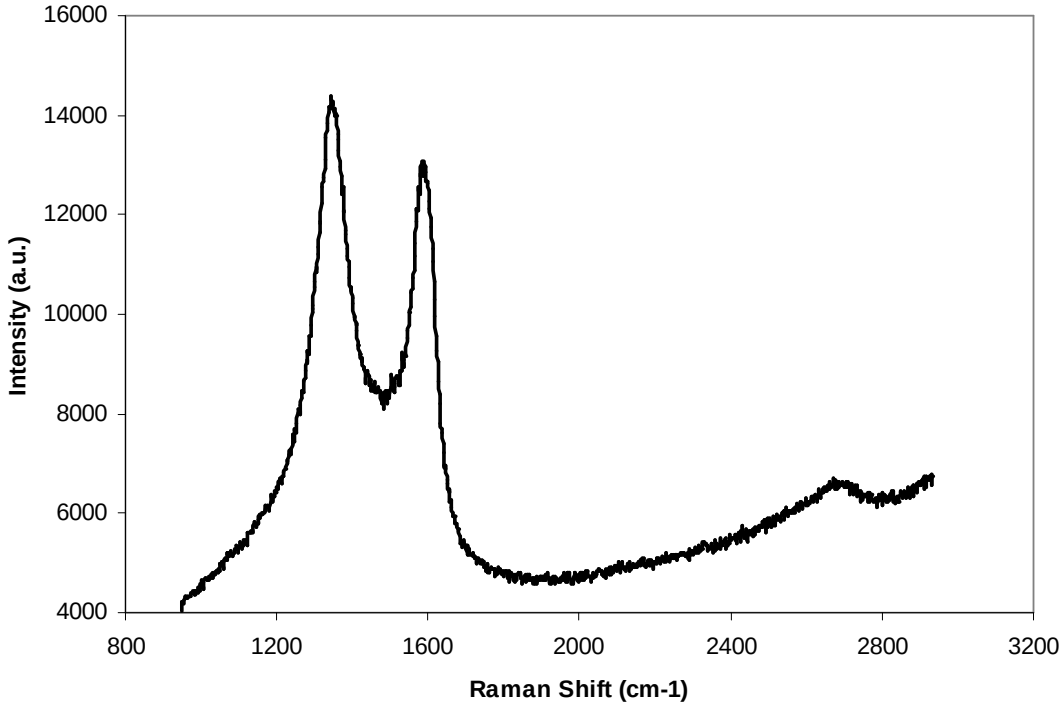


Figure 4.23: Raman spectrum of carbon produced using CO_2 at $850°C$, with the D-band at 1350 cm^{-1}, G-band at 1591 cm^{-1} and G'-band at 2685 cm^{-1}

The peaks around 1600cm^{-1}, G-band (Figures 4.20 – 4.23) corresponds to an E_{2g} mode of graphite and is related to the vibration of sp^2 – bonded carbon atoms in a two-dimensional hexagonal lattice, such as in a graphitic layer (Tuinstra and Koenig, 1970). Nanotubes with concentric multi-walled layers of hexagonal carbon lattice display the same vibration (Kasuya *et al.*, 1997). The D-band, in the region of 1350 cm^{-1}, is associated with the presence of defects in the hexagonal graphitic layers (Lou *et al.*, 2003). This means that the $LaNi_5$ catalyst is capable of producing CNFs and MWCNTs (with some defects in their structure) using CO_2.

Figure 4.24 is of a sample produced using mischmetal nickel alloy at 800°*C*. The intensity of the D-band was bigger than the G-band intensity, which indicated that there were defects in the structure of the CNTs.

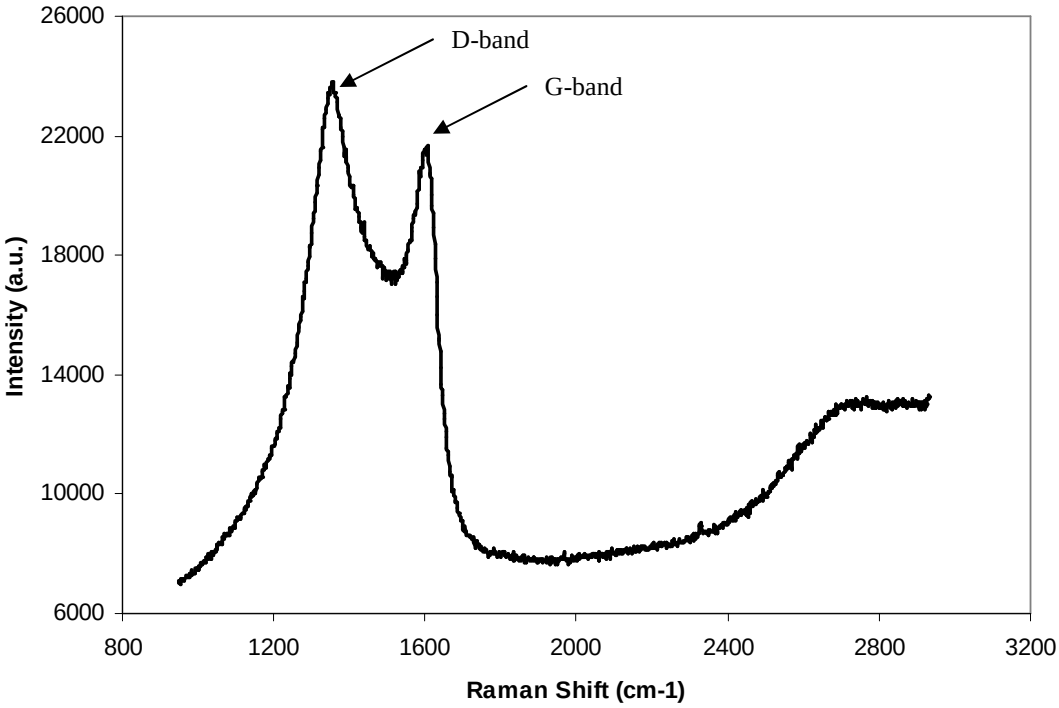


Figure 4.24: Raman spectrum of carbon produced using CO_2 at 800°*C*

Figures 4.25 shows a sample produced using a catalyst of 1% Pt on Alumina powder at 750°*C*. From Figure 4.19 it is seen that CNTs may have been formed at these conditions but this reaction is catalyzed by a noble metal, platinum. Consequently, the high cost involved in using such a catalyst may negate any economic advantage gained by using a greenhouse gas (CO_2).

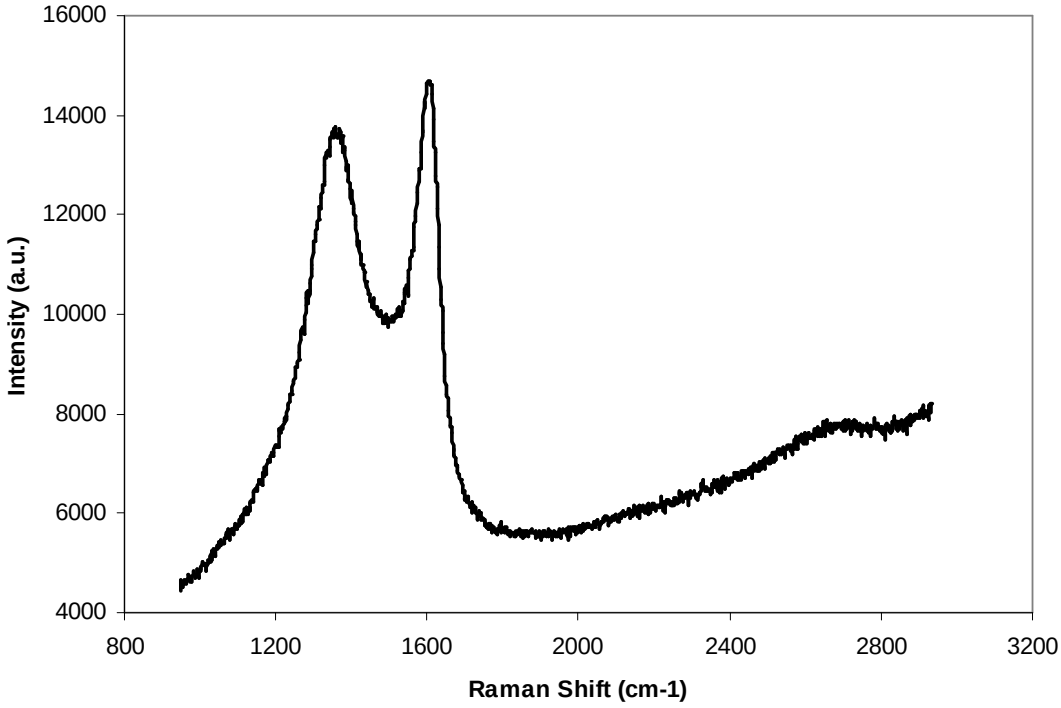


Figure 4.25: Raman spectrum of carbon produced using CO_2 at $750°C$

The Raman spectra show that CNTs and CNFs are produced during the experiments using CO_2 only. However, the CNTs were few and far between as they were not easily characterised as such using the TEM.

Figure 4.26 shows the Raman spectra of the catalyst particles tested after the reaction.

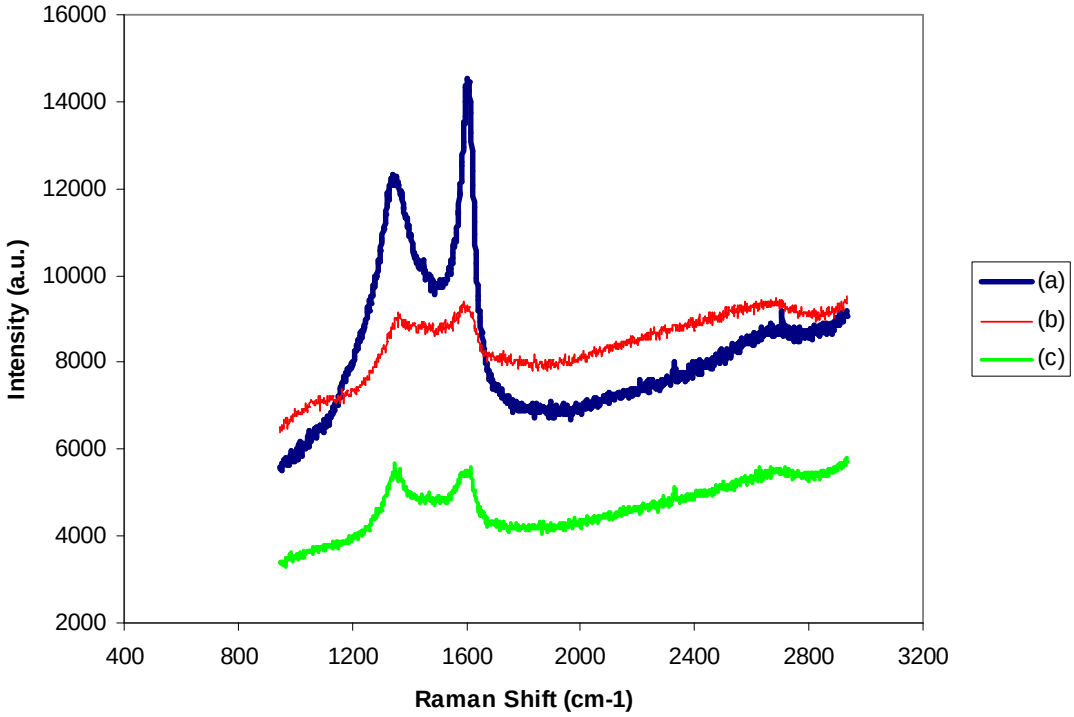


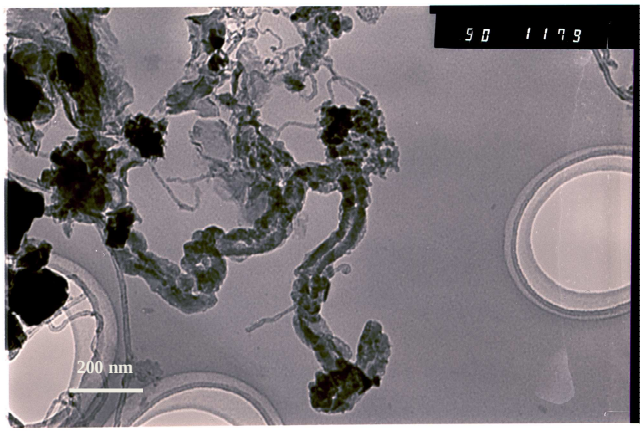
Figure 4.26: Raman spectra of catalyst particles after the reaction using CO_2 a) $LaNi_5$ at $650°C$, b) $LaNi_5$ at $700°C$ and c) mischmetal nickel alloy at $800°C$

The high intensity D-band peaks (1350 – 1400 cm^{-1}) in Figure 4.26 indicates that there is an amount of disordered carbon (CNFs or CNTs) deposited on the metallic catalyst particles.

4.3 TEM images obtained when dry reforming of CH_4 has taken place

Figures 4.27 and 4.28 show that CNTs have been formed when dry reforming of CH_4 takes place at 750°*C* and the catalysts used are $LaNi_5$ and mischmetal nickel alloy, respectively. The CNTs produced using the mischmetal nickel alloy has a better wall structure than the ones formed with the lanthanum nickel alloy.

a)



b)

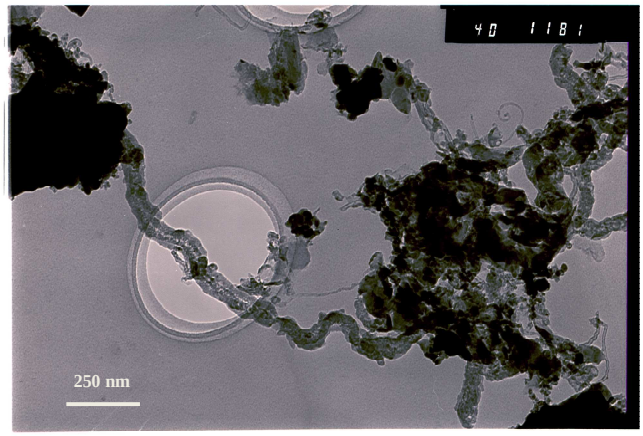
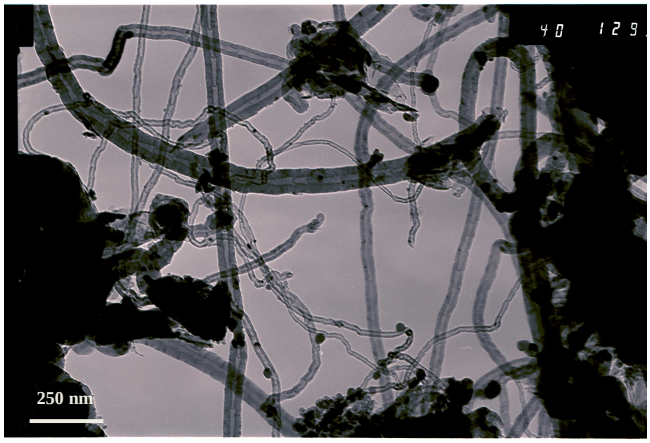


Figure 4.27: a) CNTs and b) disordered CNTs produced at 750°*C* during dry reforming using $LaNi_5$

a)



b)



c)

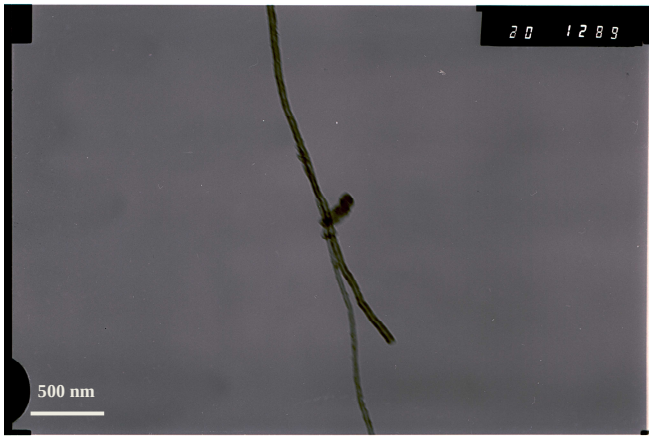
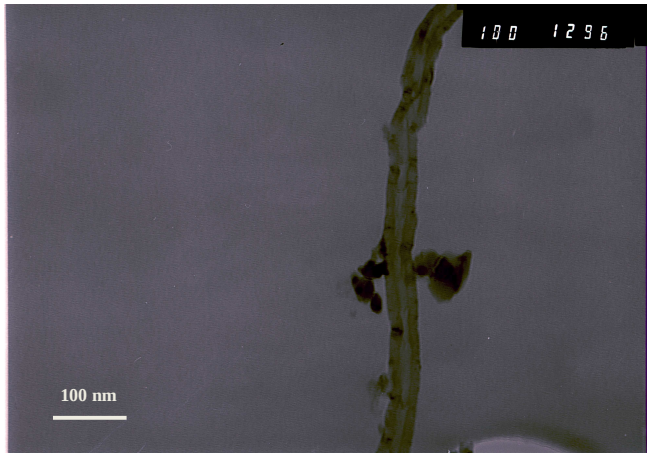


Figure 4.28: a) Network of CNTs, b) CNTs and c) CNT produced at $750°C$ during dry reforming using mischmetal nickel alloy

Figure 4.29 show CNTs produced at $850°C$ using the mischmetal nickel alloy catalyst. Some of the catalyst particles lose their circular shape before the completion of CNT growth (Figure 4.29 (b)).

a)



b)

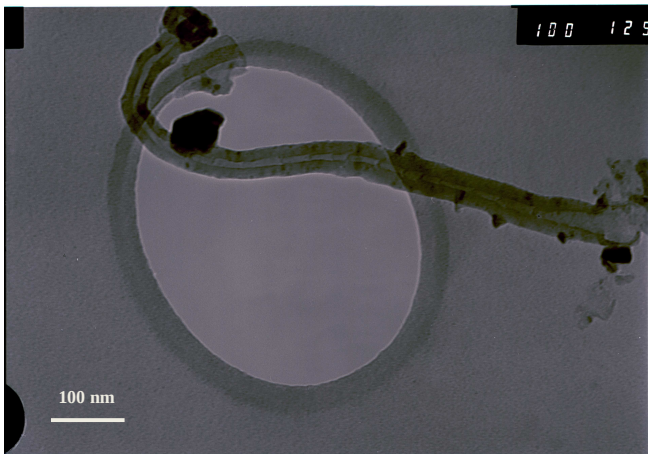


Figure 4.29: a) CNT produced at $850°C$ during dry reforming using mischmetal nickel alloy and b) CNT not fully formed

Figure 4.30 shows filamentous carbon and amorphous carbon produced at $850°C$ using the mischmetal nickel alloy catalyst.

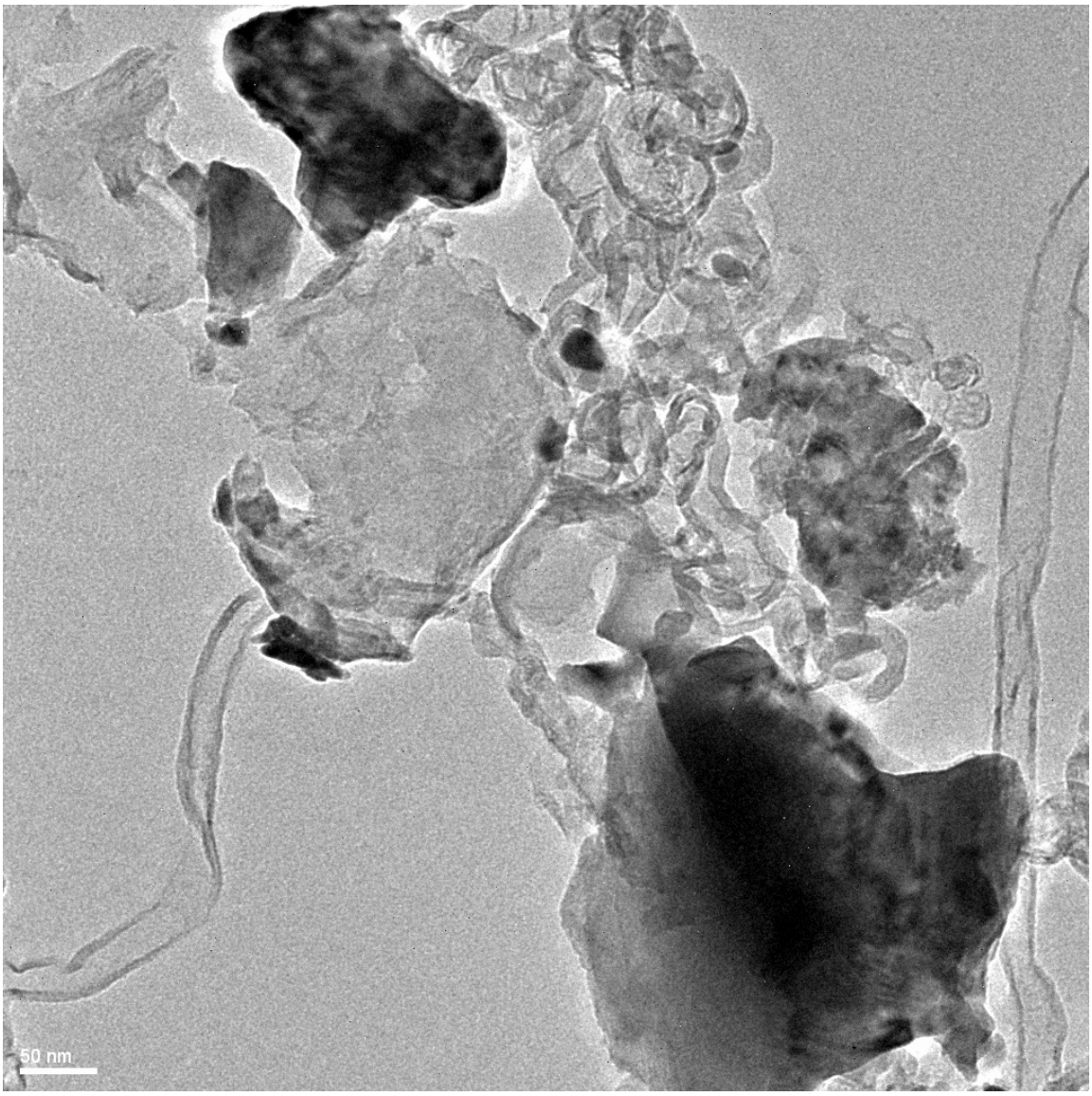


Figure 4.30: HMTEM image of the catalyst particle (dark spot) and the carbon nanostructures (grey)

At 950°*C*, using the mischmetal nickel alloy catalyst very few CNTs are formed as displayed in Figure 4.31.

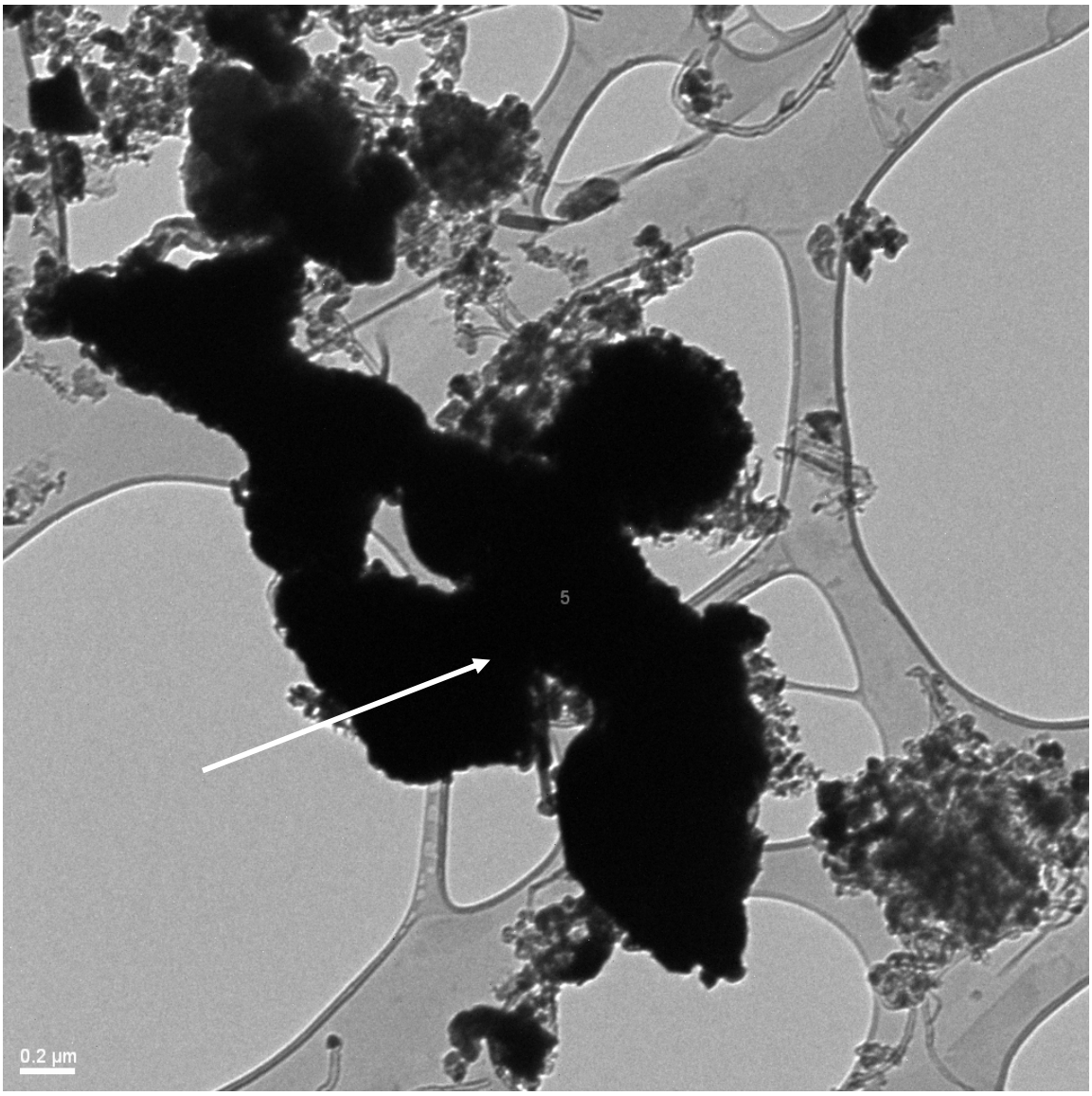


Figure 4.31: HMTEM image showing few CNTs are produced at 950°*C*

During the reforming of CH_4 with CO_2 it is shown that CNTs and CNFs are produced at 750°*C* but these carbon species become less defined at 850°*C* (Figure 4.30) and they

are almost non-existent at 950°*C* (Figure 4.31). From the TEM images it seems that hydrogen does play a role in the selection of the carbon species that is produced. When using CO_2 alone to produce CNFs it is possible to produce CNTs at relatively lower temperatures but they are not as clearly defined as those that are produced with CH_4. At higher temperatures it is only possible to produce CNTs when hydrogen is involved in any form. This proposal agrees with the conclusions drawn by Mendoza *et al*. (2006) that hydrogen may inhibit the production of other kinds of carbonaceous material and enhance the growth of crystalline nanotubes. The differences in appearances of the CNTs and CNFs (produced using CO_2 only, CH_4 only and CH_4/CO_2 reforming) can be attributed to the size, crystal imperfections and structures of the various catalyst particles.

To analyze which elements are contained on the dark part (indicated by arrow) in Figure 4.31, energy dispersive X-ray spectroscopy (EDS) was used. EDS is a technique for elemental analysis, where the radiated X-ray beam emitted from a specific material is collected after the incident electron beam is focused on it. Since each element of the periodic table has a unique atomic structure, the characteristic X-rays from each element are uniquely distinguished from others. Generally, the incident beam excites an electron in the inner shell of an element leaving a hole in the shell, which is followed by the hole filling with an electron from outer shell. The difference in energy between the electronic orbitals is released in the form of an X-ray photon. The X-rays emitted by the sample are then detected and analyzed by the energy dispersive spectrometer (Heo, 2008). Figure 4.32 shows the EDS spectra that is obtained.

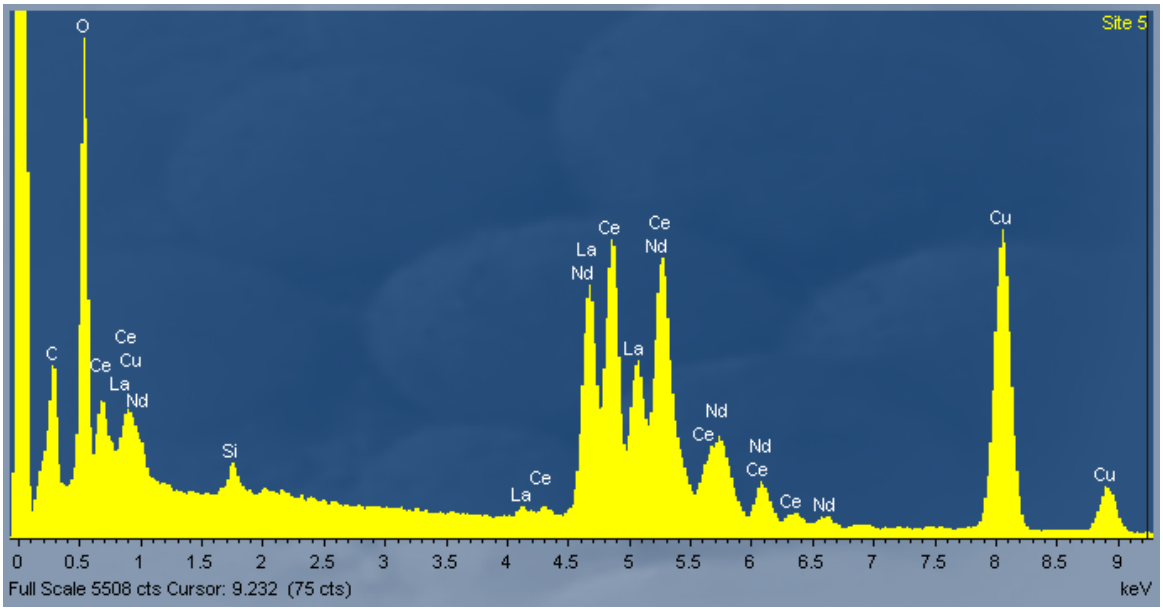


Figure 4.32: Composition of catalyst particle after dry reforming of CH_4

Figure 4.32 reveals that some carbon is deposited on the surface of the catalyst particles but it is a very small amount. This means that at high temperatures the lanthanum nickel alloy and to a greater extent the mischmetal nickel alloy do not coke as readily as some catalysts conventionally used. Thus, these catalysts could prove effective to achieve stable operation for CO_2 reforming of CH_4. The Cu peaks arise from the Cu grid used, and also shown are the key constituents of the mischmetal nickel alloy i.e. Ce, La and Nd. The stability of the $LaNi_5$ correlates with other studies done on lanthanum containing catalysts used in dry reforming (Blom *et al.*, 1994; Martinez *et al.*, 2004).

4.3.1 Raman Spectroscopy Analysis (using CO_2/CH_4 reforming)

The Raman spectra for the samples produced using $LaNi_5$ at 750°*C* and 850°*C* during the dry reforming of CH_4 are shown in Figures 4.33 and 4.34, respectively.

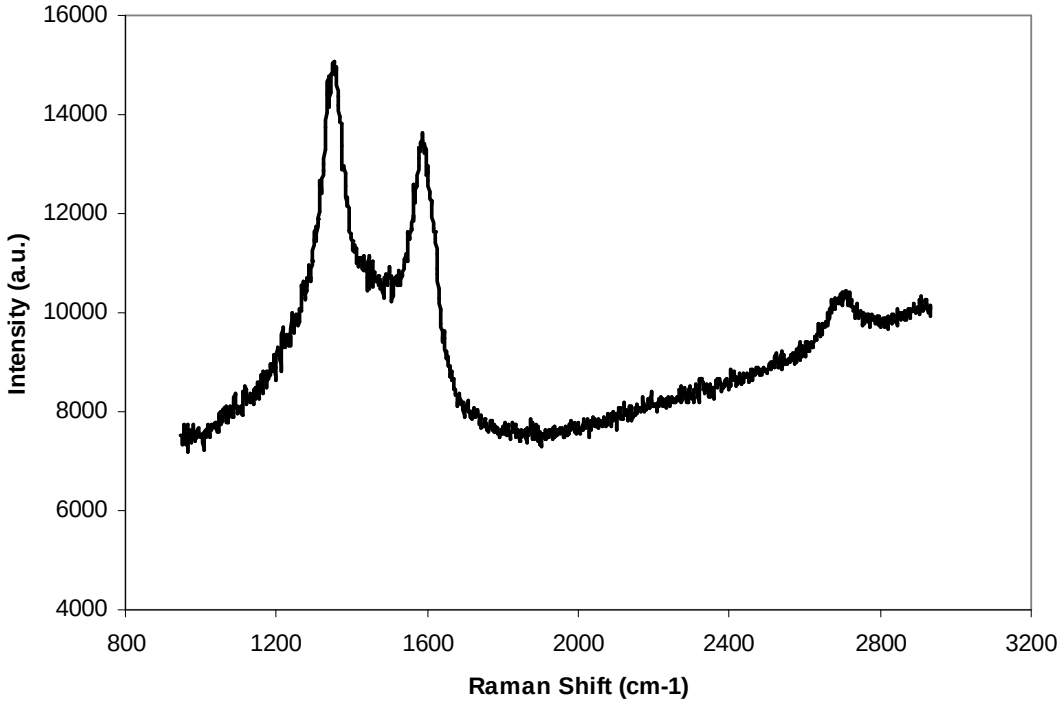


Figure 4.33: Raman spectrum of CNTs produced at 750°*C* during CO_2 reforming of CH_4, with the D-band at 1358 cm^{-1}, G-band at 1593 cm^{-1} and G'-band at 2710 cm^{-1}

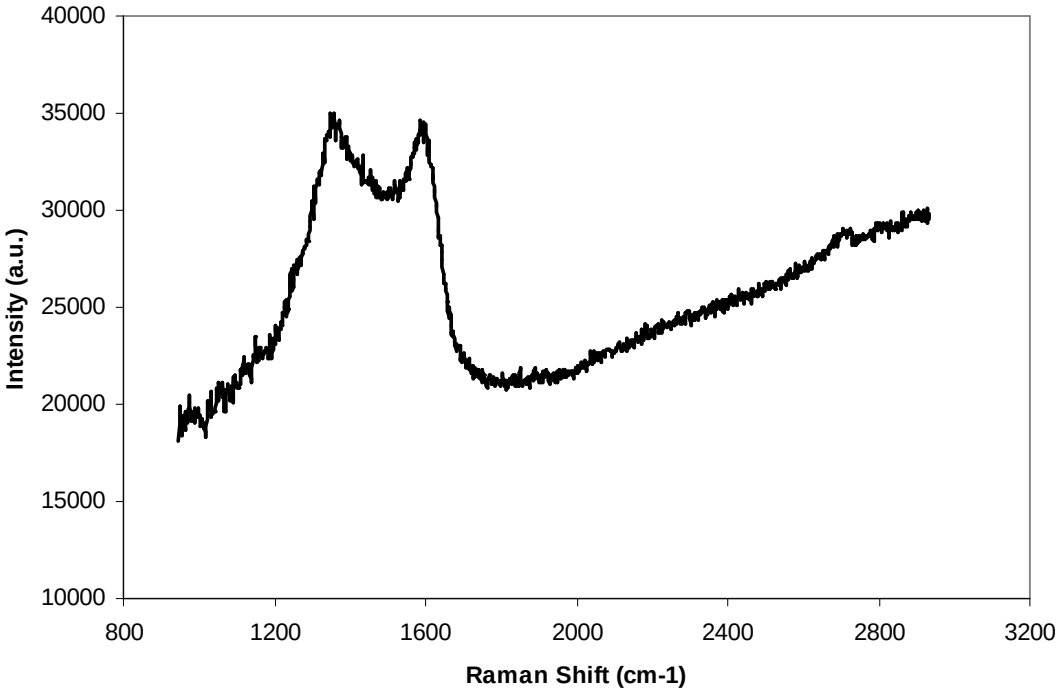


Figure 4.34: Raman spectrum of CNTs produced at 850°*C* during CO_2 reforming of CH_4, with the D-band at 1360 cm^{-1} and G-band at 1601 cm^{-1}

Figures 4.35 and 4.36 show the Raman spectra of the samples produced using mischmetal nickel alloy catalyst at $750°C$ and $850°C$, respectively.

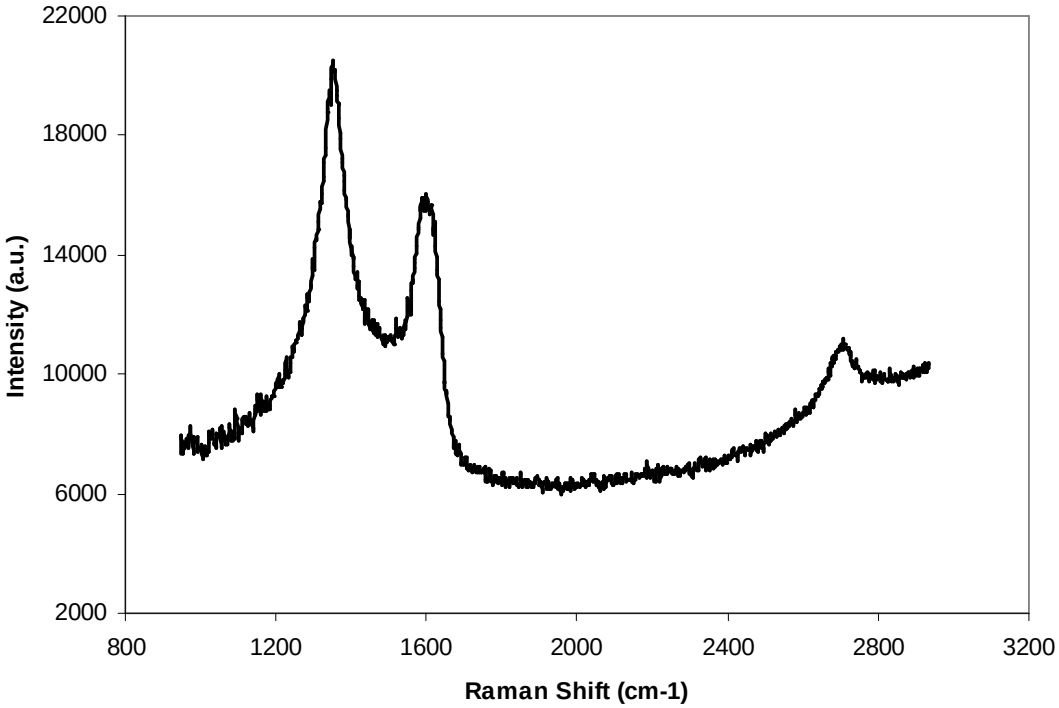


Figure 4.35: Raman spectrum of CNTs produced at $750°C$ during CO_2 reforming of CH_4, with the D-band at 1358 cm^{-1}, G-band at 1599 cm^{-1} and G'-band at 2710 cm^{-1}

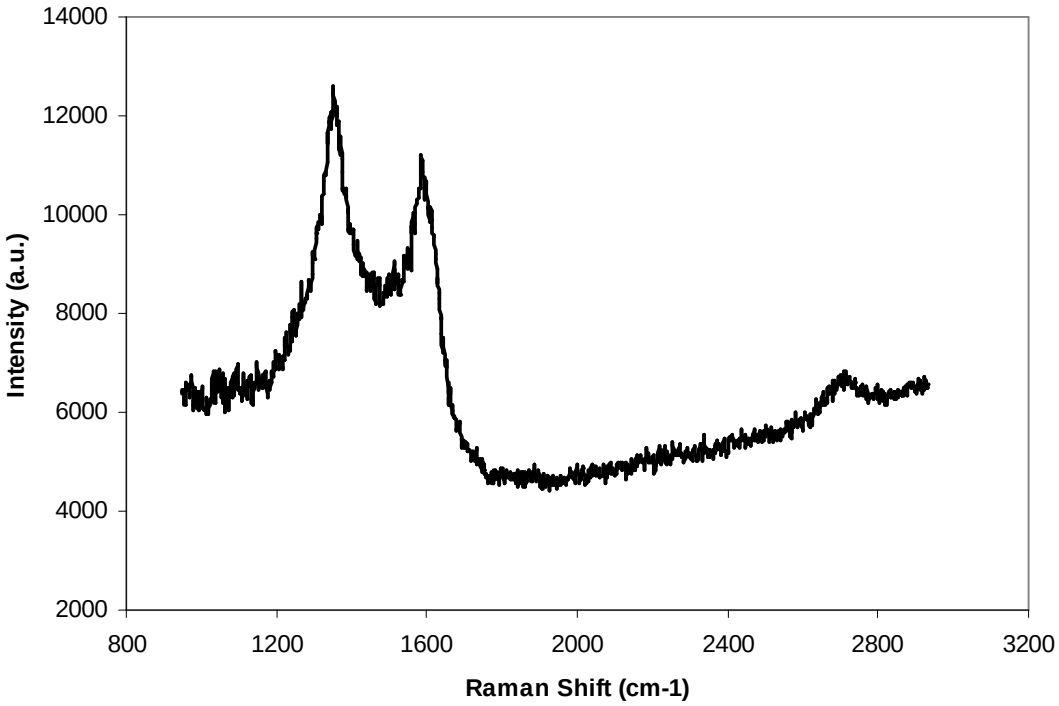


Figure 4.36: Raman spectrum of CNTs produced at 850°*C* during CO_2 reforming of CH_4, with the D-band at 1352 cm^{-1}, G-band at 1589 cm^{-1} and G'-band at 2705 cm^{-1}

These spectra (Figures 4.33 – 4.36) indicate the production of CNTs. Figure 4.37 is from a sample which did not display any CNTs being formed on the TEM images. This is re-affirmed by the Raman Shift peaks not following the same pattern as the ones in Figure 4.33 or 4.35. This sample was produced at 950°*C* using $LaNi_5$ as the catalyst. Table 4.1 is a summary of results from Figures 4.1 – 4.37 showing the gas or gasses, temperature, catalyst used and carbon produced.

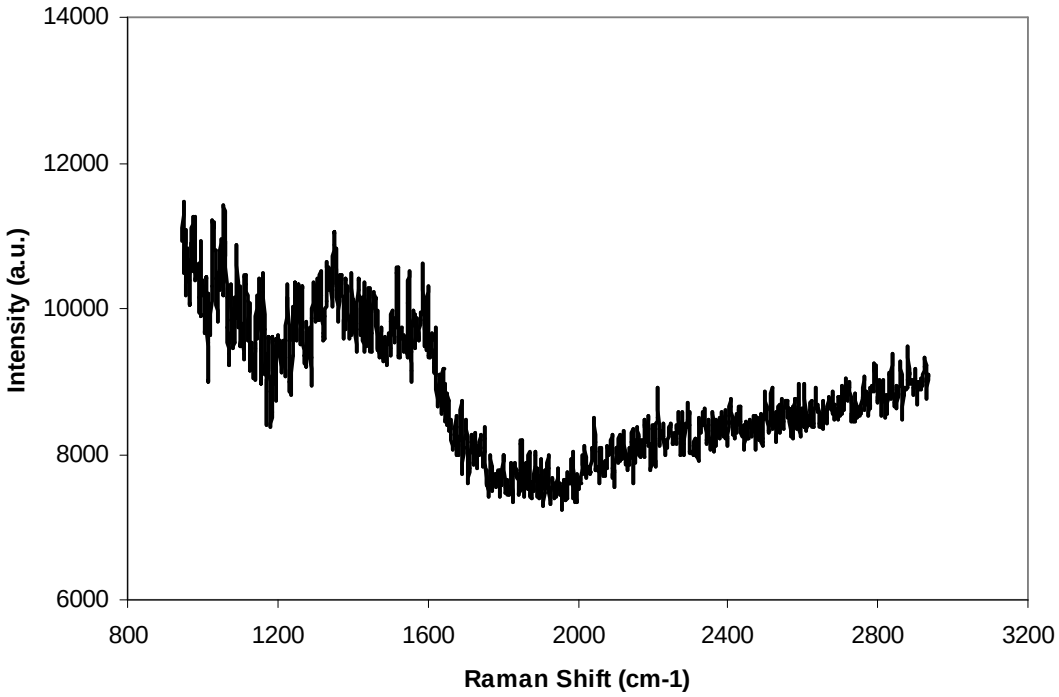


Figure 4.37: Raman spectrum of sample when CNTs were not formed during dry reforming

It is seen from Table 4.1 that the nickel catalysts of $LaNi_5$ and mischmetal nickel alloy can be used to produce MWCNTs and CNFs. Table 4.1 also shows the results for the GC analysis done whereby, the unknown gasses are those that are not calibrated for. The CNTs produced using $LaNi_5$ and CH_4 had little amorphous carbon with the multiple-wall structure of the CNTs easily seen in the HMTEM images. An increase in temperature from 650°*C* to 850°*C* leads to the CNTs and CNFs produced using CO_2 and $LaNi_5$ becoming more defined. A suitable catalyst for the dry reforming of methane with carbon dioxide is the mischmetal nickel alloy at a temperature of 950°*C* as less carbon nanotubes are produced and there is a higher percentage of synthesis gas in the outflow.

Table 4.1: Summary of carbon produced using CH_4 only, CO_2 only and CH_4/CO_2 reforming at different temperatures

Gas	Temperature (^oC)	Catalyst	Carbon Produced	Output Gas
CH_4	750	$LaNi_5$ alloy	MWCNTs	13.65% H_2 28.02% unknown 58.33% CH_4
CH_4	850	$LaNi_5$ alloy	MWCNTs	17.52% H_2 15.02% unknown 67.46% CH_4
CO_2	650	$LaNi_5$ alloy	MWCNTs, CNFs	5.33% O_2 2.02% CO 92.65% CO_2
CO_2	750	$LaNi_5$ alloy	MWCNTs, CNFs	0.06% O_2 12.03% CO 87.91% CO_2
CH_4/CO_2	750	$LaNi_5$ alloy	MWCNTs	10.27% H_2 11.3% CO 35.59% CH_4 42.84% CO_2
CH_4/CO_2	850	$LaNi_5$ alloy	MWCNTs	11.66% H_2 5.83% CO 34.51% CH_4 48% CO_2
CH_4/CO_2	750	Mischmetal Nickel alloy	MWCNTs	14.18% H_2 9.67% CO 8.97% CH_4 67.18% CO_2
CH_4/CO_2	950	Mischmetal Nickel alloy	Few MWCNTs	49.51% H_2 25.21% CO 8.61% CH_4 16.67% CO_2

4.4 Kinetics

The limitation of external mass transfer is tested through variation of feed flow rate i.e. when the reforming rate does not change with the change of flow rate, limitation of external mass transfer is negligible (Tsipouriari and Verykios, 2001; Zang, 2008; Nandini *et al*., 2006). In order to check the limitation of internal mass transfer, variation of catalyst particle size is done (Tsipouriari and Verykios, 2001; Nandini *et al*., 2006). A study undertaken by Forni (1999) showed internal mass transfer is dependent on particle radius but kinetics is independent of radius. Accordingly, rate limitations by external or internal mass transfer, under differential conditions were proven negligible by applying suitable criteria. The disappearance rate of reactant is calculated using equation 4.1 while the formation rate of product is calculated with equation 4.2. The reforming rate of CO_2 reforming of CH_4 is given in terms of CH_4 consumption rate.

$$-r_i, mol/g-s = \frac{F_i^o - F_i^f}{m_{cat} \times 60} \tag{4.1}$$

$$r_i, mol/g-s = \frac{F_i^f}{m_{cat} \times 60} \tag{4.2}$$

Where:

m_{cat} , is the mass of catalyst (g)

F_i^o , is the molar outlet flowrate

F_i^f , is the molar inlet flowrate

As discussed in the experimental design of Section 3, experiments were performed in the temperature range $750-850°C$ with an inlet feed of CO_2 and CH_4 at the flowrates listed in Table 3.1. Figures 4.38 and 4.39 show the effect of varying CO_2:CH_4 ratios on the formation rate of CO at $750°C$, $800°C$ and $850°C$. From Figure 4.38 it can be seen that the formation rate of CO increased as the CO_2 was increased. The formation rate of CO did not change considerably with an increase in CH_4 as noted in Figure 4.39. The influence of the Reverse Water-Gas Shift Reaction (RWGS) can be attributed as the difference between observations in Figures 4.38 and 4.39.

RWGS: $CO_2 + H_2 \rightarrow CO + H_2O$ (2.5)

By using constant CH_4, the reaction rate of CO_2 reforming of CH_4 was constrained due to restricted availability of CH_4. Nonetheless, the formation of CO still enhanced a lot through the RWGS reaction between H_2 and excess CO_2 when CO_2 was increased continuously as shown in Figure 4.38. At constant CO_2, the formation rate of CO only increased slightly with the increase in CH_4 (Figure 4.39).

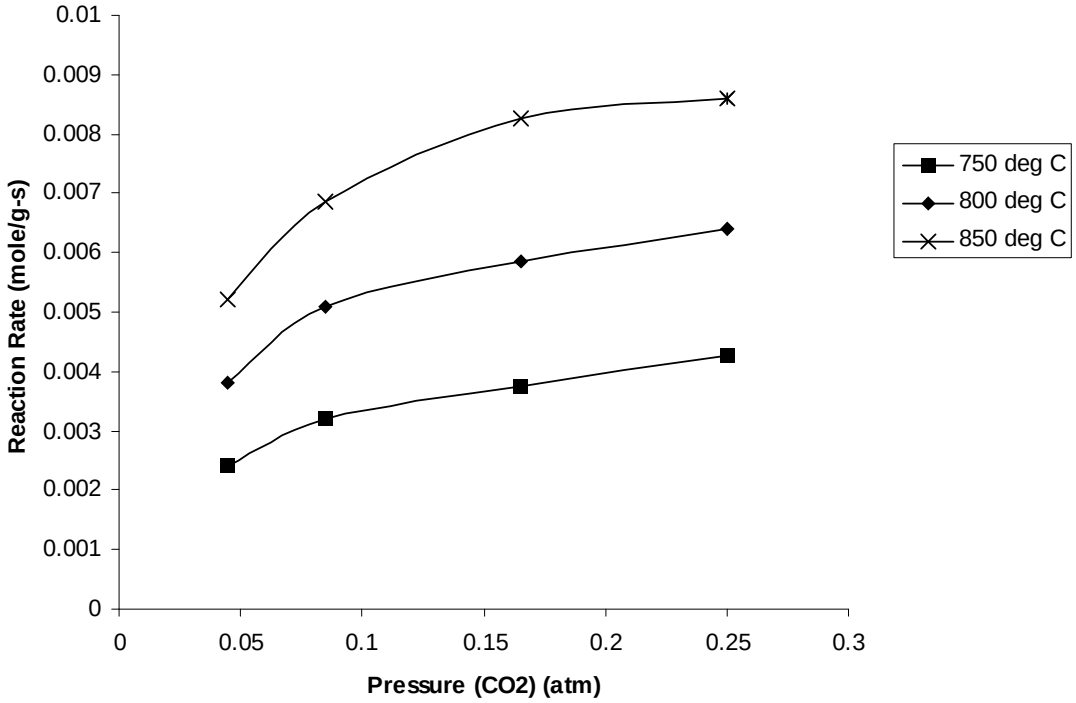


Figure 4.38: Effect of different CO_2:CH_4 ratios on formation rate of CO over the nickel alloy catalyst at $750°C$, $800°C$ and $850°C$ (CO_2 changing, CH_4 constant)

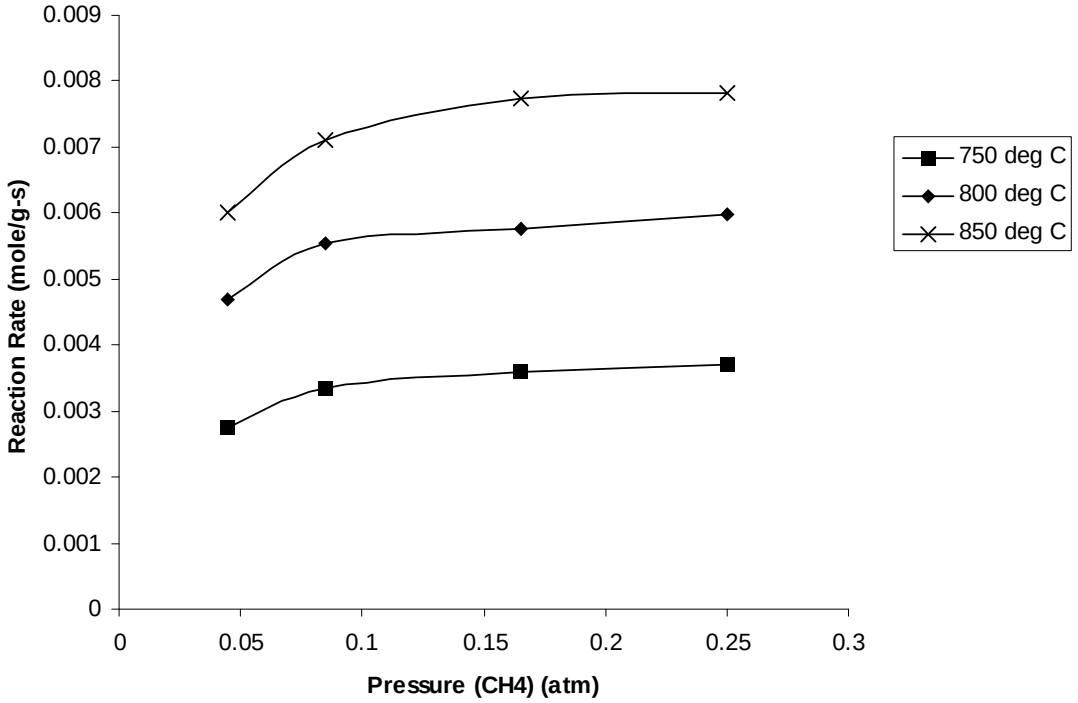


Figure 4.39: Effect of different CO_2:CH_4 ratios on formation rate of CO over the nickel alloy catalyst at $750°C$, $800°C$ and $850°C$ (CH_4 changing, CO_2 constant)

The effect of different CO_2:CH_4 ratios on the formation rate of H_2 at $750°C$, $800°C$ and $850°C$ are shown in Figures 4.40 and 4.41. At constant CH_4 (Figure 4.40), it is clear that H_2 formation rate increased at low CO_2:CH_4. The increase in H_2 formation is due to increase in reaction rate of CO_2 reforming of CH_4 when more CO_2 was available. Thereafter, the formation rate of H_2 was reasonably stable. The RWGS reaction could also be increasing with the availability of excess CO_2. Equivalence of the increase of CO_2 reforming of CH_4 to the increase of the RWGS reaction results in constant formation of H_2. However, as shown in Figure 4.38 the formation rate of CO will continue to increase. A drop in the formation rate of H_2 is seen at high CO_2:CH_4. Since the increase of the H_2

formation rate from CO_2 reforming of CH_4 reaction was less than the rate of consumption from the RWGS reaction when CH_4 was limited but CO_2 was in excess.

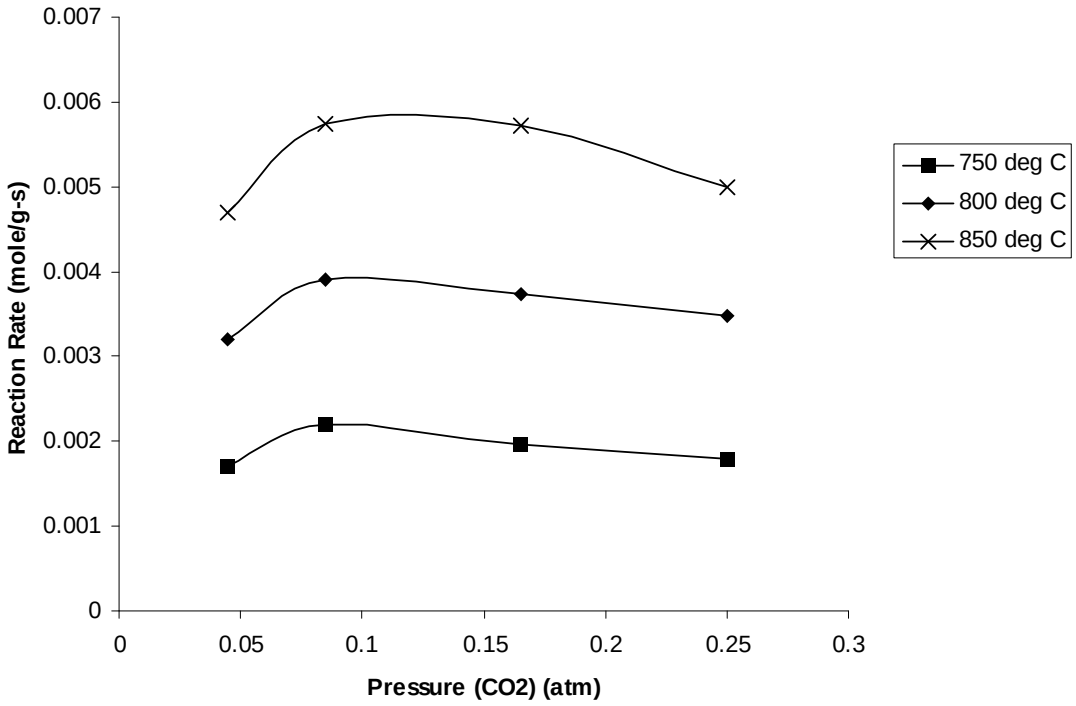


Figure 4.40: Effect of different CO_2:CH_4 ratios on formation rate of H_2 over the nickel alloy catalyst at $750°C$, $800°C$ and $850°C$ (CO_2 changing, CH_4 constant)

Figure 4.41 shows that at constant CO_2, the rate of formation of H_2 slightly increased in the beginning and was steady with an increase in CH_4:CO_2. This indicated that both the CO_2 reforming of CH_4 reaction and RWGS reaction were restricted when limited CO_2 was available.

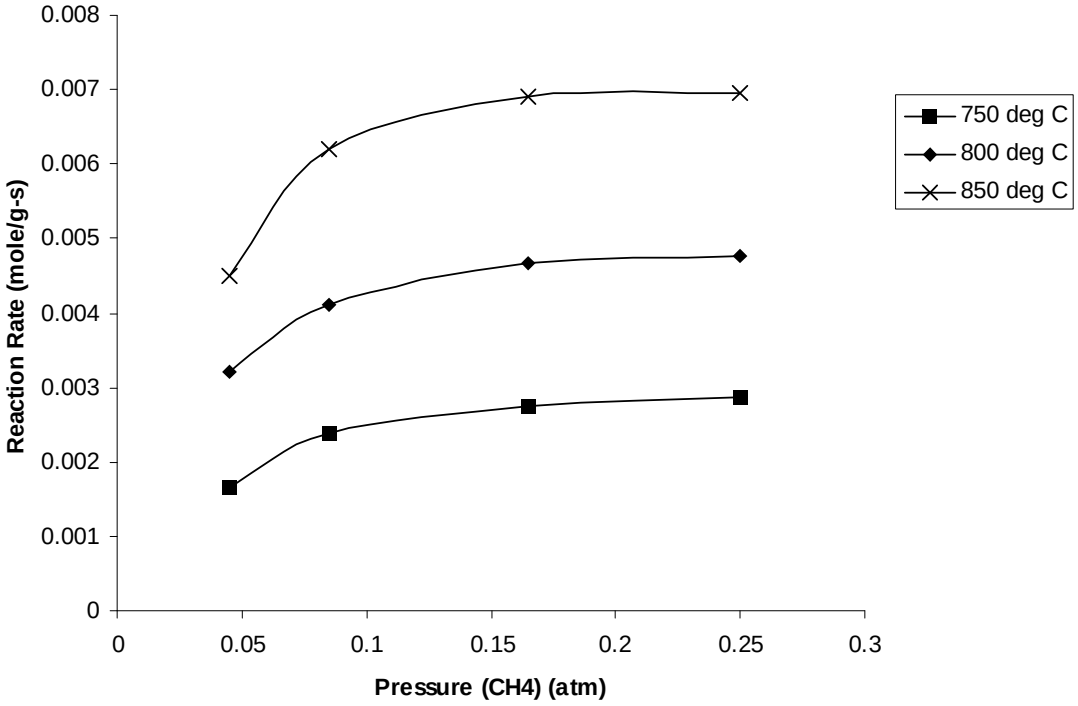


Figure 4.41: Effect of different CO_2:CH_4 ratios on formation rate of H_2 over the nickel alloy catalyst at $750°C$, $800°C$ and $850°C$ (CH_4 changing, CO_2 constant)

The effect of temperature on the reaction rate of CO_2 reforming of CH_2 over nickel alloy catalyst is investigated in the temperature range of 1023 – 1123K. In order to calculate the activation energy, Ea and rate constant, k from the slope and intercept, respectively an Arrhenius plot of reaction rate versus 1/T (K) is done, shown by Figure 4.42. Consequently, an expression for the forward rate of reaction is given by equation 4.3.

$$r_i = KP_{CH4}^{m}P_{CO2}^{n} \qquad (4.3)$$

Where:

$K= k_o\exp(-Ea/RT)$

Keeping CH_4:CO_2 ratio constant then,

$$A=k_o P_{CH4}^{m} P_{CO2}^{n}$$

The natural logarithm (equation 4.5) is taken of the simplified expression for the rate of reaction (equation 4.4) generating a convenient plot from which the apparent activation energies for CH_4, CO_2 consumption, H_2, and CO formation can be estimated.

$$r_i = A \exp(-Ea/RT) \quad (4.4)$$

$$\ln r_i = \ln A - (Ea/RT) \quad (4.5)$$

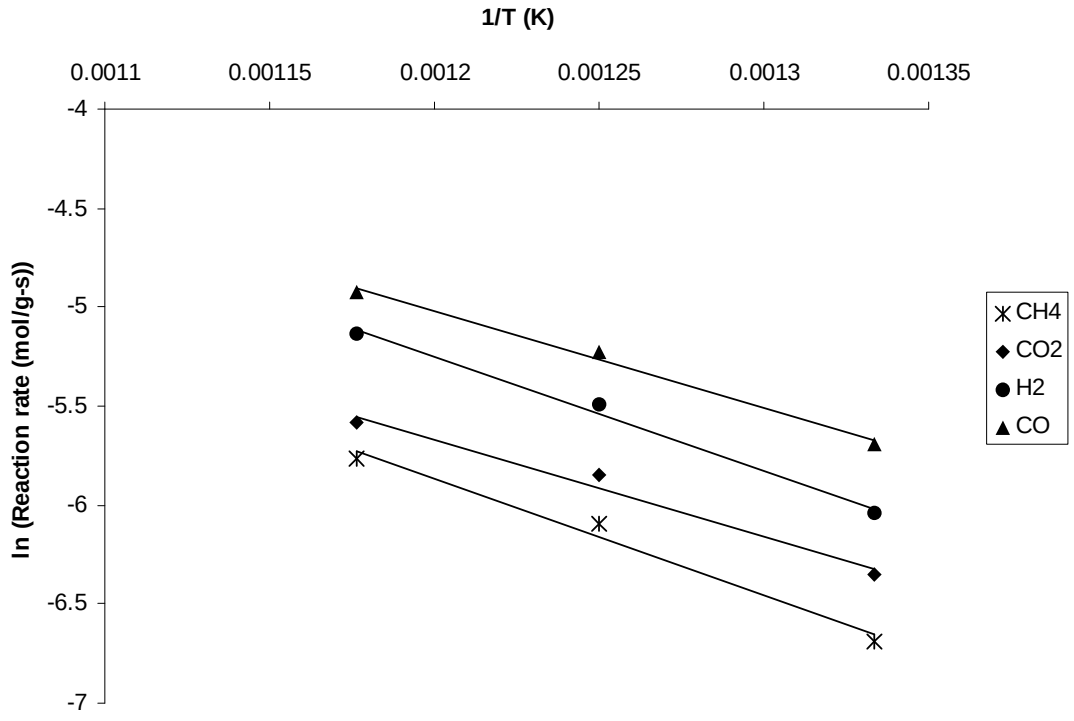


Figure 4.42: Natural logarithm of reaction rate versus 1/T (K), where CO_2:CH_4:1

The apparent activation energy for CH_4 and CO_2 consumption, and H_2 and CO production were 41.7, 47.5, 54.5 and 47.5 kJ/ mol, respectively. Comparison of apparent activation energies of lanthanum nickel catalyst with reported Ni-based catalysts shows that there is difference in apparent activation energy, possibly due to the difference of catalyst systems applied in the relevant studies (Nandini *et al*., 2006; Lemonidou and Vasalos, 2002; Zhang, 2009; Bradford and Vannice, 1999). Tsipouriari and Verykios (2002) reported that the catalyst supports of Ni may influence significantly the activation energy by altering the rate-controlling step in the reaction sequence. The proximity of apparent activation energy values for CH_4, CO_2, and CO suggests that the rate-controlling step for CO formation is the same as that for CH_4 and CO_2 consumption (Lemonidou and Vasalos, 2002; Zang, 2008). Bradford and Vannice (1999) discussed that the activation energies of CO_2 reforming of CH_4 are typically between 33 and 100 kJ/mol while high values up to 160 kJ/mol are obtained for some catalysts. The apparent energy of H_2 formation being higher than that for CO formation is ascribed to be the result of the RWGS influence on the reaction mechanism (Bradford, 1996).

CHAPTER FIVE

5.0 Conclusion and Recommendations

5.1 Conclusion

The greenhouses gases, methane and carbon dioxide were used in this study to make carbon nanofibers and synthesis gas through a vertical CVD reactor method. It was shown that carbon nanofibers and carbon nanotubes are produced using CH_4, CO_2 and dry reforming. The decomposition of CO_2 was done at realistic temperatures ($650-850°C$). The catalytic reforming of methane with CO_2 to synthesis gas at moderately high temperatures is a promising technology in utilization of CO_2. This well-known process has long had a problem of catalyst deactivation due to coking.

However, the lanthanum nickel alloy and to a greater extent, the mischmetal nickel alloy are promising catalysts in the dry reforming of CH_4 as they do not require any pre-treatment or preparation to withstand coking at the reaction temperatures used. The production of CNTs using methane (as the hydrocarbon source) is recognized as a feasible synthesis method and is quite often implemented. This synthesis technique shows that CO_2 can be used as a carbon source to produce CNTs avoiding the inflammability and toxicity from CO during operation, and is helpful for environmental protection. However, it may prove to be costly to operate at an industrial scale in order to get satisfactory conversion of CO_2.

5.2 Recommendations

A study on the reaction mechanism during CO_2 reforming of CH_4 and formation mechanism of CNTs using $LaNi_5$ will be helpful to design a catalyst system for mass production of CNTs with low cost and high quality or synthesis gas. The issue of determining whether it is tip or base growth mechanism for the CNFs needs investigation. The work regarding CO_2 production of CNFs and CNTs is interesting and requires further exploration.

REFERENCES

Abild-Pedersen, F. (2005), *Methane Activation on Ni Model Surfaces Based on Density Functional Theory*. PhD Thesis. Lyngby, Technical University of Denmark, Denmark.

Alie, C., Backham, L., Croiset, E., Douglas, P.L. (2005), *Simulation of CO_2 capture using MEA scrubbing: a flowsheet decomposition method.* Energy Conversion and Management, vol. 46, pp. 475-487.

Ando, Y., Zhao, X., Sugai, T. and Kumar, M. (2004), *Growing Carbon Nanotubes.* Materials Today, no. 7, pp. 22-29.

Arakawa, T., Suezawa, N., Adachi, G., Shiokawa, J. (1988), *Dissociation of CO_2 on some rare earth metal thin films.* Applied Surface Science, vol. 33, pp. 286-291.

Bahome, M.C. (2007), *Synthesis and Use of Carbon Nanotubes as a Support for the Fischer-Tropsch Synthesis.* PhD Thesis, University of the Witwatersrand, Johannesburg, South Africa.

Baughman, R.H., Zakhidov, A.A., Heer, W.A. (2002), *Carbon nanotubes-the route toward applications.* Science, vol. 297, pp. 787-792.

Belin, T., Epron, F. (2005), *Characterization methods of carbon nanotubes: a review.* Materials Science and Engineering B, vol. 119, pp. 105-118.

Bethune, D.S., Kiang, C.H., de Vries, M.S., Gorman, G., Savoy, R., Vazquez, J. and Beyers, R. (1993), *Cobalt-catalyzed growth of carbon nanotubes with single-atomic-layer walls.* Nature, vol. 363, pp. 605-607.

Bezemer, G.L., Radstake, P.B., Koot, V., Van Dillen, A.J., Geus, J.W., De Jong, K.P. (2006), *Preparation of Fischer-Tropsch cobalt catalysts supported on carbon nanofibers and silica using homogeneous deposition-precipitation.* Journal of Catalysis, vol. 237, pp. 291-302.

Biro, L.P., Lazarescu, S., Lambin, Ph., Thiry, P.A., Fonseca, A., Nagy, J.B. and Lucas, A.A. (1997), *Scanning tunneling microscope investigation of carbon nanotubes produced by catalytic decomposition of acetylene.* Physical Review B, vol. 56, pp. 12490-12498.

Blom, R., Dahl, I.M., Slagtem, A., Sortland, B., Spjelkavik, A., Tangstad, E. (1994), *Carbon dioxide reforming of methane over lanthanum-modified catalysts in a fluidized-bed reactor.* Catalysis Today, vol. 21, pp. 535-543.

Bodrov, I.M., Apelbaum, L.O. (1967), *Reaction kinetics of methane and carbon dioxide on a nickel surface.* Kinetika i Kataliz, vol. 8, no. 2, pp. 379-382.

Bradford, M.C.J., Vannice, M.A. (1996), *Catalytic reforming of methane with carbon dioxide over nickel catalysts II, reaction kinetics.* Applied Catalysis A, vol. 142, pp. 97-122.

Bradford, M.C.J. and Vannice, M.A. (1999), *CO_2 reforming of CH_4.* Catalysis Review Science Engineering, vol. 41, pp. 1-42.

Cassell, A., Raymakers, J.A., Kong, J., Dai, H. (1999), *Large scale CVD synthesis of single-walled carbon nanotubes.* Journal of Physical Chemistry B, vol. 103, pp. 6484-6492.

Chai, S., Hussein, S., Zein, S., Mohamed, A.R. (2007), *Synthesizing carbon nanotubes and carbon nanofibers over supported-nickel oxide catalysts via catalytic decomposition of methane.* Diamond and Related Materials, vol. 16, pp. 1656-1664.

Chen, D., Lodeng, R., Anundskas, A., Olsvik, O., Holmen, A. (2001), *Deactivation during carbon dioxide reforming of methane over Ni catalyst: microkinetic analysis.* Chemical Engineering Science, vol. 56, pp. 1371-1379.

Chen, X., Honda, K., Zhang, Z.G. (2005), *A comprehensive comparison of CH_4-CO_2 reforming activities of NiO/Al_2O_3 catalysts under fixed- and fluidized-bed operations.* Applied Catalysis A, vol. 288, pp. 86-97.

Cheung, C.L., Kurtz, A., Park, H., Lieber, C.M. (2002), *Diameter-controlled synthesis of carbon nanotubes.* Journal of Physical Chemistry B, vol. 106, no. 10, pp. 2429-2462.

Conteau, E., Hernadi, K., Seo, K., Seo, J.W., Thien-Nga, L., Miko, C., Gaal, R. and Forro, L. (2003), *CVD synthesis of high purity carbon nanotubes using $CaCO_3$ catalyst support for large scale production.* Journal of Chemical Physics Letter, vol. 378, pp 9-17.

Dresselhaus, M.S., Dresselhaus, G., Avouris, P. (2001*), Carbon Nanotubes: Synthesis, Structure, Properties and Applications.* Springer-Verlag.

Dresselhaus, M.S., Dresselhaus, G., Jorio, A., Filho, A.G.S. and Saito, R. (2002), *Raman spectroscopy on isolated single wall carbon nanotubes.* Carbon, vol. 40, pp. 2043-2061.

Dresselhaus, M.S., Dresselhaus, G., Saito, R., Jorio, A. (2005), *Raman spectroscopy of carbon nanotubes.* Physics Reports, vol. 409, pp. 47-99.

Dresselhaus, M.S., Lin, Y.M., Rabin, O., Jorio, A., Souza, A.G., Pimenta, M.A., Saito, R., Samsonidze, G.G. and Dresselhaus, G. (2003), *Nanowires and nanotubes.* Materials Science and Engineering C, vol. 23, pp. 129-140.

Ducati, C., Alexandrou, I., Chhowalla, M., Amaratunga, G.A.J. and Robertson J. (2002), *Temperature selective growth of carbon nanotubes by chemical vapour deposition.* Journal of Applied Physics, vol. 92, no. 6, pp. 3299-3303.

Ducati, C., Alexandrou, I., Chhowalla, M., Robertson, J. and Amaratunga, G.A.J. (2004), *The role of the catalytic particle in the growth of carbon nanotubes by plasma enhanced chemical vapour deposition.* Journal of Applied Physics, vol. 95, pp. 6387-6391.

Dufour, J., Serrano, D.P., Galvez J.L., Morenoa, J., Garcia, C. (2009), *Life cycle assessment of processes for hydrogen production: environmental feasibility and reduction of greenhouse gases emissions.* International Journal of Hydrogen Energy, vol. 34, pp. 1370-1376.

Durrer, L., Helbling, T., Zenger, C., Jungen, A., Stampfer, C., Hierold, C. (2008), *SWNT growth by CVD on Ferritin-based iron catalyst nanoparticles towards CNT sensors.* Sensors and Actuators B, vol. 132, pp. 485-490.

Ebbesen, T.W. (1997), *Carbon Nanotubes: Preparation and Properties.* CRC Press, Inc.

Edwards, J.H. and Maitra, A.M. (1995), *The chemistry of methane reforming with carbon dioxide and its current and potential applications.* Fuel Processing Technology, vol. 42, pp. 269-289.

Effendi, A., Hellgardt, K., Zhang, Z.G., Yoshida, T. (2003), *Characterisation of carbon deposits on Ni=SiO_2 in the reforming of CH_4–CO_2 using fixed- and fluidised-bed reactors.* Catalysis Communications, vol. 4, pp. 203-207.

Eklund, P.C., Holden, J.M. and Jishi, R.A. (1995), *Vibrational modes of carbon nanotubes, spectroscopy and theory.* Carbon, vol. 33, no. 7, pp. 959-972.

Erdohelyi, A., Cserenyi, J., Solymosi, F. (1993), *Activation of methane and its reaction with carbon dioxide over supported rhodium catalysts.* Journal of Catalysis, vol. 141, pp. 287-299.

Eswaramoorthy, M., Sen, R. and Rao, C.N.R. (1999), *A study of micropores in single-walled carbon nanotubes by the adsorption of gases and vapours.* Chemical Physical Letters, vol. 304, pp. 207-210.

Fogler, H.S. (1986), *Elements of Chemical Reaction Engineering.* Prentice-Hall International, Inc.

Forni, L. (1999), *Mass transfer and heat transfer in catalytic reactions.* Catalysis Today vol. 52, pp. 147-152.

Fujiwara, A., Ishii, K., Suematsu, H., Kataura, H., Maniwa, Y., Suzuki S. and Achiba, Y. (2001), *Gas adsorption in the inside and outside of single-walled carbon nanotubes.* Chemical Physical Letters, vol. 336, pp. 205-211.

Furer, J. (2006), *Growth of Single-Wall Carbon Nanotubes by Chemical Vapour Deposition for Electrical Devices.* University of Basel, Basel, Switzerland.

Gallego, G., Mondragon, F., Tatibouet, J., Barrault, J., Batiot-Dupeyrat, C. (2008), *Carbon dioxide reforming of methane over La_2NiO_4 as catalyst precursor-characterization of carbon deposition.* Catalysis Today, vol. 135, pp. 200-209.

Gao, L.Z., Kiwi-Minsker, L., Renken, A. (2008), *Growth of carbon nanotubes and microfibers over stainless steel mesh by cracking of methane.* Surface and Coatings Technology, vol. 202, pp. 3029-3042.

Hafner, J.H., Cheung, C.L., Lieber, C.M. (1999), *Growth of nanotubes for probe microscopy.* Nature, vol. 398, pp. 761-762.

Hafner, J.H., Cheung, C.L., Oosterkamp, T.H., Lieber, C.M. (2001), *High-yield assembly of individual single-walled carbon nanotube tips for scanning probe microscopies.* Journal of Physical Chemistry B, vol. 105, pp. 743-746.

Hamada, N., Sawada, S. and Oshiyama, A. (1992), *New one-dimensional conductors: graphitic microtubules.* Physical Review Letters, no. 68, pp. 1579-1581.

He, C., Zhao, N., Shi, C., Du, X., Li, J. (2006), *Carbon nanotubes and onions from methane decomposition using Ni/Al catalysts.* Materials Chemistry and Physics, vol. 97, pp. 109-115.

Heo, J. (2008), *Probing Electronic Properties of Carbon Nanotubes.* PhD Thesis, California Institute of Technology, California, United States of America.

Hoenlein, W., Kreupl, F., Duesberg, G.S., Graham, A.P., Liebau, M., Seidel, R.V., Unger, E. (2004), *Carbon nanotubes applications in microelectronics.* IEEE Transactions on Components and Packaging Technologies, vol. 27, no. 4, pp. 629-634.

Hone, J. (2004), C*arbon Nanotubes: Thermal Properties.* Dekker Encyclopedia of Nanoscience and Nanotechnology, CRC Press, Inc.

Hou, Z., Zheng, X. and Yashima, T. (2005), *High coke-resistance of K-Ca-promoted Ni/α-Al_2O_3 catalyst for CH_4 reforming with CO_2.* Reaction Kinetic Catalysis Letters, vol. 84, no. 2, pp. 229-235.

Hu, Y.H., Ruckenstein, E. (1997), *Transient response analysis via a broadened pulse combined with a step change or an isotopic pulse: application to CO_2 reforming of methane over NiO/SiO_2.* Journal of Physical Chemistry B, vol. 101, pp. 7563-7565.

Ichi-oka, H., Higashi, N., Yamada, Y., Miyake, T. and Suzuki, T. (2007), *Carbon nanotube and nanofiber syntheses by the decomposition of methane on group 8-10 metal-loaded MgO catalysts.* Diamond and Related Materials, vol. 16, pp. 1121-1125.

Iijima, S. (1991), *Helical microtubules of graphitic carbon.* Nature, vol. 354, pp. 56-58.

Iijima, S. and Ichihashi, T. (1993), *Single-shell carbon nanotubes of one nanometer diameter.* Nature, vol. 363, pp. 603-605.

Inoue, M., Asai, K., Nagayasu, Y., Takane, K., Iwamoto, S., Yagasaki, E., Ishii, K. (2008), *Formation of multi-walled carbon nanotubes by Ni-catalyzed decomposition of methane at 600-750°C.* Diamond and Related Materials, vol. 17, pp. 1471-1475.

Inoue, S., Ichikuni, N., Suzuki, T., Uematsu, T. and Kaneko, K. J. (1998), *Capillary condensation of nitrogen on multi-wall carbon nanotubes.* Physical Chemistry B, vol. 102, pp. 4689-4692.

Iyuke, S. and Mahalik, N. (2005), *Micromanufacturing and Nanotechnology: Fundamentals, Techniques, Platforms and Experiment.* Springer-Verlag.

Kaneto, K., Tsuruta, M., Sakai, G., Cho, W.Y. and Ando, Y. (1999), *Electrical conductivities of multi-wall carbon nanotubes.* Journal of Synthetic Metal, vol. 103, pp. 2543-2546.

Kasuya, A., Sasaki, Y., Saito, Y. (1997), *Evidence for size-dependent discrete dispersions in single-wall nanotubes.* Physics Review Letters, vol. 78, no. 23, pp. 4434-4441.

Katok, K.O., Tertykh, O.A., Brichka, S.Y. and Princhold'ko, G.P. (2006), *Pyrolytic synthesis of carbon nanostructure on Ni, Co, Fe/MCM-41 catalysts.* Journal of Material Chemistry and Physics, vol. 96, pp. 396-401.

Keidar, M. (2007), *Factors affecting synthesis of single-wall carbon nanotubes in arc discharge.* Journal of Physics D: Applied Physics, vol. 40. pp. 2388-2393.

Khedr, M.H., Omarb, A.A., Abdel-Moaty, S.A. (2006), *Reduction of carbon dioxide into carbon by freshly reduced $CoFe_2O_4$ nanoparticles.* Materials Science and Engineering A, vol. 432, pp. 26-33.

Kim, W., Choi, H.C., Shim, M., Li, Y., Wang, D. and Dai, H. (2002), *Synthesis of ultralong and high percentage of semiconducting single-walled carbon nanotubes.* Nano Letters, vol. 2, no. 7, pp. 703-708.

Kingston, C.T. and Simard, B. (2003), *Fabrication of carbon nanotubes.* Analytical Letters, vol. 36, pp. 3119-3145.

Klinke, C., Bonard, J.M. and Kern K. (2005), *Thermodynamic calculations on the catalytic growth of multi-wall carbon nanotubes.* Physical Review B, vol. 71, pp. 035403-1 – 035403-7.

Kong, J., Soh, H.T., Cassell, A.M., Quate, C.F., Dai, H. (1998), *Synthesis of individual single-walled carbon nanotubes on patterned silicon wafers.* Nature, vol. 395, pp. 878-881.

Krishnan, A., Dujardin, E., Ebbesen, T.W., Yianilos, P.N. and Treacy, M. M. J. (1998), *Young's modulus of single-walled nanotubes.* Physical Review B, vol. 58, pp. 14013-14019.

Kroto, H.W., J.R. Heath, S.C. O'Brien, R.F. Curl, R.E. Smalley. (1985), C_{60}*: buckminsterfullerene.* Nature, vol. 318, pp. 162-163.

Kukovitsky, E.F., L'vov, S.G., Sainov, N.A., Shustov, V.A. and Chernozatonskii. (2002), *Correlation between metal catalyst particle size and carbon nanotubes growth.* Chemical Physics Letters, vol. 355, pp. 497-503.

Kuwana, K., Endo, H., Saito, K., Qian, D., Andrews, R., Grulke, E.A. (2005), *Catalyst deactivation in CVD synthesis of carbon nanotubes.* Carbon, vol. 43, pp. 253-260.

Lannou, M-I., Helion, F. and Namy, J-L. (2003), *Some uses of mischmetall in organic synthesis.* Tetrahedron, vol. 59, pp. 10551-10565.

Lee, C.J., Park, J., Huh, Y. and Lee, J.Y. (2001), *Temperature effect on the growth of carbon nanotubes using thermal chemical vapour deposition.* Chemical Physics Letters, vol. 343, pp. 33-38.

Lemonidou, A.A., and Vasalos, I. (2002), *Carbon dioxide reforming of methane over 5 wt. % Ni/CaOAl_2O_3 catalyst.* Applied Catalysis A, vol. 228, pp. 227-235.

Li, H., Shi, C., Du, X., He, C., Li, J., Zhao, N. (2008), *The influences of synthesis temperature and Ni catalyst on the growth of carbon nanotubes by chemical vapor deposition.* Materials Letters, vol. 62, pp. 1472-1475.

Lou, Z., Chen, Q., Wang, W., Zhang, Y. (2003), *Synthesis of carbon nanotubes by reduction of carbon dioxide with metallic lithium*. Carbon, vol. 41, pp. 3036-3074.

Lozovik, Y.K., Minogin, A.V. and Popw, A.M. (2003), *Nanomachines based on carbon nanotubes.* Physics Letter, vol. 313, pp. 112-121.

Martinez, R., Romero, E., Guimon, C., Bilbao, R. (2004), *CO_2 reforming of methane over co-precipitated Ni-Al catalysts modified with lanthanum.* Applied Catalysis A, vol. 274, pp. 139-149.

Maser, W.K., Benito, A.M., Martinez, M.T. (2002), *Production of carbon nanotubes: the light approach.* Carbon, vol. 40, pp. 1685-1695.

Maultzsch, J., Reich, S. and Thomsen, C. (2002), *Raman scattering in carbon nanotubes revisited.* Physical Review B, vol. 65, pp. 233402-1 – 233402-4.

McBride, W. (2001), *Synthesis of Carbon Nanotubes by Chemical Vapour Deposition (CVD)*. Dissertation, College of Williamsburg, Virginia, United States of America.

Mendoza, D., Santiago, P. and Perez, E.R. (2006), *Carbon nanotubes produced from hexane and ethanol.* Revista Mexicana, vol. 52, no. 1, pp. 1-5.

Mohlala, M.S. (2006), *Organometallic Iron Complexes as Catalysts for Carbon Nanotubes Synthesis.* PhD Thesis, University of the Witwatersrand, Johannesburg, South Africa.

Mondal, K.C., Choudhary, V.R., Joshi, U.A. (2007), *CO_2 reforming of methane to syngas over highly active and stable supported CoOx (accompanied with MgO, ZrO_2 or CeO_2) catalysts.* Applied Catalysis A, vol. 316, pp. 47-52.

Motiei, M., Hacohen, Y.R., Moreno, J.S., Gedanken, A. (2001), *Preparing carbon nanotubes and nested fullerenes from supercritical CO_2 by a chemical reaction.* Journal of American Chemical Society, vol. 123, pp. 8624-8625.

Munoz, E., Maser, W.K., Benito, A.M., Martinez, M.T., de la Fuente, G.F., Maniette, Y., Righi, A., Anglaret, E. and Sauvajol, J.L. (2000), *Gas and pressure effects on the production of single-walled carbon nanotubes by laser ablation.* Carbon, vol. 38, pp. 1445-1451.

Musso, S., Porro, S., Rovere, M., Chiodoni, A. and Tagliaferro, A. (2007), *Physical and mechanical properties of thick self-standing layers of multi-wall carbon nanotubes.* Diamond and Related Materials, vol. 16, pp. 1174-1178.

Nagy, J.B., Bister, G., Fonseca, A., Mehn, D., Konya, Z., Kiricsi, I., Horvath, Z.E. and Biro, L.P. (2004), *On the growth mechanism of single-walled carbon nanotubes by catalytic carbon vapour deposition on supported metal catalysts.* Journal of Nanoscience and Nanotechnology, vol. 4, pp. 326-345.

Nandini, A., Pant, K.K., Dhingra, S.C. (2006), *Kinetic study of the catalytic carbon dioxide reforming of methane to synthesis gas over Ni-K/CeO_2-Al_2O_3.* Applied Catalysis A, vol. 308, pp. 119-127.

O'Connell, M.J. (2006), *Carbon Nanotubes: Properties and Applications.* Taylor & Francis Group, LLC.

Odom, T., Huang, J., Kim, P. and Lieber, C. (1998), *Atomic structure and electronic properties of single-walled carbon nanotubes.* Nature International Weekly Journal of Science, vol. 391, pp. 62-64.

Ohme, H., Suzuki, T. (1996), *Mechanisms of CO_2 gasification of carbon catalyzed with group VIII metals. 1. Iron-catalyzed CO_2 gasification.* Energy Fuels, vol. 10, pp. 980-987.

Park, C., Engel, E.S., Crowe, A., Gilbert, T.R., and Rodriguez, N.M. (2000), *Use of carbon nanofibers in the removal of organic solvents from water.* Langmuir, vol. 16, pp. 8050-8056.

Philip, S., Massilian, O.C. and Philippe, K. (2003), *Carbon nanotubes and nanofibers in catalysis.* Journal of Applied Catalysis A, vol. 25, pp. 337-338.

Philippe, R., Morancais, A., Corrias, M., Caussat, B., Kihn, Y., Kalck, P., Plee, D., Gaillard, P., Bernard, D., Serp, P. (2007), *Catalytic production of carbon nanotubes by fluidized-bed CVD.* Chemical Vapour Deposition, vol. 13, pp. 447-457.

Rao, A.M., Richter, E., Bandow, S., Chase, B., Eklund, P.C., Williams, K.A., Fang, S., Subbaswamy, K.R., Menon, M., Thess, A., Smalley R.E., Gresselhaus, G. and Dresselhaus, M.S. (1997), *Diameter-selective raman scattering from vibrational modes in carbon nanotubes.* Science, vol. 275, pp. 187-191.

Richardson, J.T. and S.A. Paripatyadar. (1990), *Carbon dioxide reforming of methane with supported rhodium.* Applied Catalysis, vol. 61, no. 2, pp. 293-309.

Rodriguez-Reinoso, F. (1998), *The role of carbon materials in heterogeneous catalysis.* Carbon, vol. 36, pp. 159-175.

Ross, J.R.H. (2005), *Natural gas reforming and CO_2 mitigation.* Catalysis Today, vol. 100, pp. 151-158.

Rostrup-Nielsen, J.R. (1972), *Equilibriums of decomposition reactions of carbon monoxide and methane over nickel catalysts.* Journal of Catalysis, vol. 27, no. 3, pp. 343-356.

Rostrup-Nielsen, J.R., Hansen, J.H.B. (1993), *Carbon dioxide-reforming of methane over transition metals.* Journal of Catalysis, vol. 144, pp. 38-49.

Rostrup-Nielsen, J.R. (1994), *Production of synthesis gas.* Catalysis Today, vol. 18, no. 4, pp. 305-324.

Rotkin, S. and Subramoney, S. (2005), *Applied Physics of Carbon Nanotubes: Fundamentals of Theory, Optics and Transport Devices.* Springer-Verlag.

Schlapbach, L., and Zuttel, A. (2001), *Hydrogen storage materials for mobile applications.* Nature, vol. 414, pp. 353-358.

Serp, P., Corrias, M. and Kalck, P. (2003), *Carbon nanotubes and nanofibers in catalysis.* Applied Catalysis A, vol. 253, pp. 337-358.

Shamsi, A. (2004), *Carbon formation on Ni–MgO catalyst during reaction of methane in the presence of CO_2 and CO.* Applied Catalysis A, vol. 277, pp. 23-30.

Shiri, P.R. (2007), *Raman Scattering in Carbon Nanotubes.* Dissertation, University of the Witwatersrand, Johannesburg, South Africa.

Shofner, M.L., Lozano, K., Rodriguez-Macias, F.J., Barrera, E.V. (2002), *Nanofiber-reinforced polymers prepared by fused deposition modeling.* Journal of Applied Polymer Science, vol. 89, pp. 3081-3090.

Slagtern, A., Olsbye, U., Blom, R., Dahl, I.M. (1997), *Characterization of Ni on La modified Al_2O_3 catalysts during CO_2 reforming of methane.* Applied Catalysis, vol. 165, pp. 379-390.

Smith, B.W., Monthioux, M. and Luzzi, D.E. (1998), *Encapsulated C_{60} in carbon nanotubes.* Nature, vol. 396, pp. 323-324.

Solymosi, F., Kiss, J. (1985), *Impurity effects in the adsorption and dissociation of CO_2 on Rh.* Surface Science, vol. 149, pp. 17-32.

Song, Q., Xiao, R., Li, Y. and Shen, L. (2008), *Catalytic carbon dioxide reforming of methane to synthesis gas over activated carbon catalyst.* Industrial & Engineering Chemistry Research, vol. 47, pp. 4349-4357.

Su, M., Zheng, B., Liu, J. (2001), *A scalable CVD method for the synthesis of single-walled carbon nanotubes with high catalyst productivity.* Chemical Physics Letters, vol. 322, pp. 321-326.

Szeleifer, I. and Yerushalmi-Rozen, R. (2005), *Polymers and carbon nanotubes dimensionally intersection and technology.* Journal of Polymer, vol. 46, pp. 7813-7818.

Takanabe, K., Nagaoka, K. and Aika, K. (2005), *Improved resistance against coke deposition of titania supported cobalt and nickel bimetallic catalysts for carbon dioxide reforming of methane.* Catalysis Letters, vol. 102, no. 3, pp. 153-157.

Teo, B.K., Singh, C., Chowalla, M. and Milne, W.I. (2003), *Catalytic synthesis of carbon nanotubes and nanofibers.* Journal of Nanoscience and Nanotechnology, vol. 15, pp. 1-22.

Thess, A., Lee, R., Nikolaev, P., Dai, H., Petit, P., Robert, J., Xu, C., Lee, Y.H., Kim, S.G., Rinzler, A.G., Colbert, D.T., Scuseria, G.E., Tomanek, D., Fischer, J.E. and Smalley, R.E. (1996), *Crystalline ropes of metallic carbon nanotubes.* Science, vol. 273, pp. 483-487.

Thostenson, E.T., Ren, Z. and Chou T.W. (2001), *Advances in the science and technology of carbon nanotubes and their composites: a review.* Composites Science and Technology, no. 61, pp. 1899-1912.

Tibbetts, G.G. (1985), *Lengths of carbon fibers grown from iron catalyst particles in natural gas.* Journal of Crystal Growth, vol. 73, pp. 431-438.

Treacy, M. M. J., Ebbesen, T. W. and Gibson, J. M. (1996), *Exceptionally high young's modulus observed for individual carbon nanotubes.* Nature, vol. 381, pp. 678-680.

Tsipouriari, V.A., Verykios, X.E. (2001), *Kinetic study of the catalytic reforming of methane with carbon dioxide to synthesis gas over Ni/La_2O_3 catalyst.* Catalysis Today, vol. 64, pp. 83-90.

Tsuji, M., Yamamoto, T., Tamaura, Y., Kodama, T., Kitayama, Y. (1996), *Catalytic acceleration for CO_2 decomposition into carbon by Rh, Pt or Ce impregnation onto Ni(II)-bearing ferrite.* Applied Catalysis A: General, vol. 142, pp. 31-45.

Tuinstra, F., Koenig, J.L. (1970), *Raman spectrum of graphite.* Journal of Chemical Physics, vol. 53, no. 3, pp. 1126-1156.

Van Steen, E. and Prinsloo, F.F. (2002), *Comparison of preparation methods for carbon nanotubes supported iron fischer-tropsch catalysts*. Catalysis Today, vol. 71, pp. 327-334.

Vinciguerra, V., Buonocore, F., Panzera, G. and Occhipinti, L. (2003), *Growth mechanisms in chemical vapour deposited carbon nanotubes.* Nanotechnology, vol. 14, pp. 655-660.

Wang, H.Y., Au, C.T. (1996), *CH_4/CD_4 isotope effects in the carbon dioxide reforming of methane to syngas over SiO_2 spported nickel catalysts.* Catalysis Letters, vol. 38, pp. 77-79.

Weizhong, Q., Tang, L., Zhanwen, W., Fei, W., Zhifei, L., Guohua, L., Yongdan, L. (2004), *Production of hydrogen and carbon nanotubes from methane decomposition in a two-stage fluidized bed reactor*. Applied Catalysis A, vol. 260, pp. 223-228.

Witmore, N.H. (2007), *Greenhouse Gas Catalytic Reforming to Syngas.* Dissertation, Columbia University, New York, United States of America.

Winter, C. J. and Nitsch, J.J. (1998), *Hydrogen as an Energy Carrier: Technologies, Systems, Economy.* Springer-Verlag.

Xiang, R., Luo, G., Qian, W., Wang, Y., Wei, F., Li, Q. (2007), *Large area growth of aligned CNT arrays on spheres: towards large scale and continuous production.* Chemical Vapour Deposition, vol. 13, pp. 533-536.

Xu, X-J., Huang, S-M. (2007), *Carbon dioxide as a carbon source for synthesis of carbon nanotubes by chemical vapour deposition.* Materials Letters, vol. 61, pp. 4235-4237.

Xu, A., Indala, S., Hertwig, T.A., Pike, R.W., Knopf. F.C., Yaws, C.L., Hopper, J.R. (2005), *Development and integration of new processes consuming carbon dioxide in multi-plant chemical production complexes.* Clean Technology Environment Policy, vol. 7, pp. 97-115.

Yang, Q.H., Hou, P.X., Bai, S., Wang, M.Z. and Cheng H.M. (2001), *Adsorption and capillarity of nitrogen in aggregated multi-walled carbon nanotubes.* Chemical Physical Letters, vol. 345, pp. 18-24.

Yang, Y., Li, W., Xu, H. (2002), *A new explanation for the carbon deposition and elimination over supported Ni, Ni-Ce and Ni-Co catalysts for CO_2-reforming of methane.* Reaction Kinetic Catalysis Letters, vol. 77, no. 1, pp. 155-162.

Yi, S., Zhang, H., Pei, L., Zhu, Y., Chen, X., Xue, X. (2006), *The electrochemical hydrogen storage of CNTs synthesized by CVD using $LaNi_5$ alloy particles as catalyst and treated with different temperature in nitrogen.* Journal of Alloys and Compounds, vol. 420, pp. 312-316.

Yu, J., Lucas, J., Strezov, V. and Wall, T. (2003), *Coal and carbon nanotube production.* Fuelfirst, vol. 82, pp. 2025-2032.

Zeng, Q., Li, Z. and Zhou, Y. (2006), *Synthesis and application of carbon nanotubes.* Journal of Natural Gas Chemistry, vol. 15, pp. 235-246.

Zhang, H., Fu, X., Chen, Y., Yi, S., Li, S., Zhu, Y., Wang, L. (2004), *The electrochemical hydrogen storage of multi-walled carbon nanotubes synthesized by chemical vapor deposition using a lanthanum nickel hydrogen storage alloy as catalyst.* Physica B, vol. 352, pp. 66-72.

Zhang, C., Li, S., Wu, T., Shao-Yi, P. (1999*), Reduction of carbon dioxide into carbon by the active wustite and the mechanism of the reaction.* Materials Chemistry and Physics, vol. 58, pp. 139-145.

Zhang, Z., Verykios, X.E., MacDonald, S.M., Affrossman, S. (1996), *Comparative study of carbon dioxide reforming of methane to synthesis gas over Ni/La_2O_3 and conventional nickel-based catalysts.* Journal of Physical Chemistry, vol. 100, pp. 744-754.

Zang, J. (2008), *Research and Development of Nickel Based Catalysts for Carbon Dioxide Reforming of Methane.* PhD Thesis, University of Saskatchewan, Saskatchewan, Canada.

Zhang, J., Wang, H., Dalai, A.K. (2009), *Kinetic studies of CO_2 reforming of CH_4 over Ni-Co/AlMgOx bimetallic catalyst.* Industrial and Engineering Chemistry Research, vol. 88, no. 2, pp. 677-684.

Zhao, N., Cui, Q., He, C., Shi, C., Li, J., Li, H., Du, X. (2007), *Synthesis of carbon nanostructures with different morphologies by CVD of methane.* Materials Science and Engineering A, vol. 460-461, pp. 255-260.

Zwaan, B. and Gerlagh, R. (2006), *Climate sensitivity uncertainty and the necessity to transform global energy supply.* Energy, vol. 31, pp. 2571-2587.

APPENDIX 1: POSTER, ORAL PRESENTATIONS AND PUBLICATIONS

K.Moothi, S.K. Maphutha and S.E. Iyuke. (2008), *Carbon Nanofiber Production from Carbon Dioxide*. Poster Presentation. Postgraduate Student Symposium in Process Engineering, SAIChE Gauteng Branch in collaboration with SAIMM, Gauteng, South Africa.

S.K. Maphutha, K.Moothi and S.E. Iyuke. (2008), *Carbon Dioxide used for the Production of Carbon Nanofibers using Nickel Alloy*. Poster Presentation. Wits Postgraduate Symposium 2008, 7-8 November, University of the Witwatersrand, Gauteng, South Africa.

K. Moothi, S. Maphutha and S.E Iyuke. (2009), *CO_2 and CH_4 are used for the production of Carbon Nanofibers and Carbon Nanotubes using Nickel Alloy*. Oral Presentation. South African Chemical Engineering Conference 2009: Sustainable Engineering Development, 20-23 September, Western Cape, South Africa.

S.K. Maphutha, K.Moothi and S.E. Iyuke. (2009), *Thermodynamic Study on Carbon Nanotube Production during Dry Reforming of Methane* (Submitted to Chemical Engineering Science).

K.Moothi, S.K. Maphutha and S.E. Iyuke. (2009), *Carbon Nanotube and Carbon Nanofiber Production from CO_2 and CH_4.* (Submit to Industrial and Engineering Chemistry Research).